Design and development of a multi-modal aerial-ground vehicle for long-endurance inspection applications

Teodoro Afonso de Sousa Clemente Pinto Dias

Thesis to obtain the Master of Science Degree in

Electrical and Computer Engineering

Supervisor(s): Dr. Meysam Basiri

Examination Committee

Chairperson: Prof. João Fernando Cardoso Silva Sequeira
Supervisor: Dr. Meysam Basiri
Member of the Committee: Prof. Rita Maria Mendes de Almeida Correia da Cunha

Dez 2021

O que foi sempre será.

Declaração

Declaro que o presente documento é um trabalho original da minha autoria e que cumpre todos os requisitos do Código de Conduta e Boas Práticas da Universidade de Lisboa.

Declaration

I declare that this document is an original work of my own authorship and that it fulfills all the requirements of the Code of Conduct and Good Practices of the Universidade de Lisboa.

Acknowledgments

First, I would like to thank my supervisor Dr. Meysam Basiri, without whom this thesis wouldn't be possible. I'm grateful for the opportunity that you gave me, and I hope I was up to your expectations. I also appreciate all the guidance and your availability throughout the whole work, which allowed me to deliver this thesis.

To my parents, who always supported me. If I am the man I am today is thanks to you. Thank you for the opportunities you provided me. Thank you for your availability and support throughout this work.

To my official English reviewer, Teresa, a special thank you. Thank you for always being there supporting me throughout this year, and thank you for making the time to help me with this work. I'm fortunate to have you in my life.

For all others not mentioned that helped me with this dissertation, thank you.

x

Resumo

Durante a última década, a utilização de Micro Veículos Aéreos (MVAs) em aplicações como inspeção e vigilância tem demonstrado ser extremamente útil. Porém, a sua usabilidade é negativamente impactada pelos requerimentos energéticos da locomoção aérea, tendo uma capacidade de transporte e autonomia de voo limitados. Pelo contrário, os veículos terrestres são capazes de transportar maiores cargas e têm uma maior autonomia, sendo limitados pela sua capacidade de ultrapassar obstáculos no seu trajeto. Devido a estas características, tem havido um aumento do número de aplicações em que os dois tipos de veículos são utilizados em conjunto. Esta dissertação descreve o design e o desenvolvimento de um veículo híbrido aéreo-terrestre, BogieCopter, capaz de locomoção multimodal em ambientes apinhados e estreitos, e que tem uma maior autonomia que a alcançada por veículos puramente aéreos. O design consiste num MVA com dois eixos inclináveis e quatro rodas, independentes e passivas, que possibilitam ao veículo voar, aproximar-se e mover-se em superfícies planas e inclinadas. Em comparação com outros veículos híbridos com rodas passivas, o design do BogieCopter permite-lhe atingir uma maior eficiência no movimento terrestre e transportar a carga necessária para a realização da maioria dos tipos de inspeção, e apresenta o mecanismo que adiciona a multimodalidade com uma das menores massas. Adicionalmente, o desempenho do veículo é avaliado através de múltiplos testes, demonstrando a sua capacidade para voar, mover-se no chão e, até, para subir paredes. Finalmente, uma comparação entre a energia gasta pelos diferentes modos de operação é apresentada.

Palavras-chave: Desenvolvimento de Protótipo, Design de Protótipo, Inspeções, Locomoção Aérea-Terrestre, Micro Veículo Aéreo, Multimodalidade

Abstract

During the last decade, the use of Micro Aerial Vehicles (MAVs) in applications such as inspection and surveillance has proved to be extremely useful. However, the usability of these vehicles is negatively impacted by the large power requirements of flight consumption, limited payload and operating time. On the other hand, ground vehicles are able to transport larger payloads and have a higher operating time, being limited by their capacity to overcome obstacles in their path. Thus, applications in which both types of robots are used in combination have started to emerge. This thesis describes the design and development of a hybrid aerial-ground vehicle, BogieCopter, enabling multi-modal mobility in challenging terrains, enabling the locomotion in potentially cluttered and narrow spaces, and having a higher operating time when compared to aerial-only vehicles. The design consists of a MAV with two tiltable axles and four independent passive actuated wheels, allowing the vehicle to fly, approach, land and move on flat and inclined surfaces. In comparison to existing multi-modal vehicles with passive actuated wheels, the design of BogieCopter enables a higher ground locomotion efficiency, provides a higher payload capacity suitable for inspection applications, and presents one of the lowest mass increases due to the ground actuation mechanism. Furthermore, the vehicle's performance is evaluated through a series of real experiments, demonstrating its flying, ground locomotion and wall-climbing capabilities. Finally, the energy consumption for different modes of locomotion is demonstrated.

Contents

List of Tables

List of Figures

Nomenclature

Greek symbols

η	Efficiency
γ	Slope inclination [^{o}]
ω	Angular velocity [rad/s]
ϕ	Roll [^{o}]
ψ	Yaw [^{o}]
ρ	Density [kg/m^3]
τ	Torque [$N \cdot m$]
θ	Angle [^{o}]

Roman symbols

$\dot{m}$	Mass flow rate [kg/s]
$\partial \vec{S}$	Unit normal area vector
A	Rotor disk area [m^2]
a	Acceleration [m/s^2]
B	Propeller number of blades
C	Center of mass
D	Diameter [m]
d	Half the wheelbase [m]
E	Energy [J]
F	Force [N]
g	Gravity [m/s^2]
I	Moment of inertia [kg/m^2]
L	Half the trackwidth [m]
m	Mass [kg]
P	Power [W]
p	Pressure [Pa]
r	Position [m]
S	Slipstream boundary surface [m^2]
s	Span [m]

T Thrust $[N]$

t Time $[s]$

T_w Thrust-to-weight ratio

U Voltage $[V]$

u Propellers' induced moments $[N \cdot m]$

u_d Magnitude of the drag force $[N]$

u_f Magnitude of total thrust $[N]$

V, v Velocity $[m/s]$

v_i Inflow velocity $[m/s]$

W Weight $[N]$

w Flow velocity in the far wake plane $[m/s]$

Subscripts

2_rotors Relative to two non-interacting rotors

$\parallel$ Parallel

$\perp$ Perpendicular

A Relative to the motors' arms

B^* Frame in the center of mass of the vehicle

$co - axial$ Relative to the co-axial rotor

$hover$ Relative to the hover

L Left

max Maximum

$nominal$ Nominal

$prop$ Relative to the propeller

R Right

r Robot body reference frame

$rotor$ Relative to the rotor

s Relative to the servo

$system$ Relative to the system

u Relative to longitudinal motion

w Relative to lateral motion

X, Y, Z Cartesian components

x, y, z Cartesian components

Superscripts

$*$ In the center of mass

$\ddot{}$ Second order derivative

$\dot{}$ First order derivative

B Relative to the body coordinate frame

E, I Relative to the Inertial or Earth coordinate frame

Acronyms

μ**UAV** Micro Unmanned Aerial Vehicle

CFD Computational Fluid Dynamics

CFRP Carbon Fiber Reinforced Plastic

CoM Center of Mass

CRC Cyclic Redundancy Check

DDMR Differential Drive Mobile Robot

DoF Degrees of Freedom

EKF Extended Kalman Filter

ESC Electronic Speed Controller

FoS Factor of Safety

GAM Ground Actuation Mechanism

GV Ground Vehicle

LED Light Emitting Diode

LIDAR Light Detection And Ranging

MAV Micro Aerial Vehicle

MTOM Maximum Take-off Mass

NAV Nano Aerial Vehicle

NS Not Specified

P Proportional

PAV Pico Aerial Vehicle

PCB Printed Circuit Board

PID Proportional Integral Derivative

PWM Pulse Width Modulation

ROS Robot Operating System

RPM Revolutions per minute

SD Smart Dust

SF Safety Factor

SoC State of Charge

T/W ratio Thrust-to-weight ratio

ToF Time-of-Flight

UAV Unmanned Aerial Vehicle

UGV Unmanned Ground Vehicle

VTOL Vertical Take-off and Landing

Chapter 1

Introduction

1.1 Motivation and Goals

Due to advances in the field of electronics and in the field of microsystems, unmanned aerial vehicles (UAVs) have become a prevalent commercial technology. More specifically, micro aerial vehicles (MAVs) have become ubiquitous in many fields. One of those fields is the cinematography/photography industry, which saw an exponential increase in the use of MAVs, due to the fact that such platforms are able to fly over cluttered and inaccessible areas and provide an elevated and bird-eye view of the environment. Such important features allied with the capacity to fly over obstacles and to reach regions of interest, which may be of impossible access to humans or other types of robots, meant that MAVs could be used for other applications, such as inspection (examples include agriculture [1, 2], oil and gas [3], power generation [4], mining [5], chemicals [6], marine vessels [7], structural [8] and others), search and rescue missions [9, 10], surveillance [11], and many others [12]. The application of MAVs in these different use cases has contributed to the reduction in downtime and operating costs [13], increase of the safety of human operators [3, 6] and it has even helped to save lives [14]. These contributions have led to a tremendous growth in the inspection drone's market, in the last 3 years, being expected to more than double by 2027 [15].

Despite their desirable characteristics, the usability of MAVs has been strongly impacted by their limitations. When compared to ground vehicles (GVs), MAVs offer a very limited payload capacity, have a lower operating time, and don't present robustness to collisions, meaning that their use in potentially cluttered and narrow spaces where there is potential for physical interaction is very limited or, even, non existent. On the other hand, GVs lack the capability to overcome obstacles and reach hard to reach places, which come inherently with the use of aerial vehicles. The undesirable characteristics of both of these types of vehicles means that their ability to operate in different environments and in different applications is limited. Most flying vehicles are only able to fly away from the ground and from structures, consuming a big percentage of its power source in reaching a desired place and not in performing the desired task while a ground vehicle may not be able to reach that desired place, due to the requirement to overcome some obstacle on its path, or will require the operator to waste time on the positioning of the

GV in the region of interest. As an example, we can think about a structure that needs to be inspected on the top of a building, for example, some photovoltaic panels. While a MAV can be positioned on the bottom of the building and fly to its top, the GV needs to be taken by the operator to the top. However, while a GV will consume a low amount of energy during the inspection (it is almost static, only moving between photovoltaic panels), the MAV is spending a high amount of energy to maintain its flying state, which isn't really necessary neither desirable. Use cases as these are the ones that would benefit from the use of multi-modal vehicles. We could think of a hybrid aerial-ground vehicle that could fly to the top of the building and then move on the ground to a desired point and perform the desired task. Despite the fact that we can think of many multi-modal types of vehicles, in this work, we will focus our attention on hybrid aerial-ground vehicles.

This project aims at designing an aerial-ground MAV that can both fly and move on surfaces, hence extending the adaptability and applicability of MAVs for applications such as inspection, search and rescue missions, surveillance, and cinematography. The MAV will be designed with the goals of being cost-effective, in order to promote its easy adoption, being easily manufactured and having a platform as open to modifications as possible, in order for the system to be upgradeable and to be easily adapted to as many applications as possible. We envision many potential advantages for such a system such as the ability to get close to surfaces and move on inclined surfaces, being able to move into tight spaces or inside buildings, move safely around humans in buildings, increase the total operating time due to the use of the more energy-efficient ground locomotion and being accessible to the common MAV operator.

1.2 Objectives

The goal of this thesis is to design, develop and test a multi-modal MAV capable of flying and of ground locomotion, both in flat and inclined surfaces, with the main goal of it being used in inspection applications.

The design and development of such vehicles can be divided into two different work categories: hardware and software/firmware. In this work, the hardware of the platform will be developed from scratch while the firmware will be developed through the extension of the capabilities of a readily available open-source firmware.

To be able to reach the proposed goal, a set of objectives have been identified and will be followed throughout the next chapters. They are:

- Analysis of the State-of-the-Art inspection vehicles (with a focus in aerial vehicles) and multi-modal MAVs;

- Analysis of the multi-modal vehicle's mechanics which can lead to a lighter and more efficient multi-modal MAV;

- Design of the multi-modal MAV, with mechanical and propulsive system optimization;

- Development of a simulation model of the multi-modal MAV, for the design of future controllers and path following algorithms;

- Firmware development of the ground locomotion mode, enabling the drone to move on flat and inclined surfaces;

- Test of the developed multi-modal MAV, in all the possible actuation modes: aerial, ground, and multi-modal mode, with analysis of its performance.

1.3 Thesis Outline

This thesis is divided into six chapters, which are explained next.

The present chapter serves the purpose of being an introduction to the topic developed on the remainder of this work. In section 1.1, the motivation behind developing an aerial-ground MAV is presented as are the goals of this work. This section is followed by section 1.2, in which the objectives that need to be completed to develop the aerial-ground MAV are presented.

Chapter 2 is divided into three main parts: UAV state-of-the-art, in section 2.1, inspection rotary wings MAVs state-of-the-art, in section 2.2, and a review of the multi-modal rotary wings MAVs literature, in section 2.3. In section 2.1, as the name "Unmanned Aerial Vehicles" suggests, the main topic will be UAVs, in general. A brief historical overview of UAVs is given and the state-of-the-art classifications of UAVs are analysed, in order to narrow the classification of the developed multi-modal UAV and give a better sense of its characteristics. Section 2.2 starts with a brief introduction to the topic of inspection rotary wings MAVs and further explores the different inspection methods that make use of MAVs. In the last section of this chapter, section 2.3, the state-of-the-art multi-modal rotary-wing MAVs are reviewed, in order to define the advantages and the shortcomings of each design and draw the path for the design of the developed MAV.

Chapter 3 presents the background information necessary to develop a multi-modal MAV. The information presented here is summarized to only the necessary, in order to keep this chapter as short as possible while still providing all the required background information to develop the MAV. It is divided into three sections. Section 3.1 explains, shortly, how the performance of a rotor is influenced by its shape and operating characteristics, enabling a better selection of the propulsive system. Section 3.2, introduces quadrotors, presenting their working principle and how they are controlled. The last section, 3.3, is focused on unicycle type robots, ending with the determination of their equations of motion.

Chapter 4, throughout its seven sections, presents the hardware of the developed MAV. Baseline and requirement specifications are set and the design procedure is presented. It is followed by the determination of the mass of the vehicle and by the selection of the different parts that compose the propulsive and electronic systems. It culminates in the mechanical design of the MAV, ending with the presentation of a developed prototype.

Chapter 5 focus on the code side of the developed MAV. It is divided into two sections. In section 5.1, a simulator model for the developed MAV is presented. In section 5.2, the open-source autopilot firmware is selected and the developed firmware is presented, depicting the decisions that led to the final code.

Chapter 6 is divided into four sections. In these sections, results from different experiments are

3

presented and the developed MAV is validated. In section 6.1, the developed vehicle's mass is presented and analysed. In section 6.2, the used rotor is tested and its performance is compared with the performance of other (tested) rotors. Different real experiments that were conducted with the developed vehicle, in order to validate its design, are presented in section 6.3. Finally, in section 6.4, the power consumptions and the throttle required to maintain different operating states are presented and compared.

Chapter 7 is divided into two parts: achievements, in section 7.1, and future work, in section 7.2. In the first section, section 7.1, we conclude about the state of the project and about what was performed and accomplished with this work. We finish this thesis with the future work, in section 7.2, where objectives for the continuity of this project are presented, pointing improvements and features to be made, in order to get the best possible multi-modal MAV.

Chapter 2

State-of-the-Art and Literature Review

This chapter is dedicated to the analysis of the state-of-the-art UAVs, inspection rotary-wing MAVs and multi-modal rotary-wing MAVs. It is divided into three sections. In section 2.1, brief background information on UAVs will be provided. This section serves the purpose of presenting an overview of the different types of UAVs available, narrowing the classification of the developed UAV. After this section, we will narrow the scope of the analysis of the state-of-the-art to rotary-wing MAVs. In section 2.2, the state-of-the-art inspection vehicles will be analysed. Finally, in section 2.3, the state-of-the-art multi-modal vehicles, mainly hybrid aerial-ground robots is presented. In this last section, a comparison between all the analysed multi-modal vehicles will be given, with the intention of easing the design process.

2.1 Unmanned Aerial Vehicles

Unmanned aerial vehicles (also known commonly as drones), as the name suggests, refer to aircraft systems without any human operator on-board, which flies remotely or autonomously [12, 16]. Given the absence of a human operator, they are commonly used where the presence of humans is difficult, dangerous, or even impossible [6, 8, 17]. More recently, their use in civilian/recreational applications has had an impressive growth [15, 16], derived from the miniaturization of electronic/electromechanical components and advances in power storage systems [16, 18], leading to cost-effective solutions.

2.1.1 History of Unmanned Aerial Vehicles

The history of UAVs dates back to more than 2500 years, to ancient Greece, where Archytas of Tarentum developed a mechanical bird that, by moving its wings, was able to fly, allegedly, 200m before falling to the ground, after its energy had all been used [16]. More recently, UAVs were used during World War I (1917, figure 2.1). Those early UAVs were very unreliable and inaccurate [16]. Their usefulness, their ability to change the battlefield, and their overall impact on military applications were only recognized by a handful of individuals who kept alive (over the post World War I years) the concept of an unmanned vehicle by pushing for political support and funding [16]. The perception about UAVs

was completely changed during the war in Afghanistan and Operation Iraqi Freedom where UAVs were successfully used on the battlefield and were deployed successfully for a multitude of missions. This resulted in a huge increase in funding for the development of UAVs [16]. More recently, in 2006, after the Federal Aviation Administration issued its first commercial drone permit, non-military ventures began [15]. The last decade has seen an explosion in the use of drones for diverse applications such as cinematography/photography, delivery [19], search and rescue [9, 10], inspection (examples include Oil and Gas, Power Generation, Mining, Chemicals, Marine Vessels, and others) [6, 8, 17], and surveillance [11]. This booming in the use of drones is related to the performance of tasks that were almost impossible before, a reduction in downtime and operating costs and an increase of the safety of human operators [3, 6, 13]. Furthermore, the use of drones has even helped to save lives [14].

Figure 2.1: World War One drone: the Kettering Bug [20].

2.1.2 Classification of Drones

The increasing use of drones in both military and civilian applications has led to the creation of drones specialized in a given purpose, being that their configuration is dependent on the platform and the mission [12, 21]. Different classifications for drones exist in the literature, based on different parameters. These classifications can be divided into two categories: conventional and unconventional classification. The purpose of this subsection is to narrow the classification of the developed vehicle and doesn't have the objective of being an extensive analysis of the drone classification state-of-the-art. Several articles have been published in the drone's classification area, but a review can be found in [12]. For the conventional classification, we will be using the classification presented in [12] and for the unconventional classification, we will be presenting the classification given in [21].

2.1.2.1 Conventional Classification of Drones

The conventional classification of drones is based on the size, mass, and flight endurance of the drone [12, 21]. The conventional classification of drones used is reproduced in table 2.1. We can classify the developed drone in terms of mass and size as being a MAV, so, onward in this chapter, we will be analysing and focusing our attention on this small group of drones.

The first comprehensive research on MAVs dates back to 1993 [12]. MAVs have received a great deal of attention during the past two decades, both from the scientific community as commercially, derived

6

from technology advances, mainly in the area of microtechnology [12]. The success of MAVs inherits from their small dimensions, which allows them to fly in confined/cluttered spaces, making them the ideal flying platform for operations in urban environments, particularly within buildings, and enables them to be manufactured at large scale and at low costs [12, 21], making them the ideal type of vehicle for a custom made platform. In comparison with smaller flying vehicles, MAVs make use of readily available electronics and mechanical components, contributing to their lower development cost. A comparison of the development cost of different types of aerial vehicles is presented in figure 2.2.

Drone Classification	Size	Mass
SD	< 0.25 cm	< 0.5 g
PAV	0.25 to 2.5 cm	0.5 to 3 g
NAV	2.5 to 15 cm	3 to 50 g
MAV	15 cm to 1 m	50 g to 2 kg
μUAV	1 to 2 m	2 to 5 kg
UAV	> 2 m	> 5 kg
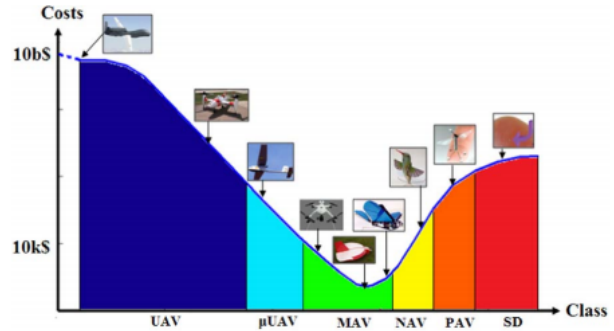
Table 2.1: Drone conventional classification, according to [12].

Figure 2.2: Design and fabrication costs of different types of drones [12].

2.1.2.2 Unconventional Classification of Drones

The unconventional classification of drones, presented in [12, 21], is given by the vehicle's configuration. Here we are only going to analyse the classifications given for MAVs, but many of them are similar for other kinds of aerial vehicles (in terms of the conventional classification). MAVs can be classified according to nine categories: fixed-wing, flapping wing, vertical take-off and landing (VTOL), rotary-wing, tilt-rotor, ducted fan, helicopter, ornicopter, and unconventional type [12]. Even with these classifications, drones can share features, for example, a rotary-wing can also be a VTOL and a helicopter is a type of rotary-wing [21]. Following [21], we can classify drones as:

Fixed-wing: Often consist of a rigid wing, fuselage, and tails which use a motor and propeller as their propulsion system, requiring a runway to take-off and land or a catapult to launch [12, 21]. Generally, this type of MAV has the highest allowed flying altitude and the highest cruising speed among all types of drones, allowing it to cover a vast area with the same energy storage system of other MAVs [12, 21].

Rotary-wing: This type of MAV uses rotary-wing systems (rotors) to generate lift, thrust, and control forces [12]. Contrary to other types of MAVs, rotary-wing MAVs have high manoeuvrability, being able to fly in every direction, horizontally and vertically, and are also able to hover in a fixed position [12, 21]. These capabilities make them the perfect drone type for surveying hard-to-reach areas, such as pipelines, bridges, etc [12]. Rotary-wing MAVs are the preferred type of drone for indoor use [12]. Compared to fixed-wing drones, they have lower endurance, lower cruising velocity, and lower maximum flying altitude [12, 21]. They can have multiple configurations: main and tail rotors (conventional helicopter), co-axial rotors, tandem rotors, and multirotors [21]. Among multirotors,

quadrotors and hexarotors are the best-known drones [12]. Because of the advantages of rotary-wings for inspection applications, during the rest of this work, we will focus solely on them.

Flapping-wing: Take inspiration from animals, being that flapping wings MAVs take inspiration from birds. They have flexible and/or flapper small wings which use an actuation mechanism for their flapping motion [12, 21]. The flapping wings are made from flexible and light materials. Compared to the previous drones, their endurance and velocity are small and are more difficult to control (caused by their complex aerodynamics) [12].

Blimps: The only type of drone which is lighter than air (like balloons and airships). They are large, fly at low speeds, and have the highest endurance [21].

<table>
<tr><td>(a)</td><td>(b)</td><td>(c)</td><td>(d)</td></tr>
</table>
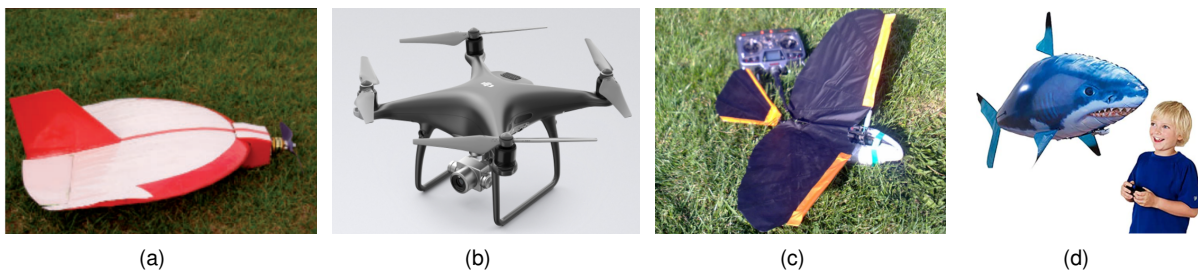
Figure 2.3: UAV unconventional classification: (a) Fixed-wing [22] (b) Rotary-wing [23] (c) Flapping-wing [24] (d) Blimp [25].

2.2 Inspection Rotary-Wing MAVs

In recent years, rotary-wing MAVs have received a great deal of attention for inspection purposes, due to their advantages, presented in the previous subsection 2.1.2. While MAVs present a low development cost and the ideal balance between payload capacity and size, enabling them to work both outdoors as indoors [12], rotary-wings have the ability to hover in place, fly at low speeds as at a higher speed [12, 21], making them ideal for inspection applications, where a high velocity is desirable to reach the inspection point and hover/low velocity is desirable for the inspection task.

Inspection applications where these MAVs have been used are increasing and include crop evaluation [1, 2], pipeline inspection [3], bridge inspection [26, 27], photovoltaic panels inspection [4, 28, 29] and many others. The use of MAVs for inspection in hazardous or hard-to-reach places has become the norm, due to the increased safety for the human operator [3, 6]. On other sites, it is becoming standard, due to the reduction in downtime and inspection costs [13]. For example, the use of MAVs for photovoltaic panels inspection instead of human ground inspections can lead to a reduction of 90% in the inspection costs and in the inspection time [13]. Lower inspection costs and time can lead to more regular inspections which in turn can lead to better failure anticipation and prevention.

Almost all the analysed research work done in the use of MAVs for inspection applications relies on the use of commercially available MAVs [4, 8, 17, 28, 29]. The commercially available MAVs are tailored to the required application, with the addition of sensors [4, 8, 17, 28, 29]. These additions led, sometimes, to poor vehicle operating times, due to the increase in mass and the lack of optimization of the propulsive system to those weights [17] (payload capacity of those commercially available MAVs

doesn't take into account the sensors used in inspection applications). This wouldn't be the case if the MAV was designed and developed for that specific use case and to be able to carry those sensors.

Based on the sensors that are added to the MAV platform, it is possible to distinguish two inspection methods: visual inspection and contact-based inspection. It should be noted that in both inspection methods, usually, Time-of-Flight (ToF) sensors (such as Light Detection And Ranging (LIDAR)) were added to the platform, enabling the vehicle to operate autonomously.

2.2.1 Visual Inspection

Visual inspection methods are based on the use of optical sensors. These sensors can work on the visual spectrum of light (RGB cameras) or in the infrared spectrum (thermal cameras). The procedure of inspection for both sensors is the same, a picture of a point of interest is taken and then analysed, by a human operator or by an image processing algorithm. Although the use of an aerial vehicle has sped up the inspection process duration, most of the time, it is still required a closer inspection by a human operator, due to the inability of the MAV to get close to structures.

Visual inspection by RGB cameras: Visual inspection with the use of RGB cameras is mainly done on concrete, brick or steel constructions, where the goal is to find defects on the structure, for example, fractures or even microfractures [7, 8, 17, 27].

Visual inspection by thermal cameras: Visual inspection using thermal cameras is the most common method for inspection of electrical infrastructure, mainly high voltage cables and photovoltaic panels, where differences in temperature between points can indicate the existence of defects (for example, hot spots on photovoltaic panels) [4, 28–31]. For photovoltaic panel inspection, the use of high-resolution thermal cameras is a must [30, 31].

2.2.2 Contact-based Inspection

Contact-based inspection, as the name indicates, refers to inspection methods where contact between the sensor used and the surface to be analysed is required. The inspection is done through the hammer test or using ultrasounds. The hammer test is a common approach to the inspection of concrete structures whereas the use of ultrasounds is a common approach for the inspection of steel structures. To perform these tests, the most common approach is the addition of a manipulator with multiple degrees of freedom (DoF) to a MAV, being that the literature reviewed focuses on the development of the manipulator, its dynamics and the interaction of the vehicle with the surface to be inspected [3, 32–34]. Due to the mass added by the manipulator to the MAV, the vehicle's operating time is reduced, given that commercially available MAVs don't take into account on its design the mass required for these sensors. Some research exists in which the use of the additional manipulator for contact-based inspection isn't required. Examples are [6, 35], where electromagnets are used to stick to the wall and where tilt-rotors are used to enable the vehicle to stick and climb a wall, respectively.
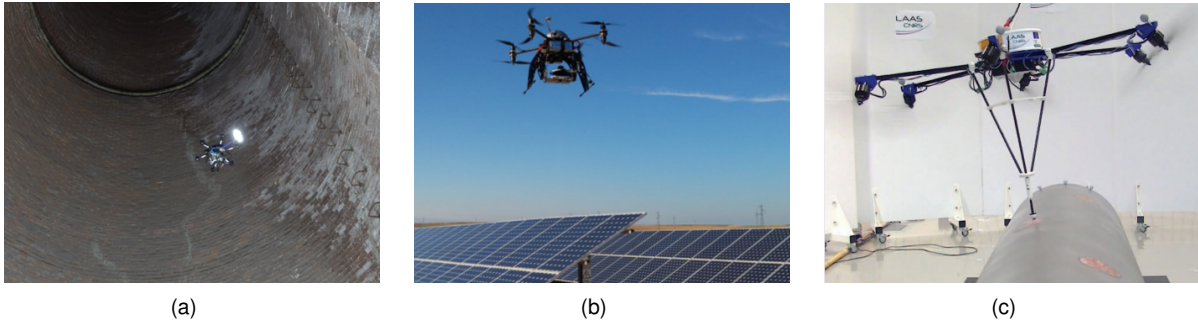
Figure 2.4: Examples of different inspection MAVs: (a) ChimneySpector [8] inspecting an old industrial chimney (b) Inspection of a photovoltaic plant in Spain [30] (c) The AEROMARS project contact-based inspection platform [3].

2.3 Multi-modal Rotary-wing MAVs

During the last decade, there has been a great deal of interest in developing hybrid aerial-ground vehicles [12, 36], being that the first research done on hybrid rotary-wing MAVs seems to date back to 2013 [37, 38]. The interest in the development of a hybrid aerial-ground vehicle derives from trying to combine the advantages of MAVs with those from unmanned ground vehicles (UGVs), in a single platform. While UGVs have desirable characteristics such as long operating time, high payload capacity, and robustness to collisions, they lack the capability to overcome obstacles in their path and reach hard to reach places (many points of interest are often inaccessible from the ground [36]), which come inherently with the use of aerial vehicles [36] (if an aerial vehicle faces an obstacle, it simply has to fly over it). On the other hand, aerial vehicles lack the robustness to resist collisions, have a low operating time, due to the high energy requirements of flight, and low payload capacity but are able to traverse difficult terrain and overcome almost any obstacle [36]. A hybrid aerial-ground vehicle is designed to combine the advantages of both locomotion methods, by moving on the ground to save energy when possible, and flying when terrain constraints do not allow otherwise [36]. In this section, we will analyse the state-of-the-art of scientific and commercially available multi-modal vehicles, with a focus on hybrid aerial-ground vehicles.

We can divide multi-modal vehicles into two categories depending on their ground actuation mechanism (GAM): active and passive actuated vehicles [5, 36]. Active actuated multi-modal vehicles use an active source of actuation for the ground locomotion, for example motors, which are added to the flying platform (additionally to the actuators used for flight). This design presents advantages such as the increased operating time in ground locomotion, due to the efficiency of wheel rolling locomotion, and decoupling and independence between the flight and ground controllers [5]. On the other hand, the additional mass added by the GAM's actuators impacts negatively the flight operating time. Contrary to active actuated multi-modal vehicles, passive actuated multi-modal vehicles use the same flight actuation mechanisms to enable the ground locomotion. The impact on the flight operating time is reduced and the design of the vehicle is simpler. However, the use of the propellers to move on the ground is less efficient than a wheel-based one (caused by a commonly used design) and the dust generation in ground mode can cause errors in state estimation [5]. Opposing to [36] and similar to [5], in this work

we will consider active actuated vehicles those in which extra actuators are added to the flying platform to enable the ground locomotion and we will consider passive actuated vehicles those who rely on the same actuators used for flight to move on the ground.

2.3.1 Active Actuated Multi-modal MAVs

As mentioned previously in this section, active actuated multi-modal vehicles rely on additional actuators to enable the ground locomotion (others than those used for flight). The majority of the design of commercially available products relies on this approach, with many different types of vehicles available. Those vehicles can be further divided into tracked, two-wheeled, three-wheeled, and four-wheeled vehicles.

2.3.1.1 Tracked Vehicles

Two examples of tracked aerial-ground vehicles are the Pegasus [11] and the B-Unstoppable [39] (figures 2.5(a) and 2.5(c), respectively). Pegasus was designed for military applications [11] while B-Unstoppable is designed for the hobby market. There isn't much information about Pegasus available other than [11] but the working principle is similar to B-Unstoppable. Both vehicles have two tracks, each one driven by one DC motor, enabling the vehicle to move on the ground and implementing skid steering. In the case of Pegasus, there is an extra motor, which, in flight mode, moves the tracks to a position to protect the propellers of the vehicle (figure 2.5(b)). B-Unstoppable has a maximum flight endurance of nine minutes and a maximum ground locomotion endurance of eighteen minutes (driving saves up to 60% of the energy) [39] while Pegasus has a maximum ground locomotion endurance of six hours (to the best of our knowledge, there isn't information about the flight endurance). Both vehicles are equipped with RGB cameras [11, 39] and Pegasus is also equipped with a LIDAR [11].

| (a) | (b) | (c) |
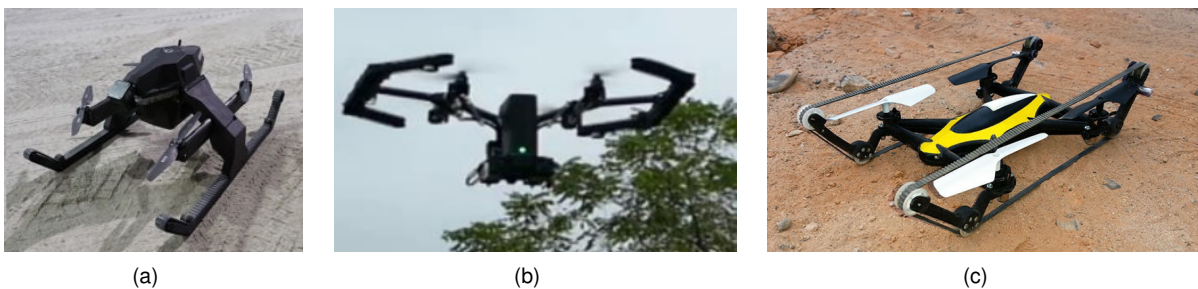
Figure 2.5: Examples of tracked aerial-ground vehicles: (a) Pegasus in ground mode [11] (b) Pegasus in fly mode, with the tracks protecting the propellers [11] (c) B-Unstoppable in ground mode [39].

2.3.1.2 Two-wheeled Vehicles

Morton and Papanikolopoulos [40] developed a two-wheeled active actuated multi-modal MAV (figure 2.6). The biggest advantage of this vehicle is that it morphs using a single actuator, protecting the propellers while on the ground mode [40]. Despite this feature, the vehicle needs a flat surface to be able to do the transformation, which limits its usability [5]. It uses two motors for ground locomotion, implementing skid-steer drive, and behaves as a quadrotor on flight mode. The design doesn't include any sensor for the performance of tasks and its inclusion seems to require a design change. It weighs

946 g and in loiter it was estimated that the average power consumption was 187.5 W. The power consumption in ground mode is unknown. It's also unknown if the design took into consideration any payload.

Figure 2.6: Morphing two-wheeled quadrotor [40].

2.3.1.3 Three-wheeled Vehicles

WAMORN's [41] design started from the assumption that ground operability of two-wheeled passive aerial-ground MAVs is remarkably bad due to the use of the reaction force from the wind generated by the rotors [41]. To solve this issue, an active actuated vehicle was developed, using a skid-steer drive and having a support wheel (stabilizer) to protect the MAV from rollovers while braking or moving on inclined surfaces, and to make the run more stable [41]. The skid-steer drive mechanism was designed for a maximum velocity of 1.1 m/s, similar to the velocities of vehicles used in disaster situations [41]. Due to the use of a commercially available MAV, a test was conducted to verify the maximum take-off mass (MTOM), which was confirmed to be 350g. The total mass of the developed MAV is 329 g, which doesn't have a high enough safety factor (SF) to be operated in windy conditions. To the best of our knowledge, this mass didn't take into consideration the mass of any extra sensor neither it is presented the total mass percentage of the active GAM. Compared with the Skywalker passive actuated caged MAV, it was presented that the active GAM has a better energy efficiency than the passive one, showing improvements of, almost, 8 times in the operating time and, almost, 23 times in the operating distance, for a MAV which weighs 4.7 times more. WAMORN is, also, able to withstand higher slope angles (27.5 times higher pitch). To the best of our knowledge, it is also unknown how the flight operating time was impacted by the added mass of the active GAM.
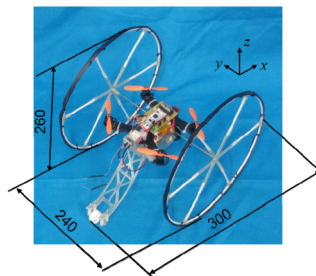
Figure 2.7: WAMORN [41].

2.3.1.4 Four-wheeled Vehicles

The work developed in [42] is one of the simplest approaches to an aerial-ground MAV, being a quadrotor mounted on top of a rover (see figure 2.8(a)). Its main use case was agricultural applications.

The ground mode was designed to have a top speed of 7-10 m/min and have a curb weight of 5.5 kg. Flight tests showed that the vehicle was able to fly for 15 minutes and to hover for 20 minutes while ground testing showed that the vehicle was able to operate for 40 minutes on flat surfaces and for 35 minutes on uneven surfaces, without any load [42]. Flight tests were performed with the aerial-ground vehicle while the ground tests were only performed with the rover and so, the multi-modality of the vehicle wasn't demonstrated in ground mode. Also, to the best of our knowledge, power consumptions are unknown as is the mass of the vehicle.

Although the work of Myeong and Myung [35] (figure 2.8(b)) didn't have a focus or a goal on the design of an aerial-ground vehicle, we need to refer to it as a source of inspiration. Furthermore, there is a possibility for it to move on the ground, given its characteristics. The main goal of this work was to develop a wall-climbing vehicle. The vehicle is a quadrotor, with the rotors mounted on tiltable axles. These axles are actuated by servos. On the far end side of each motor arm, wheels were assembled, enabling the robot to move on walls. Each pair of wheels (on each side), is actuated by a servo. The propulsive system is composed by EDF rotors, due to their size although being very inefficient [35]. It is demonstrated that this MAV is able to move on the wall and that, with the rotors tilted at 65º, facing the wall, its power consumption is, approximately, 25% lower than the one required to hover. To the best of our knowledge, the total mass of the MAV is unknown as is its payload.

R S and Dharmana [43] proposed an air-land-water vehicle concept (figure 2.8(c)), based on a birotor design for flight, due to its benefits over quadrotors [43, 44], and a differential drive system for ground movement. The vehicle is able of water locomotion due to the design of its wheels, which act like paddles. By using a servo in each rotor arm, the vehicle is able of wall-climbing. It has four wheels, two acting as actuators and two acting as supporting wheels. To the best of our knowledge, and according to [45], this concept was never developed and the only real data available is the thrust produced by its rotors, which is, approximately, 12.5 N, and the design vehicle's mass of 1.5 kg.

NASA's Jet Propulsion Laboratory has also been developing its own multi-modal MAVs. An example of an active actuated is Drivocopter [5] (figure 2.8(d)). It was designed to tackle the DARPA Subterranean (SubT) Challenge [5]. Due to the requirements of the challenge, Drivocopter requires a minimum sensor payload of, approximately, 1.2 kg. For ground mode, Drivocopter uses four coreless DC motors, one in each wheel. The wheels are manufactured from carbon fibre and create a protecting cage around the rotors. The design of Drivocopter assumed a MTOM of 4.5 kg, consisting of 2 kg for the airframe and GAM, 1.2 kg for sensors, and 1.3 kg for the batteries, which would enable 10 minutes of hovering time [5]. Due to the requirements and the need for a compact system, Drivocopter uses co-axial rotors in a quadrotor configuration, meaning, it uses a total of eight motors [5]. Drivocopter ended up weighing 5.1 kg, with the GAM weighting 900 g, which corresponds to, approximately, 17.6% of the vehicle's total mass [5]. While in ground mode on a flat surface, the vehicle consumes about 130 W, and in flight mode, it consumes 1060 W, a value, approximately, 8 times higher than the first one [5]. It is estimated that the vehicle can drive for about 90 minutes and fly for about 8 minutes, with a full charge [5].

Examples of hobby four-wheeled active actuated aerial-ground vehicles are JJRC H3 [46] and Syma X9 [47] (figures 2.8(e) and 2.8(f), respectively). Although more models exist, these two were selected

due to their GAM, which represent all the GAM's design available in the hobby market. While JJRC H3 uses a skid-steer drive, Syma X9 uses a servo to provide Ackermann steering and a rear motor for propulsion. JJRC H3 wheels are built around their rotors, providing some protection for the propellers. It is able to fly for, approximately, 6 minutes and its ground operating time, payload capacity, and power consumption are unknown. Syma X9 has four wheels, one at the end of each motor's arm. It is able to fly for, approximately, 8 minutes. Its ground operating time, payload capacity, and power consumption are also unknown.
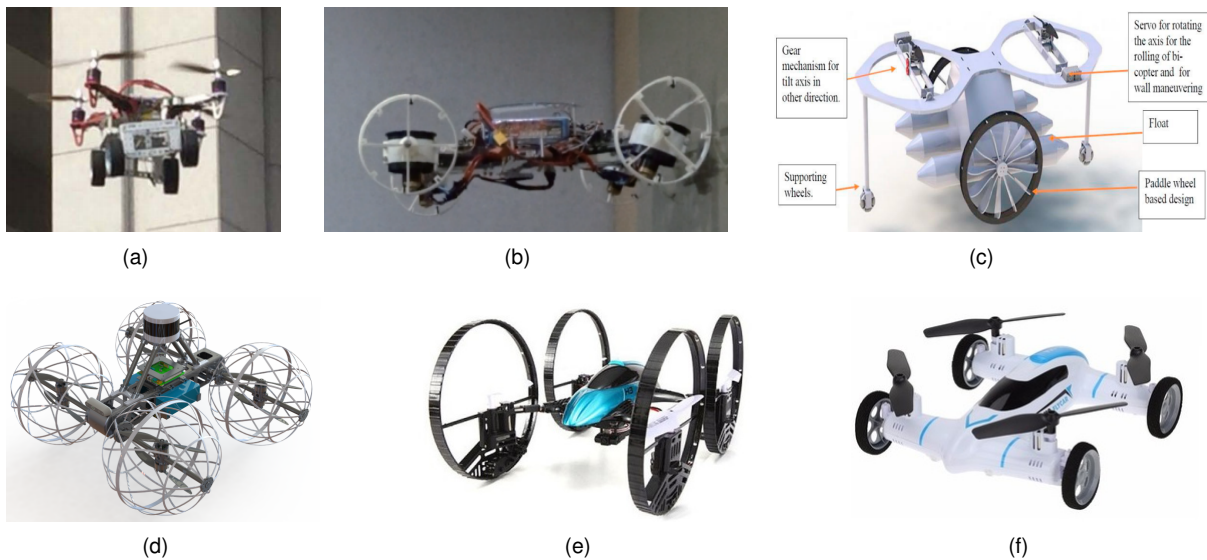
Figure 2.8: Four-wheeled active actuated MAVs: (a) [42] (b) Wall-climb quadrotor [35] (c) MTMUR [43] (d) Drivocopter [5] (e) JJRC H3 [46] (f) Syma X9 [47].

2.3.2 Passive Actuated Multi-modal MAVs

As explained at the beginning of this section (2.3), passive actuated multi-modal vehicles rely solely on the actuators used for flight to move on the ground. Most of the scientific work done in multi-modal rotary-wing MAVs rely on this approach, with many different types of vehicles available. Those vehicles can be further divided into caged, mono-wheeled, two-wheeled, four-wheeled, six-wheeled, and eight-wheeled vehicles, depending on their design.

2.3.2.1 Caged Vehicles

The first approach to multi-modal rotary-wing MAVs relied on rolling cage designs [37, 38, 48]. It is possible to consider that a vehicle uses a cage design when there is a cage-like structure surrounding the vehicle, providing additional protection for the propellers, and enabling the ground locomotion.

The first design that we are aware of, that used a cage for ground locomotion and not only for protection of the MAV was HyTAQ [37, 48] (figure 2.9(a)). In this MAV, two shafts are fixed to the quadrotor and extended from its sides, attaching the quadrotor to the rolling cage through two revolute joints, allowing the cage to roll freely with respect to the main quadrotor body [37, 48]. The total mass of HyTAQ is 570 g, with the cage weighing 120 g, which corresponds to 21.1% of the total mass of the MAV. Each one of its rotors is able to produce a maximum thrust of 3.3 N, consuming, on average, 70

W, corresponding to a total efficiency of 4.8 g/W at maximum thrust. Experiments with HyTAQ showed that the operating time of the multi-modal robot increased 5.4x when used in terrestrial mode when compared to the aerial mode and that the terrestrial range was about 4 times the flight range [37]. Due to problems in the capture of relevant system dynamics, the vehicle didn't perform as intended, being improved on [48], taking the drag into consideration. It was presented that the cage causes a slight increase (less than 10%) in the power consumption when compared with the MAV without cage [48]. It was also showed that, at velocities higher than 8 m/s, flying was more efficient than moving on the ground, at least on a carpet, linoleum, and turf [48]. For the aerial mode, the maximum range can be obtained at a pitch angle of 24º, with HyTAQ being able to travel 3.6 km with a fully charged battery while for the ground mode the maximum range of HyTAQ is 8.5 km when it moves at 3 m/s, and the pitch angle is maintained at 90º [48]. The operating range for ground mode is about 2.4x more than the aerial range [48]. HyTAQ, to the best of our knowledge, doesn't seem to offer any payload capacity.

One of the limitations of HyTAQ [37, 48] is related to its ground turning ability [26]. The two sides of the cage are connected through two revolute joints to the MAV, with the rolling cage rotating as a single component. This implies that the turning of the vehicle along the yaw axis on the ground is dependent on slip friction between the ground surface and the cage. This slip friction is higher than the rolling friction and is difficult to measure exactly [26]. Due to this, the control of the turning against the slip friction is a difficult problem to solve [26]. Another limitation is the cage shafts [26]. Due to the lightweight design of the shafts, they tend to easily break when the MAV falls to the ground or lands badly [26]. Rolling cage designs also impact the acquisition of data, since the visual sensors are obstructed by the cage [5, 26]. To overcome these limitations, a vehicle that relies on a cage with two independent rotating wheels is presented in [26] (figure 2.9(b)). In this design, a quadrotor is fixed to the cage through multiple supports and the wheels rotate around the cage of the MAV. The vehicle is designed and tested to reduce as much as possible its air resistance, in order to reduce the wind influences and interferences on its locomotion. It was demonstrated that the spokeless cage design reduced the air resistance by about 40% when compared with rolling cage designs [26]. The MAV has a total mass of 1.36 kg and was tested for inspection applications, namely bridge inspection. A comparison between the power consumption of the aerial and ground locomotion was not presented nor was the payload capacity of the MAV.

The other early example of a multi-modal MAV is MUWA [38] (figure 2.9(c)). MUWA is capable of air, land, and sea movement. It is designed as a quadrotor inside a styrofoam structure, being able of buoyancy. This styrofoam structure acts as a cage, enabling ground locomotion. Contrary to the previous mentioned MAVs which use fixed-pitch propellers, MUWA relies on variable-pitch propellers (also known as collective-pitch propellers). This feature makes the MUWA a high manoeuvrability vehicle, being able of sharp movements. The MAV is designed to be used in disaster scenarios. Cameras and/or sensors can be added depending on the application, being exemplified the use of the vehicle to perform 3D measurements of a room. Each propeller of MUWA is capable of producing 11.1 N of thrust, which means MUWA is able to produce a total thrust of 44.4 N. To the best of our knowledge, its MTOM is 2.1 kg. A comparison between the power requirements of the different modes of locomotion isn't presented.

PRSS UAV [49] (figure 2.9(d)) is a quadrotor mounted on a gimbal with three DoF, inside a spherical

structure, enabling it to move on the ground and protecting it from collisions. PRSS UAV was built around a commercially available MAV, with 1 kg and 2 kg MTOM [49]. The cage was designed to weigh 332g (not considering the gimbal), which corresponds to 18.1% of the total system weight. The only sensor that PRSS UAV included was a camera [49]. To the best of our knowledge, ground locomotion wasn't demonstrated nor are the power consumptions for the different modes known.

The first design of Rollocopter [50] (figure 2.9(e)) was based on a hexacopter surrounded by a spherical cage. The non-standard position of the rotors enabled the spherical cage to be easily propelled in any direction. To the best of our knowledge, this work was never implemented, being that the only data available is from simulations.

A special case of an aerial-ground MAV is the Cobot Shapeshifter [51, 52] (figure 2.9(f)). While a single Cobot is not able to move on the ground, two connected Cobots are. This is due to the fact that the Cobot Shapeshifter is surrounded by a cage similar to half a cylinder. When two Cobot Shapeshifters come together, the cage is similar to a full cylinder. Forward motion is based on the combination of the pitching momentum of both quadrotor MAVs and turning is based on the slippage of the cage, similar to HyTAQ [37, 48]. Due to this fact, the intended use case of Cobot Shapeshifter is for extra-terrestrial missions, where the drones roll together to a desired point to save energy and only fly to perform their mission at the desired place. Each Cobot weighs 0.8 kg and has a total thrust capacity of 32 N [51, 52]. Theoretical results showed that, for terrains other than consolidated soil and with slopes higher than 0°, flying was better than rolling with this configuration [51, 52].

(a)   (b)   (c)

(d)   (e)   (f)
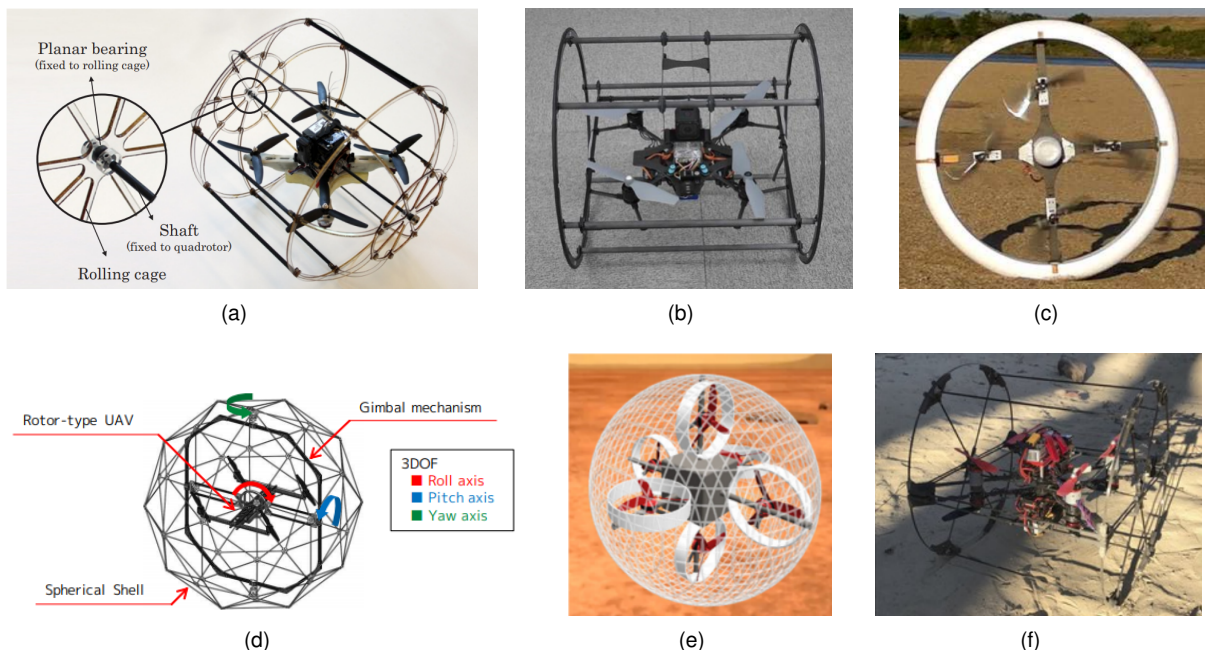
Figure 2.9: Caged passive actuated MAVs: (a) HyTAQ [37, 48] (b) Caged with passive wheels [26] (c) MUWA [38] (d) PRSS UAV [49] (e) Rollocopter [50] (f) Shapeshifter [51, 52].

2.3.2.2 Mono-wheeled Vehicles

Due to the added mass of the GAM on multi-modal MAVs, which impacts, negatively, their flight operating time [53], Qin et al. [44, 45] set up to design and implement a minimal viable GAM. Their MAV

is a bicopter and uses a single wheel for ground locomotion. Such design simplified the implementation and reduced the add-on weight, adding 20 g to the MAV, which corresponds to merely 1.03% of the MAV's mass, contributing to a lower impact on the flight operating time and to a lower flight power consumption. The vehicle weighs 1950 g, taking into consideration a payload of 500 g. The MAV consumes 454.5 W while flying. The use of a design with a single passive wheel implies that the vehicle requires active actuation while on the ground, having to keep its rotors spinning, consuming 176 W while rolling and 106 W while maintaining its still state. This corresponds to 61% and 77% less energy required, when compared to the required energy to fly, respectively. The difference in the power required between the rolling and still states comes from the energy needed to overcome friction. To the best of our knowledge, the MAV was only tested on a horizontal and planar surface.
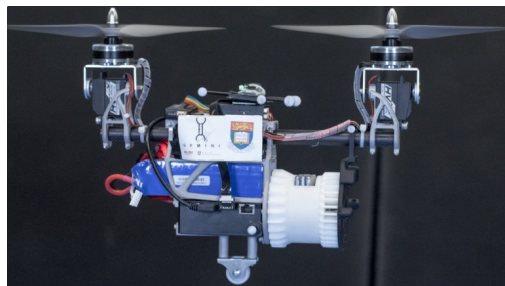
Figure 2.10: Gemini [44, 45].

2.3.2.3 Two-wheeled Vehicles

Another MAV that tried to overcome the limitations of HyTAQ [37, 48] was NINJA UAV (figure 2.11(a)), an air-ground-water multi-modal MAV, being a previous work of [26]. Similar to [43], the water locomotion is enabled by the wheel design, which resembles paddles. Unlike [26], it tries to solve the turning motion issues of a single connected cage, reduce the mass of the ground-water mechanism, and the obstruction of a camera by the cage, all with the same modification. Instead of using a rolling cage, NINJA UAV [54] uses two independent wheels, which are free to pitch, connected to the quadrotor by a shaft, which acts as a revolute joint. The design of the wheels can also be made in such a way that it protects the rotors of the quadrotor. NINJA UAV weighs 2.122 kg, including the mass of the wheels [54]. The capabilities of NINJA UAV were demonstrated by showing the MAV moving on water, on the ground, on the ceiling, and even climbing stairs. To the best of our knowledge, a comparison between the power consumptions of the aerial mode and ground mode is unavailable as is the payload of the MAV.

Another work from NASA's Jet Propulsion Laboratory for the DARPA Subterranean (SubT) Challenge is Rollocopter [36] (figure 2.11(b)). It consists of a quadrotor connected to two wheels, which can spin freely, through a shaft, which seems to be stronger than the shaft in other two-wheeled MAVs. In terms of sensors, Rollocopter is equipped with a LIDAR, an RGB-D camera, ToF sensors and wheel encoders [36]. The system weighs 4.231 kg, with the ground locomotion totalizing 500 g, which corresponds to 11.8% of the total system mass [36]. The vehicle has a maximum lift capacity of 62.5 N [36]. The system consumed 194.5 W while moving on the ground and 971.9 W while flying, which means that the system consumes only 20% of the energy required to fly [36] while moving on the ground. The authors still think that this value could be improved with the reduction of the rolling of the MAV during ground locomotion.

The authors have also approximated the total power consumption of the vehicle without wheels to be 650 W [36]. This means that for the hybrid aerial-ground configuration to compensate over the purely flying configuration, Rollocopter needs to move on the ground at least 41.4% of its operating time [36].

One of the first commercially available aerial-mode MAVs was Parrot Rolling Spider [55] (figure 2.11(c)). Similar to the rest of the two-wheeled passive vehicles, Parrot Rolling Spider is a quadrotor that has two small axles attached to it and to the wheels. The forward motion is based on the pitch of the quadrotor and the steering is based on a combination of rolling with yawing. The flight operating time of the MAV is, approximately, 9 minutes. The ground operating time is unknown as is its power consumption and its payload.

(a)   (b)   (c)
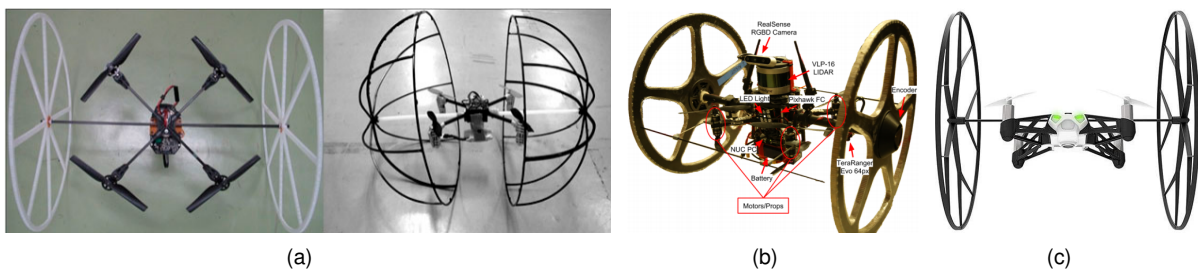
Figure 2.11: Two-wheeled passive actuated MAVs: (a) NINJA UAV [54] (b) Rollocopter [36] (c) Parrot Rolling Spider [55].

2.3.2.4 Four-wheeled Vehicles

One of the most different approaches to a passive actuated aerial-ground MAV is Flying STAR [56] (figure 2.12(a)). Flying STAR takes advantage of dual shaft motors to create the mechanism which enables it to move on the ground. By connecting the shaft of the motors to wheels, through gearboxes, it creates active wheels. The MAV was designed using two active wheels and 2 passive wheels. Although the MAV uses active wheels, we have considered this vehicle as being passive actuated since it uses the same actuators for flight and for ground locomotion. The only actuator which was added to the vehicle was a servo, which controls the sprawl mechanism. Since this servo doesn't actuate the wheels and only changes the height of the vehicle for and during the ground mode, we still consider this MAV as being passive actuated. The sprawl mechanism enables the drone to change its height, so it can pass through short passages. Most of the Flying STAR mechanical parts are 3D printed [56], which makes this MAV a very accessible one. The MAV weights 900 g and although it is referred it was designed taking into consideration the payload of sensors needed for search and rescue missions [56], this payload is unknown. Flying STAR is able to move on the ground on a multitude of surfaces, such as concrete, grass, and terrain [56]. Each rotor is able to produce, approximately, 3 N of lift, meaning that the total lift produced by Flying STAR is, approximately, 12 N. This value doesn't have a high enough SF for the vehicle to be able to operate in windy conditions. The active actuation of the wheels impacted the power consumption of the motors by 2.5% [56]. One disadvantage of this MAV is that in ground mode it cannot go faster than 2.82 m/s or it will start flying, due to the lift produced by the motors used to actuate the wheels. A comparison between the flight operating time and the ground operating time is not presented.

Similar in design to the wall-climbing MAV [35] presented in 2.3.1.4, that we mentioned that could implement a ground locomotion mode, there is Inkonova Tilt Scout [57]. Instead of using a servo to

actuate the wheels, Inkonova seems to use the rotors for ground propulsion, implementing a tilt-rotor mechanism. The MAV seems to use co-axial rotors, in a quadrotor configuration. It has a payload capacity of 300 g. It is unknown if this payload takes the cameras that are depicted in figure 2.12(b) into consideration. Due to the lack of information available, the power consumptions and operating times of the drone in both operating modes are unknown.

(a)   (b)

Figure 2.12: Four-wheeled passive actuated MAVs: (a) Flying STAR [56] (b) Inkonova Tilt Scout [57].

2.3.2.5 Six-wheeled Vehicles

To the best of our knowledge, the Quadroller [58] (figure 2.13) is the only example of a passive actuated multi-modal six-wheeled MAV. Quadroller uses an off-the-shelf quadrotor platform to which three sets of two passive wheels were added, to enable the motion on the ground. During ground locomotion, only two sets of wheels are in contact with the ground, with the other set of wheels enabling the vehicle to pitch forward or backwards to reverse the direction of travel [58]. The two sets of wheels in the furthest ends of the quadrotor (see figure 2.13) are free to rotate, enabling steering, similar to bogie steering. Ground driving uses the same control mixing used in flight without any alteration to the avionics. Quadroller weighs 1300 g and the GAM weighs 290 g, corresponding to 22.4% of the total vehicle mass. A comparison between the power consumption in flying mode and ground mode is provided and it shows that the average power consumption while moving on the ground is, approximately, 4 times lower than while flying, with the operating distance almost doubling, depending on the surface. The Quadroller was tested on different surfaces, including concrete, carpet, grass and gravel [58]. It can be concluded that for Quadroller, it is preferable to fly than move on grass. To the best of our knowledge, Quadroller didn't carry any sensor and its payload capacity is unknown.

Figure 2.13: Quadroller [58].

2.3.2.6 Eight-wheeled Vehicles

Although not really implementing an aerial-ground mode, as the previously mentioned MAVs, and not being the focus or the goal of the work, we need to refer the work of Kawasaki et al. [27] (figure 2.14(a)), which was one of the main inspirations for this thesis. In [27], a quadrotor with tilting rotors is designed and implemented. By having the front rotors connected to an axle and the rear rotors connected to another axle, the MAV is able to hover at any given pitch angle, as depicted in figure 2.14(b). This is an advantage for inspection applications, where the MAV can change its flight attitude in order to overcome obstacles, adapt itself to the shape of ducts and passages, or change its upward-facing side, meaning that sensors can be used downwards and upwards. This MAV uses eight passive wheels, which enables it to come into contact with walls and ceilings. Due to the wheel's design, it can only move on flat surfaces, which limits its application on ground mode. Since the ground locomotion is not a goal of the work presented in [27], a comparison between flight operating time and ground operating time isn't provided. The MAV weighs 2.5 kg and its payload is, approximately, 2.34 kg. Each rotor is able to produce 15 N of thrust while consuming 400 W, which corresponds to a maximum efficiency of 3.75 g/W.
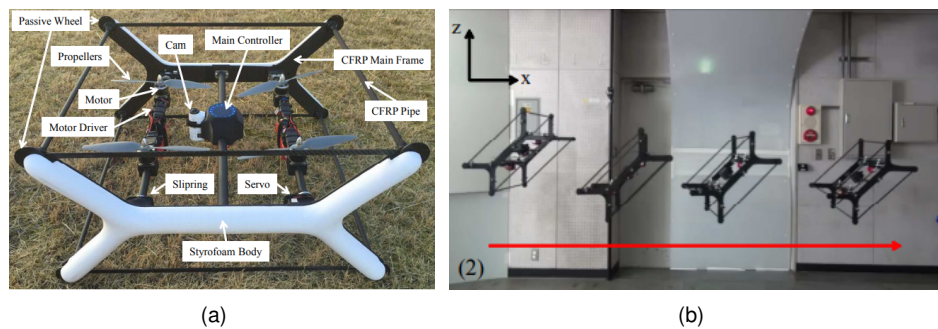
Figure 2.14: Eight-wheeled passive actuated MAV: (a) Bi^{2}Copter [27] (b) Bi^{2}Copter flying at any given pitch angle [27].

2.3.3 Comparison between Multi-modal MAVs

During this last section, multiple multi-modal MAVs have been presented as well as their characteristics and the results achieved during experiments with those vehicles. Table 2.2 summarizes what was presented throughout this section, depicting some of the vehicle's characteristics that are of interest for this work.

Analysing the designs of the reviewed multi-modal MAVs, it is possible to reach the following conclusions:

- From the passive actuated multi-modal MAVs analysed, it is possible to verify that there is a common approach to solve the passive actuated multi-modality problem. The design solution is to assemble the MAV in a structure that allows it to pitch, which couples the flight controller to the ground controller;

- Most of the reviewed MAVs can't be considered fit to be used in more than the designed use case since important details aren't specified (for example, the payload). This limits the use of the

platform by other operators other than its creators;

- To the best of our knowledge, many multi-modal MAVs aren't designed with any payload capacity. This heavily impacts the usability of the vehicle, since sensors can't be mounted on the platform;

- Most of the reviewed MAVs have a low thrust-to-weight ratio (T/W ratio) (lower than 1.5). This heavily impacts the usability of the vehicle, since perfect conditions were admitted for its design, with the MAV not being able to operate in windy conditions;

- By having a GAM, the ground operating time was increased by a minimum of 1.33x and by a maximum of 11.25x when compared with the flight operating time. This means that the MAV could be able to have a higher operating range or able to do a given task for a longer period of time (example of Pegasus [11], which is able to perform a surveillance up to 6h while perched);

- To the best of our knowledge, the problem of locomotion on inclined surfaces was rarely tackled by the previous work done in the multi-modal MAV area. In fact, only Shapeshifter [51, 52] explores the problem theoretically and NINJA UAV [54] experimentally, by demonstrating the capabilities of the vehicle to climb stairs;

- Gemini [44, 45] is the MAV with the lowest ground actuation mechanism (GAM)'s mass, corresponding to 1.03% of the vehicle's mass. Although this lower mass, Gemini requires active actuation while being static on flat surfaces, due to the mono-wheel design, requiring 0.6x the energy required while moving. Considering only designs that don't require actuation to be static on flat surfaces, the minimum mass added by the GAM corresponds to 11.8% of the vehicle's mass, by [36].

MAV	Main Use Case	Payload	MTOM	T/W Ratio	Type of Ground Actuation	Mass[1] in MTOM (%)	Ground Operating Time[2]
Pegasus [11]	Surveillance	NS[3]	NS	NS	Active	NS	NS
B-Unstoppable [39]	Hobby	NS	NS	NS	Active	NS	> 1.33x
[40]	NS	NS	946 g[4]	NS	Active	NS	NS
WAMORN [41]	Disaster Sites	NS	350 g	~1.06	Active	NS	NS
[42]	Crop Evaluation	NS	NS	NS	Active	NS	< 1.75x
[35]	Inspection	NS	NS	NS	Active	NS	NS
MTMUR [43]	NS	NS	1.5 kg[4]	~3.4	Active	NS	NS
Drivocopter [5]	DARPA SubT Challenge	850 g	5.1 kg	NS	Active	~17.6	~11.25x
JJRC H3 [46]	Hobby	NS	NS	NS	Active	NS	NS
Syma X9 [47]	Hobby	NS	NS	NS	Active	NS	NS
HyTAQ [37, 48]	NS	NS	570 g[4]	~2.36	Passive	NS	≲ 6x
[26]	Bridge Inspection	≥ 74 g	1.36 kg[4]	NS	Passive	NS	NS
MUWA [38]	Disaster Sites	NS	2.1 kg	~2.16	Passive	NS	NS
PRSS UAV [49]	Disaster Sites	≥ 76 g	2 kg	< 1.5	Passive	~33.2	NS
Rollocopter [50]	Space Exploration	NS	NS	NS	Passive	NS	NS
Shapeshifter [51, 52]	Space Exploration	NS	~800 g	~4.08	Passive	NS	NS[6]
Gemini [44, 45]	Confined Spaces	500 g	1.95 kg[4]	~1.28	Passive	~1.03	≲ 2.58x
NINJA UAV [54]	NS	NS	2.122 kg[4]	NS	Passive	NS	NS
Rollocopter [36]	NS	850 g[5]	4.231 kg	~1.47	Passive	~11.8	~5
Parrot Rolling Spider [55]	Hobby	NS	NS	NS	Passive	NS	NS
Flying STAR [56]	Confined Spaces	NS	900 g[4]	~1.36	Passive	NS	NS
Inkonova Tilt Scout [57]	Subterranean Inspection	300 g	NS	NS	Passive	NS	NS
Quadroller [58]	NS	NS	1.3 kg[4]	NS	Passive	~22.3	~2
Bi^{2}Copter [27]	Bridge Inspection	~2.34 kg	~4.84 kg	~1.26	Passive	NS	NS

[1] Ground mechanism   [2] Increase when compared to flight operating time   [3] Not Specified
[4] Unknown if it is higher   [5] Similar payload to [5]   [6] Presented theoretical operating ranges

Table 2.2: Characteristics of interest of the different analysed multi-modal rotary-wing MAVs.

Chapter 3

Theoretical Background

This chapter serves the purpose of presenting the basic concepts that enable the design of an aerial-ground MAV. It isn't supposed to be an extensive chapter and only a summary of the topics will be presented, following different information's sources, which will be cited throughout each section. This chapter is divided into three sections. The first section is relative to propellers and aerodynamic forces, enabling the optimization of the rotors and easing the selection process of the developed MAV's rotors. The second section is about quadrotors and their dynamics, since the developed vehicle will be of this type of multirotor. The third and last section refers to unicycle type systems, the same that the developed MAV presents for ground locomotion.

3.1 Rotor's Performance

A multirotor is a vehicle that generates its aerodynamic forces through the spinning blades of the rotors. To understand these aerodynamic forces, different approaches have been used, such as analytical theories, numerical modeling, and experimentation. Two main theories have been developed to evaluate helicopter rotor's performance, which can be used for multirotor rotor's performance evaluation: momentum theory and blade element theory. In this section, only an overview of momentum theory will be presented, giving a better understanding of the aerodynamic forces, and enabling the choice of propellers and motors (elements of the rotors) for the developed MAV. More specifically, it is of our interest to analyse the hovering flight and the performance of single and co-axial rotor systems, being that the other topics of these theories are out-of-scope of this work. A detailed description of the theories can be found in [53].

3.1.1 Momemtum Theory

Although momentum theory doesn't take into consideration complex vortex wake structures neither the local flow around the rotor's blades, which are responsible for a loss of 1% to 5% in the propeller's produced thrust (for well-designed propellers) [59], it allows for a first-order prediction of the thrust generated and power required for a given flight condition, laying out the physical principles that can be used in more elaborate analysis of rotor dynamics. A propeller accelerates incoming air particles, "throwing"

them towards its rear, and thus feeling a force on itself - the so-called thrust - according to Newton's Third Law of Motion. The first half of this acceleration takes place in front of the propeller, and the second half behind the propeller. This increase doesn't apply to pressure, meaning that a wake boundary is clearly defined. Due to the assumptions of momentum theory, in which the flow is assumed to be one dimensional, quasi-steady, incompressible and inviscid, the increased velocity of the airflow leads to a contraction of the stream passing through the rotor disk area, as depicted in figure 3.1.
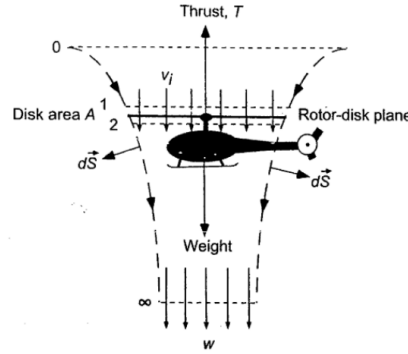
Figure 3.1: Flow model for momentum theory in hovering flight [53].

To estimate the performance of the rotor, we need to apply the Rankine-Froude momentum theory, which is simply the application of basic fluid mechanics principles to the rotor flow, depicted in figure 3.1. Equation 3.1, presents the application of the continuity equation (conservation of mass):

$$\iint_S \rho \overrightarrow{V} \cdot \partial \overrightarrow{S} = 0 \tag{3.1}$$

Where ρ is the density of the medium, $\overrightarrow{V}$ is the flow velocity, and $\partial \overrightarrow{S}$ is the unit vector normal to the control volume surface S.

In equation 3.2, the momentum principle is applied:

$$\iint_S p \cdot \partial \overrightarrow{S} + \iint_S \left(p \overrightarrow{V} \cdot \partial \overrightarrow{S} \right) \overrightarrow{V} = \overrightarrow{F} = -\overrightarrow{T} \tag{3.2}$$

Where p is the pressure, $\overrightarrow{F}$ the resultant force, and $\overrightarrow{T}$ the thrust produced by the rotor.

Finally, equation 3.3, presents the energy equation:

$$\iint_S \frac{1}{2} \left(p \overrightarrow{V} \cdot \partial \overrightarrow{S} \right) \left| \overrightarrow{V} \right|^2 = E \tag{3.3}$$

Where E is the work done on the fluid by the rotor.

3.1.1.1 Hovering Flight

During hovering, the vehicle has zero velocity (longitudinal, lateral and vertical), which means that the flow field is azimuthally axisymmetric.

Considering an unconstrained flow, the net pressure force on the control volume is zero. Therefore the net force, $\overrightarrow{F}$, is equal to the rate of change of fluid momentum across the surface, S.

24

Applying the previous presented equations to the hovering rotor case, several results can be derived. For the sake of simplicity and brevity, only the equations that matter for this work are presented next. A fully detailed analysis is given in [53].

The rotor thrust, T, and induced velocity, v_i, can be related as:

$$T = \dot{m}w = 2\dot{m}v_i = 2\rho A v_i^2 = \rho \frac{\pi}{2} D^2 v_i^2 \tag{3.4}$$

Where $\dot{m}$ is the mass flow rate, w is the inflow velocity at the fully developed wake (see figure 3.1), A is the rotor disk area and D is the diameter of the propeller.

The power P is given by:

$$P = Tv_i = T\sqrt{\frac{T}{2\rho A}} = \sqrt{\frac{T^3}{\rho \frac{\pi}{2} D^2}} \tag{3.5}$$

The efficiency of a propeller can be defined as the ratio of available power to the engine power which is described by:

$$\eta = \frac{P_{prop}}{P_{motor}} \tag{3.6}$$

The previous equation can be used to get a relation between the velocity and the efficiency of a rotor with a given power and diameter, which can't be solved analytically [59]:

$$v_i = \eta \cdot \left(\frac{2 \cdot P}{\pi \rho D^2 (1 - \eta)}\right)^{\frac{1}{3}} \tag{3.7}$$

Another way to affect the thrust, power and efficiency of a propeller is by changing its pitch angle and number of blades. This analysis is out-of-the-scope of this work but, as of interest, we can determine the relation between the power and number of blades of two fixed diameter, pitch and shape propellers as being:

$$P_2 = P_1 \frac{B_2}{B_1} \tag{3.8}$$

Where P_1 and B_1, and P_2 and B_2 are the power and number of blades of propeller 1 and 2, respectively.

Examining equation 3.4 we can determine that the thrust produced by a rotor increases when the diameter of the propeller increases or when the density of the medium increases. This influence of the density of the medium in the thrust produced by the rotor is what greatly influences the altitude that rotary-wing vehicles can reach. It is also possible to conclude that increasing the rotational velocity of a fixed size propeller, increases the thrust produced by the rotor. From equations 3.4, 3.5, and 3.8 it is possible to determine that the power required to turn a propeller depends directly on its number of blades and on its diameter, being an exponential relation. Another important conclusion, which can be derived from equations 3.5 and 3.7 is that to have the most efficient rotor for a specific application (most thrust produced while requiring the lowest possible amount of power), with a required given power, P, it is always mandatory to use the largest possible propeller diameter, which is limited by mechanical constraints and tip Mach number.

3.1.1.2 Co-axial Rotor Systems

In a co-axial rotor system, two counter-rotating rotors are assembled in an arrangement on the same axis. Co-axial rotors are used when there are mechanical constraints to the size of the propellers and the thrust required is unattainable with the constrained propeller size for a single rotor. We intend to demonstrate that this configuration comes at a cost, impacting negatively the efficiency of the rotors, due to the strong interaction between the rotor wakes. For a complete analysis, [53] should be consulted. The power required for a co-axial rotor system is given by:

$$P_{co-axial} = 2T(v_i)_{system} = \frac{(2T)^{\frac{3}{2}}}{\sqrt{2\rho A}}$$ (3.9)

While the power required for two non-interacting rotors is given by:

$$P_{2\_rotors} = \frac{2(T)^{\frac{3}{2}}}{\sqrt{2\rho A}}$$ (3.10)

Comparing the two power requirements as in equation 3.11, it is possible to conclude that a co-axial configuration requires 41.4% more energy than an identical system with two non-interacting rotors while producing the same thrust amount. Experiments have showed that this value is lower, corresponding to, approximately, 16% [53]. Due to this higher power requirement of co-axial rotors when compared to single rotors for the same produced thrust, the use of co-axial rotors requires an extensive study of the interaction between wakes in order to reduce this increase in power consumption as much as possible [60].

$$\frac{P_{co-axial} - P_{2rotors}}{P_{2rotors}} = \frac{\left(\frac{(2T)^{\frac{3}{2}}}{\sqrt{2\rho A}} - \frac{2(T)^{\frac{3}{2}}}{\sqrt{2\rho A}}\right)}{\frac{2(T)^{\frac{3}{2}}}{\sqrt{2\rho A}}} = 0.414$$ (3.11)

3.2 Quadrotors

In this section, a basic understanding of the multi-modal flying vehicle that will be developed, a quadrotor, is provided. The addition of a ground actuation mechanism only changes the mass and the moments of inertia of the developed MAV, being that its flying dynamics are equal to those of common quadrotors, which have already been explored and presented on multiple articles [61–64].

Quadrotors, commonly called quadcopters, are a subset of rotary-wing vehicles, with VTOL capabilities, that use four rotors, actuated independently, to control the position and attitude of the vehicle. Two of the rotors on the quadrotor rotate clockwise while the other two rotate counter-clockwise and each type is mounted on an opposite side of the quadrotor, as depicted in figure 3.2. The reason for such assembly is to cancel out the moment that each rotor creates while rotating, since a counter-clockwise rotating rotor is able to cancel out the moment of a clockwise rotating rotor, if both have the same shaped propeller (diameter, number of blades, pitch, etc, while being designed for different rotation directions), have the same motor, and are spinning with the exact same rotational velocity, making the quadrotor a very stable platform. Due to theirs characteristics, quadrotors are one of the best rotary-wing MAVs

[16, 44, 61], being widely used in inspection applications [3, 4, 6–8, 17, 27–34], as presented in section 2.2.
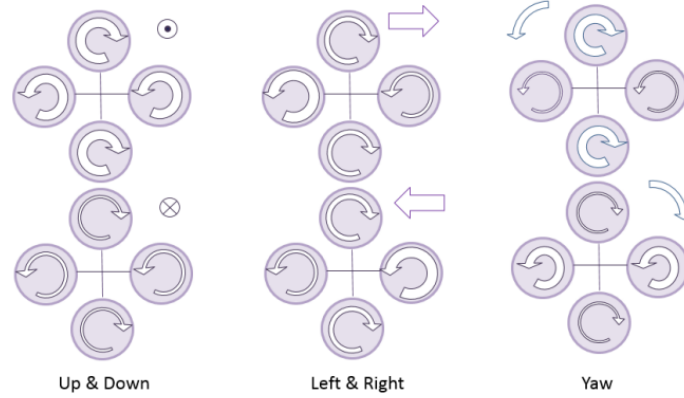
Figure 3.2: The quadrotor concept, demonstrating the required rotor actuation for the different locomotions. The width of the arrows is proportional to the rotors' angular speed [62].

3.2.1 Dynamics

To determine the equations of motion of quadrotors, Newton-Euler Equations are used. Two coordinate frames are defined, an inertial frame (or fixed to the environment), the so called Earth fixed or Inertial frame (represented by the letter E in figure 3.3) and the body-fixed coordinate frame, which is fixed to the quadrotor's body (represented by the letter B in figure 3.3).
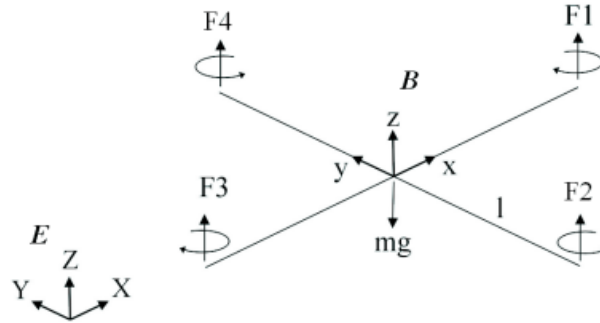
Figure 3.3: Usual coordinate frames used to derive the dynamics of quadrotors [61]. Earth fixed frame, body frame and thrust produced by the rotors represented by the letters E, B, and F, respectively.

Using these reference frames, the equations of motion for a quadrotor can be estimated:

$$m \cdot {}^{E}\ddot{\mathbf{r}}^{B^*} = -m\mathbf{g} + u_f\widehat{\mathbf{z}} - u_d \cdot \frac{{}^{E}\dot{\mathbf{r}}^{B^*}}{\left\|{}^{E}\ddot{\mathbf{r}}^{B^*}\right\|} \quad (3.12)$$

$$\mathbf{I}_{B^*}^{B} \cdot {}^{E}\dot{\boldsymbol{\omega}}^{B} = \begin{bmatrix} u_\phi \\ u_\theta \\ u_\psi \end{bmatrix} - {}^{E}\boldsymbol{\omega}^{B} \times \mathbf{I}_{B^*}^{B}\,{}^{E}\boldsymbol{\omega}^{B} \quad (3.13)$$

Where m is the vehicles' mass; B^* represents the frame in the center of mass (CoM) of the vehicle; ${}^{E}\mathbf{r}^{B^*}$ is the position vector from a fixed point in the earth fixed frame to the CoM of the vehicle; $\mathbf{g}$ is the gravity vector; u_f is the net force along the $\widehat{\mathbf{z}}$ axis; u_d is the magnitude of the drag force; $\mathbf{I}_{B^*}^{B}$ is the vehicle's moment of inertia about its CoM, along the $\widehat{\mathbf{x}}$, $\widehat{\mathbf{y}}$, and $\widehat{\mathbf{z}}$ axes; ${}^{E}\boldsymbol{\omega}^{B}$ is the Earth-observed rotational velocity of body frame, $\mathbf{B}$; ϕ, θ, and ψ are the Euler angles specifying the vehicle's attitude; u_ϕ, u_θ, and u_ψ are the propellers' induced moments along the $\widehat{\mathbf{x}}$, $\widehat{\mathbf{y}}$, and $\widehat{\mathbf{z}}$ axes, respectively.

3.2.2 Controller

Quadrotors are underactuated systems with six degrees of freedom and only four independent control inputs. Although many different types of approaches to the quadrotor's control problem exist, in this work we will be using one of the earliest control systems: a cascaded control architecture [65]. Cascaded feedback strategy is the most used one due to its practicality and simplicity [65], since it divides the system into two subsystems, completely decoupling the position and attitude control designs [66], simplifying the control problem. It uses a hierarchical control structure in which the attitude dynamics of the vehicle are designed as an inner loop to govern the position dynamics of the system [67]. A diagram of the flight controller that will be used on the developed MAV (implemented on the open-source autpilot firmware used) is presented in figure 3.4. In this controller, the outer loop (position controller) views the system 3.12 as a fully actuated point-mass system and produces a thrust controller. The inner loop is an attitude controller for the rotational subsystem 3.13, which orients the thrust of the vehicle to match the desired thrust assigned by the outer loop controller [66]. The feedback control of the inner loop runs with a higher frequency, around 5–10 times faster than the feedback control of the outer loop. On the open-source autopilot firmware used, the outer loop (position controller) is bypassed depending on the flight mode being used, the controllers are a mix of proportional (P) and proportional integral derivative (PID) controllers and an Extended Kalman Filter (EKF) is used to provide the required feedback (estimations).
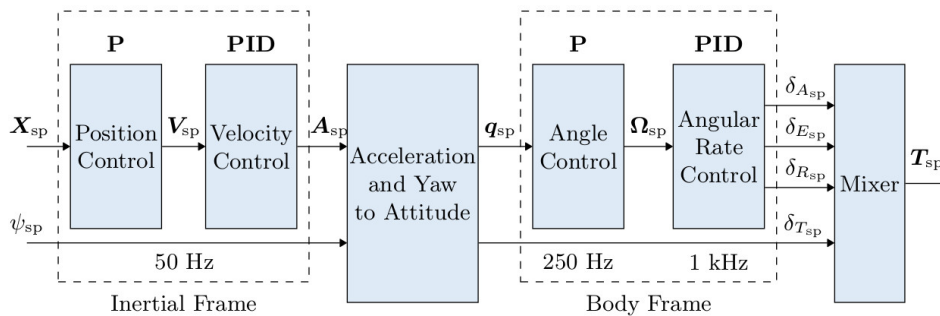
Figure 3.4: Diagram of the flight controller used [68].

3.3 Unicycle Type Robots

The purpose of this section is to provide a basic understanding of the dynamics that rule a unicycle type drive system. In this section, only the dynamic equations of a differential drive mobile robot (DDMR) will be derived (one of the types of unicyle robots). For a more complete analysis of the kinematics and dynamics of unicycle robots, [69–72] should be consulted. As of interest for this work, the dynamics of the differential drive system will be derived according to the Newton-Euler approach, which describes the system through the forces being applied to the body and its constraints.

3.3.1 Differential Drive Systems

Unicycle robots are actuated by two (identical) motors, attached to (identical) wheels, and located on each side of the vehicle platform (same distance to the CoM of the vehicle), enabling the longitudinal and lateral motion of the vehicle (figure 3.5). By changing the angular velocity of each wheel, it is possible

to change the direction and the velocity of the vehicle. For longitudinal motion, the two wheels should be rotating at the same velocity, while to turn, one of the wheels should spin faster than the other (for example, to rotate counter-clockwise, the right side wheel should spin faster than the left side wheel). An example of a unicycle vehicle turning, with this difference in the angular velocities of the wheels, is depicted in figure 3.5. Turn in place is also possible by having one of the wheels rotating forward and the other backwards.

Differential drive systems are a type of unicycle vehicle, where a third wheel is added for support, usually a caster wheel (figure 3.6). Although the developed MAV can't be classified as a differential drive system but as a skid-steer drive system (figure 3.7), the dynamics of both systems are identical [73]. For the derivation of the dynamics, the "caster wheel effect" will be ignored.
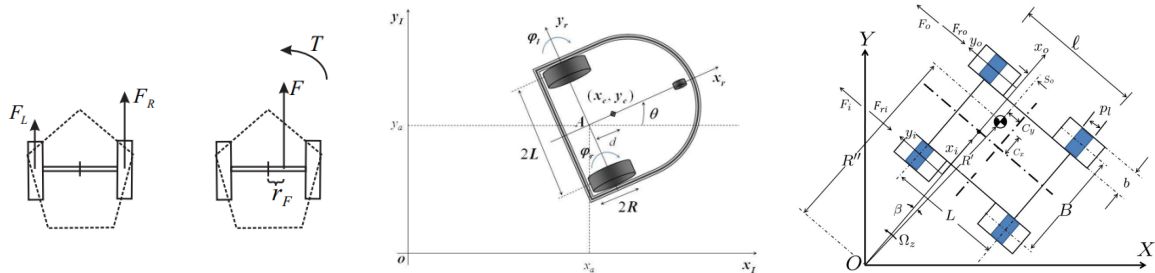
Figure 3.5: Unicycle showing forces acting on the wheels (left side) and resultant force, causing the vehicle to turn (right side) [74].

Figure 3.6: Differential Drive Mobile Robot [72].

Figure 3.7: Top view of a skid-steered vehicle performing a steady state turning maneuver, showing the forces acting on the platform [75].

3.3.1.1 Newton-Euler Dynamic Approach

Dynamics is the study of the motion of a mechanical system taking into consideration the different forces that affect its motion. It differs from kinematics, where the forces are not taken into consideration [72]. For this analysis, it is assumed that the DDMR is characterized by two non-holonomic constraints: there is no lateral slip motion and each wheel maintains one contact point with the ground [72]. Furthermore, the vehicle will be considered as one rigid body [72]. The Newton-Euler dynamic modelling presented follows [72]. The free body diagram of the system is presented in figure 3.8, with the forces acting on it represented and the notation following the body reference frame $\{x_r, y_r\}$.
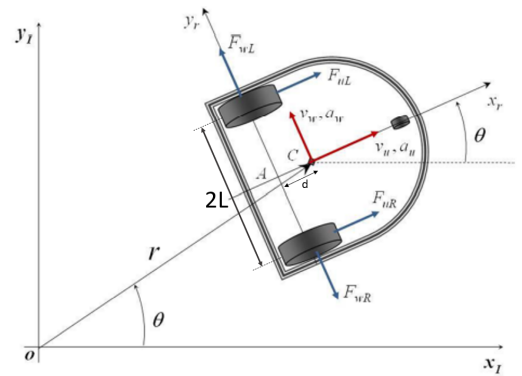
Figure 3.8: DDMR free body diagram for Newtonian dynamic modeling, with forces represented. Adapted from [72].

The notation v_u and v_w represents the velocity of the CoM, C, of the vehicle in its body frame with the subscript $_u$ and $_w$ meaning longitudinal and lateral, respectively; the acceleration of the vehicle in its CoM is represented by a_u and a_w; F_{u_R}, F_{w_R}, F_{u_L}, F_{w_L} are the forces exerted on the vehicle by the right and left wheels, respectively; θ is the orientation of the robot; ω represents the angular velocity; d corresponds to half the wheelbase; and L is half the trackwidth.

To start the modeling, the robot position in its inertial frame ($\{x_I, y_I\}$, in figure 3.8), r, is represented using polar coordinates:

$$\hat{r} = re^{j\theta} \tag{3.14}$$

Differentiating the above position vector (equation 3.14) in respect to time, it is possible to obtain the velocity and acceleration of the robot in its inertial frame [72]. The obtained equations, simplified and described in terms of the radial and tangential components are given by:

$$\dot{\hat{r}} = [\dot{r}]e^{j\theta} + [r\dot{\theta}]e^{j(\theta + \frac{\pi}{2})} \tag{3.15} \qquad \ddot{\hat{r}} = [\ddot{r} - \dot{r}\theta^2]e^{j\theta} + [2\dot{r}\dot{\theta} + r\ddot{\theta}]e^{j(\theta + \frac{\pi}{2})} \tag{3.16}$$

The longitudinal and lateral velocity and acceleration terms can be defined as:

$$v_u = \dot{r} \tag{3.17} \qquad\qquad v_w = r\dot{\theta} \tag{3.18}$$

$$a_u = \ddot{r} - \dot{r}\theta^2 = \dot{v_u} - v_w\dot{\theta} \tag{3.19} \qquad a_w = 2\dot{r}\dot{\theta} + r\ddot{\theta} = \dot{v_w} - v_u\dot{\theta} \tag{3.20}$$

Applying Newton's second law of motion, in the robot frame, we are able to find the relationship between the forces and accelerations. The DDMR exhibits two types of motion: translations in the radial and tangential directions, and rotation around the vertical axis at the CoM. Assuming that m is the total mass of the robot and representing the moment of inertia with respect to the CoM by I, the dynamic equations are defined as [72]:

$$ma_u = F_{u_R} + F_{u_L} \tag{3.21} \qquad\qquad ma_w = F_{w_L} - F_{w_R} \tag{3.22}$$

$$I\ddot{\theta} = (F_{u_R} - F_{u_L})L + (F_{w_R} - F_{w_L})d \tag{3.23}$$

Replacing the acceleration terms from equations 3.19 and 3.20 in the previous three equations, and, according to the assumptions of absence of slipping (pure rolling) in the longitudinal direction and no sliding in the lateral direction, we can determine the dynamic equations of the DDMR from equations 3.21, 3.22 and 3.23 [72]:

$$\dot{v_u} = d\dot{\theta}^2 + \frac{1}{m}(F_{u_R} + F_{u_L}) \tag{3.24}$$

$$\ddot{\theta} = \frac{L}{md^2 + I}(F_{u_R} - F_{u_L}) - \frac{mdv_u}{md^2 + I}\dot{\theta} \tag{3.25}$$

Chapter 4

Design

This chapter focuses on the design of a multi-modal MAV, more specifically, a passive actuated aerial-ground MAV. The design is influenced by the multi-modal MAVs reviewed in section 2.3, trying to take advantage of the different approaches to the aerial-ground problem and solving the issues identified in the inspection MAVs, in section 2.2. The design process will be presented, starting from the baseline requirements and including the estimation of an initial vehicle payload and mass, analysis and selection of the propellers, motors, and batteries, presentation of different vehicle concepts, mechanical design, and stress analysis of custom parts. In the end, the final prototype will be presented. In this chapter, we will also address some challenges that arise from the concept design.

4.1 Baseline and Requirements Specification

The main goal of this work is to develop a multi-modal aerial-ground platform, that can locomote in the air, and on flat and inclined surfaces, allowing long-endurance missions. Inspection is one example of the applications for this platform, but it can have many other applications such as surveillance or maintenance. Contrary to [42], the payload for both ground and aerial locomotion will be considered the same.

4.1.1 Baseline Specifications

Some baseline specifications were set previously to the start of this work. They are:

- The developed MAV should be able of VTOL and hovering, with a quadrotor being the selected platform, given its advantages over other multirotor's designs [16, 61];

- The MAV will make use of Li-po batteries, due to their advantages over other power sources [76, 77];

- The MAV size should be similar to that of commonly available quadrotors used for outdoor industrial applications. The well known DJI Flamewheel F450 [78] was used as the reference for the dimensions of the distance between the motor axis and for the maximum MAV span. The F450

31

frame [78] has a lateral motor axis distance of 322 mm and a diagonal motor axis distance of 455 mm, as represented in figure 4.1. To determine the maximum span for the developed MAV, the use of propeller guards was considered, limiting the span to a maximum value of 700 mm (propeller guards have a radius of 190 mm);

- The MAV should implement a passive actuated ground actuation mechanism (GAM);

- The MAV should be able to move on flat and inclined surfaces, and be able to fly;

- The autopilot unit should be a Pixhawk 1;

- A single autopilot unit should be used to implement the locomotion in air, and on flat and inclined surfaces;

- The developed MAV should have enough payload capacity to be able to carry the most usual sensors used in inspection applications.
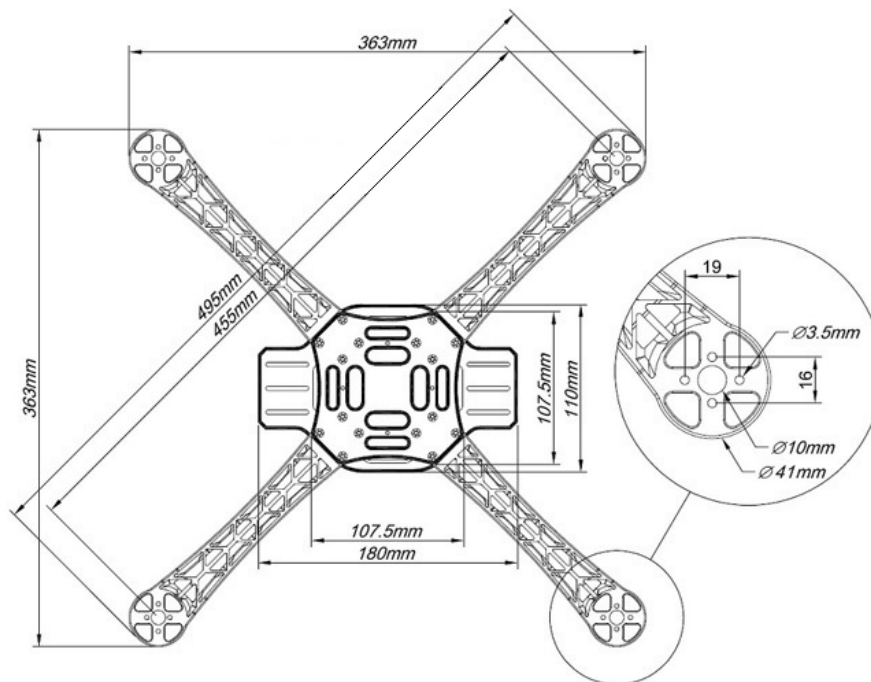
Figure 4.1: Dimensional drawing of the HJ450 frame, a copy of DJI FlameWheel F450 [78].

4.1.2 Requeriments Specification

From the literature reviewed on inspection rotary-wing MAVs, some requirements for the MAV were identified. They are:

- The MAV's mass should be as small as possible;

- The efficiency of the rotors should be as high as possible;

- The ground locomotion's efficiency should be as high as possible;

- The MAV should have a flight operating time of, at least, 10 minutes, with full payload.

4.2 Design Procedure

In any phase of the design of an aerial vehicle, the interdependency of components makes the choice of any component dependent on the choice of all other components and vice-versa [16]. This means that the design is an iterative process and only finishes once the design achieves all the requirements and objectives of the project.

A general method for the design of aerial vehicles can be formulated. The method is based on the assumption that the mass of an aerial vehicle is one of its most important design constraints. In fact, the mass of the vehicle is directly related to the required thrust. As analysed and demonstrated in section 3.1.1.1, the thrust is directly proportional to the size of the propellers. The power requirements of the rotors are directly proportional to the size of the propellers as is the total size of the vehicle (in our case, a quadrotor, which has four propellers). The power requirements influence the size of the batteries, which in turn influences the vehicle's mass. By explaining the importance of the mass constraint, we have just exemplified the interdependency of components.

The design process starts by defining three important design constraints for aerial vehicles: MTOM, the maximum span, s_{max} and the target T/W ratio, T_w. These three constraints are directly related to the application in which the vehicle will be used, so, this needs to be defined beforehand. Once these constraints are defined, it is possible to have a good idea of the required propeller diameter, D_{prop}, which ends up defining the total span of the vehicle [16]. Afterwards, the design can be divided into the selection of the propulsion system (propellers, motors, batteries, and motor controllers) and the mechanical design (design of the structure of the vehicle itself). A flowchart of the design method used throughout this chapter is presented in figure 4.2.
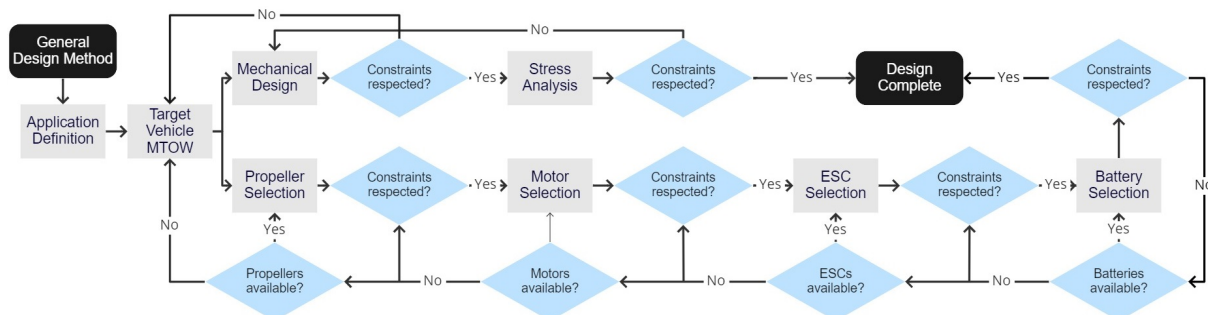
Figure 4.2: Design method flowchart.

4.3 Maximum Take-off Mass

As has been previously presented, one of the most important constraints in the design of an aerial vehicle is its MTOM. The mass of the aerial vehicle depends on its intended use case and can be divided into two categories, the mass associated with the payload (for example, sensors) and the vehicle's mass (mechanical structure, propulsion system, batteries, and any other required hardware, for example, the autopilot.

4.3.1 Payload

The payload is directly related to the application in which the aerial vehicle will be used. It corresponds to the extra mass, besides the vehicle's mass, that the vehicle is able to lift. For example, in transport applications, it usually refers to the maximum mass of the transported object while in inspection applications it corresponds to the mass of sensors and computational platforms required to perform a given task. The design starts by defining the use case for the vehicle, which defines the payload. As has been mentioned earlier in this chapter, in section 4.1, the use case for the developed MAV is inspection applications, with a focus on photovoltaic panels inspection. The literature reviewed in subsection 2.2.1, presented that, for such applications, the most used sensors are a combination of RGB cameras with thermal (IR) cameras. For inspection applications on enclosed spaces (pipelines, sewers, mines, etc), the use of LIDARs is also a must.

As presented in appendix A, namely in A.3, the maximum payload, taking into account the use of RGB and IR camera's sensors and a LIDAR, and including a SF, can be estimated to be 2 kg. This will be the design maximum payload for the developed MAV.

4.3.2 MAV Mass

The MAV's mass estimation is a difficult process since the mass of the vehicle, without any payload, depends on the selection of the propulsive system, which in turn can only be selected knowing the MTOM. Although several articles can be found on the design and optimization of aerial vehicles [76, 79–83], none of them relates the MAV's mass to its payload. To estimate an initial vehicle's mass, we looked at [79], more specifically, to the example of the Ascending Technologies Pelican (without any payload). Pelican has a total mass of 967 g and a payload capacity of 1 kg [79]. Since only a single example doesn't allow the extrapolation of a relation between payload and vehicle's mass, for this work, we also considered the relation in multi-modal MAVs whose payload was known. The relation between payload and vehicle's mass of Drivocopter [5], Rollocopter [36], and Bi^{2}Copter [27] were taken into consideration. In the case of Drivocopter, since it is an active actuated design and the developed MAV will be of passive actuation type, the vehicle's active ground actuation mechanism (GAM)'s mass was considered as being payload, with its payload capacity totalizing 1.75 kg. From these four examples, we can reach the following relation between payload and vehicle's mass:

$$0.967 \leq \frac{vehicle\,mass}{payload} \leq 4.08 \tag{4.1}$$

For the developed MAV, the vehicle's mass should be as low as possible, meaning its payload capacity is maximized. Given this, the relation between the vehicle's mass and the payload was assumed to be equal to one. This relation is similar to the value achieved by one of the designs that influenced this work, the design of Bi^{2}Copter, which achieved a relation of 1.07, and is higher than the value achieved for a uni-modal MAV, the Ascending Technologies Pelican, whose relation is 0.967.

Having the vehicle mass estimated, it is possible to estimate the mass of the different systems that compose the MAV [79]. This estimation is based on empirical data from the mass distribution of different real MAV systems. This distribution is reproduced in figure 4.3. The distribution mass of the developed

MAV is presented in table 4.1. It should be noted that these values are only estimations and are not fixed values, being that their purpose is to ease the design process. For example, the frame mass value is considered based on uni-modal quadrotors and not based on multi-modal quadrotors, being expected that the final value for the mass of the frame will be higher than the estimated one.
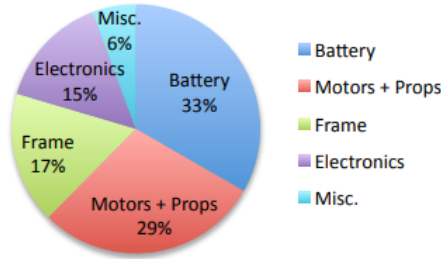
Figure 4.3: Average mass distribution for quadrotors [79].

Components	Mass (g)
Battery	660
Electronics	300
Frame	340
Motors + Propellers	580
Miscellaneous	120

Table 4.1: Estimation of the mass for the developed MAV, distributed throughout its systems.

4.4 Propulsion System Design

To proceed with the design of the propulsion system, according to the design procedure presented in section 4.2, having determined s_{max} to be 700 mm (one of the baseline specifications, subsection 4.1.1) and MTOM to be 4 kg (section 4.3), it is still necessary to determine one of the constraints, the target T/W ratio.

The T/W ratio dictates how the aerial vehicle behaves. A vehicle designed with a T_W lower than one won't be able to lift its MTOM, not being able to fly, and one designed with a T_W equal to one is only able to hover, given perfect conditions, not being able to ascend. It is possible to verify that a T_W value higher than one is required for a normal operation of an aerial vehicle. Usually, a minimum T_W value of two is used [37, 43, 81, 84]. This minimum value provides the ability for the aerial vehicle to respond to commands in certain windy conditions. Most MAVs don't operate in ideal conditions and the design with a safety factor (SF) is required to enable the MAV to perform, as expected, outdoors [43, 81, 84]. The T/W ratio is dependent on the use case of the aerial vehicle, since the application defines the conditions in which the vehicle will be operating. The use case of the developed MAV is intended to be inspection applications, being that high manoeuvrability is not a requirement. Given this, T_W will be constrained to its recommended value of two [37, 43, 81, 84] (for example, racing drones use a T/W ratio of more than seven [81]).

4.4.1 Propeller

The selection of a propeller for the developed MAV depends on three main factors: the propeller's maximum produced thrust, its efficiency and its diameter. Relatively to thrust, the developed MAV should be able to achieve a total thrust of $T_W * MTOM = 8$ kg. Being a quadrotor, this means that each rotor should be able to produce a thrust of $\frac{T_W * MTOM}{4} = 2$ kg. One of the requirements is to have the highest possible rotor efficiency. As was analysed in 3.1, to achieve that, the propeller diameter should be as large as possible. Due to design size constraints, the propeller maximum diameter is limited to 254 mm. A rule of thumb is that the efficiency of the rotor should be higher than 7 g/W (thrust per power required)

[84]. Following an iterative process to limit the number of available propellers, the efficiency value of 7 g/W was considered as being the minimum allowed efficiency for hovering while for the maximum thrust, the minimum acceptable value admitted was 4 g/W, although the optimal value admitted was 5 g/W. Still, taking efficiency into consideration, given the results in [44], the minimum propeller diameter was constrained to 228.6 mm. The selection process is also constrained by the fact that the propeller chosen needs to exist in both clockwise and anti-clockwise shapes, as required by a multirotor.

Due to the lack of propeller's performance data from most of the manufacturers, the propellers' selection was limited to APC [85], which makes available its simulated propeller data [86]. It should be noted that some of the propellers whose data is available in [86] are not available for purchase, that the data doesn't include three-blade propellers and that the real data may differ from the simulated data. Despite these disadvantages, this propeller database is the best tool for an initial propeller selection.

To analyse the propeller performance data, a script was created to automatically select the propellers that conformed to the constraints [87]. By constraining the characteristics of the propellers, it was possible to reduce the number of propellers to be analysed from 526 to 17. The data for the propellers to be analysed can be found in appendix B.1 and the propeller selection process from the constrained propeller database can be found in appendix B.2.

The propeller selected was the: APC 10x5E [88]. Two three-blade propellers were also taken into consideration, although performance data wasn't available for them: Dynam 10x7x3 and HQ Prop 10x6x3. The reason for taking into consideration these three-blade propellers is that, in theory, they are expected to produce the same thrust of a two-blade propeller with a diameter of 279.4 mm, according to equation 3.8. Besides, three-blade propellers present benefits for tilt rotor designs [89]. It was also taken into consideration the APC 10x7E [90], despite not being in the available APC data. The higher pitch from this propeller should enable it to produce a higher maximum thrust [91], with an impact on the responsiveness of the rotor (lower manoeuvrability), which, as mentioned previously, shouldn't impact significantly the performance of the MAV, given its use case.

4.4.2 Motor

With the propeller selected, the APC 10x5E, it is possible to find the motor that attains the best performance when assembled with it (creates the best rotor). Considering that each propeller weighs around 20 g, and given the mass distribution estimated in table 4.1, the motors' total mass should be 500 g, corresponding to a maximum individual motor mass of 125 g.

The motor selection process can be performed using readily available tools, such as Drive Calculator [92] or eCalc [93]. Unfortunately, eCalc requires a license to use the full version and the database from Drive Calculator seems to be very outdated. Although being outdated, Drive Calculator allowed to determine the manufacturers that had motors that corresponded to the required specifications and provided an overview of the motors' efficiency. A list of these manufacturers was created, which included AXi [94], BrotherHobby [95], Cobra [96], D-Power [97], Dualsky [98], Dymond [99], EMAX [100], Hacker [101], Plettenberg [102], Scorpion [103], Sunnysky [104], Racerstar [105], and T-Motor [106]. Their current in-production motors were analysed, looking for performance charts or simulating their perfor-

mance from their characteristics. From the analysed motors, five were selected, having performances that fulfilled the requirements. The selected motors and a summary of their characteristics of interest are presented in table 4.2.

Manufacturer	Dualsky	Racerstar	Sunnysky	T-Motor	
Model	ECO 2814C-V2 [107]	BR2814 [108]	X2814-III [109]	AS2814 [110]	AT2814 [111]
Rated Voltage (Lipo)	3-4s	3-4s	3-4s	3-4S	3-4S
Kv	970	1000	1000	1050	1050
Max Current (A)	33 @ 15s	NS [1]	55 @ 30s	49 @ 180s	50 @ 180s
Max Power (W)	400 @ 15s	NS	750	718 @ 180s	700 @ 180s
Diameter (mm)	35.2	36.4 [2]	35	36.2	35.2
Length (mm)	34.2	33.8 [2]	36	34 [2]	34 [2]
Weight (g)	105	106	113	112	107
Price (€)[3]	25.52	17.2	27.52	29.24	43

[1] Not Specified   [2] Measured   [2] Converted from $ to € using 1$ = 0.86€

Table 4.2: Characteristic's comparison between the identified motors.

The motor to be used in the developed MAV was selected taking into consideration three factors: availability, the existence of performance charts, and their efficiency in those performance charts, if available. At the time of selection, the Sunnysky motor was out of stock and the Racerstar motor didn't have any performance charts for propellers with a diameter of 254 mm, being excluded for these reasons, respectively. Despite the availability of performance charts for the Dualsky motor for a propeller with 254 mm, the APC 10x6E, these presented that the motor, for the required maximum thrust of 2 kg, has a maximum power requirement above the allowed 400W. This means that the motor could easily get damaged, due to overheating, causing malfunctioning, having been excluded for this reason. Between the T-Motor AS2814 and AT2814, as illustrated in appendix C the AT2814 is overall more efficient than the AS2814 for the same propeller. Despite the higher cost when compared with the AS2814 (more 13.76€), the increased efficiency would have a positive impact on the operating time of the vehicle (10% higher operating time, only due to the use of a more efficient motor, as demonstrated in appendix C), having a higher impact on the MAV over the increased price, when analysing the operation of the vehicle at the long term. The selected motor for the developed MAV was the T-Motor AT2814 1050kV.

4.4.3   Electronic Speed Controller (ESC)

ESCs are the electronic drivers of brushless motors, the selected motor type. They receive an electric signal, representing the motor throttle, and generate a tri-phase pulse width modulation (PWM) signal that drives the motor.

The selection of an ESC is based on three characteristics: maximum operating current, ESC's mass, and price. The selected ESC had also to respect three constraints: it should be controllable using a digital communication protocol, such as DShot [112, 113], its configuration should be a 4-in-1 esc (four ESCs in a single PCB, sharing the same characteristics) and the ESC should output a signal corresponding to the instantaneous current. The reasons for using a digital communication protocol is that these are less prone to be affected by noise, when compared to analog signals, such as PWM, and to have a protocol that uses error-detecting algorithms, such as CRC[1] [114], reducing even further the possibility of communication errors. Considering that motors can induce a lot of noise in the cable harnessing, we want to avoid as much as possible communication errors between the autopilot and the ESC. The reason for using a 4-in-1 ESC that is able to output a current signal, is to avoid the use of an extra PCB to measure the instantaneous current and avoid the use of extra harnessing to connect two single ESCs to the battery, which ends up weighing more than a single 4-in-1 ESC. The ideal solution for the developed MAV would be a 2-in-1 esc (two ESCs built on the same PCB), but, unfortunately, such solution doesn't exist for the required currents.

Looking at the motor specifications, we can determine that the ESC should be able to handle at peak, at least, 50 A. Online, readily available tables, such as [115], were used to compare the characteristics of different ESCs. From these resources, the selection of the ESC was simplified, with the Racerstar Air50 [116] being the selected ESC. This 4-in-1 ESC is able to handle 55 A continuously in each one of the individual ESCs (220 A for the 4-in-1 ESC), has a total mass of 12.1 g (without cabling) and is priced at 29.99 USD.

4.4.4 Propulsive System Battery

The selection of a battery is based on five parameters: voltage, capacity, discharge rate (depends on the selected rotor), total mass and price. The motor manufacturer provides testing data at, approximately, 15.5 V [111]. This voltage level is attained by a 4S Li-po battery, with four cells in series, having a nominal voltage[2] of 14.8 V. It is possible to determine the required battery capacity (in Ah) using equation 4.2, which relates the motor efficiency at the hovering thrust (in g/W), the hovering thrust (in g), the required hovering time (in seconds) and the nominal battery voltage (in V).

$$Ah = \frac{T_{hover}}{\eta_{hover} \cdot U_{nominal} \cdot \frac{3600}{t_{hover}}} \qquad (4.2) \qquad\qquad Ah = \frac{4000}{5.63 \cdot 14.8 \cdot \frac{60}{10}} = 8 \qquad (4.3)$$

Replacing the variables in equation 4.2 for the known values, we obtain a value of 8 Ah for the battery capacity (equation 4.3). It should be noted that the value for the efficiency at hover used was 5.63 g/W, which is the one provided by the manufacturer for a thrust of 1008 g [111], which corresponds to, approximately, 1/4 of the total required thrust at hovering.

Due to the configuration of the developed MAV, as will be presented in section 4.6, two equal batteries are used in the propulsive system. This means that each battery should have a capacity of 4 Ah. Having

---

[1]Cyclic Redundancy Check is an error-detecting algorithm commonly used in communication protocol to detect accidental changes to raw data.

[2]The battery nominal voltage corresponds to the voltage of a fully charged battery when delivering the current equivalent to its rated capacity at a specific discharge rate.

the capacity determined, we are able to estimate the required discharge rate (C)[3]. For example, a battery with a maximum discharge rate of 2C corresponds to a battery able to output a maximum current of $2 \cdot bat_{capacity}$ A. Analysing the motor data provided by the manufacturer [111], it is possible to determine that the maximum required current for two motors at full thrust is 79.66 A. This means that a required discharge rate of, at least, 20C ($79.66/4 = 20$, rounding to the unit) is required. Practically, a higher C-rating will be required in order to avoid battery's voltage sag.

The best battery for the developed MAV was selected through an analysis of the available offer from battery manufacturers and from hobby stores. The battery selected was the Gens Ace Bashing 4S 5000 mAh [117], due to having one of the highest specific energy densities (Wh/kg) among the analysed batteries ($\sim$ 187Wh/kg), meaning it is able to provide the highest operating time while impacting as less as possible the vehicle's total mass. Unfortunately, when the parts were ordered, this battery was out of stock, and a temporary replacement was chosen, ZOP Power 4S 3200 mAh [118], which should enable a flight operating time of eight minutes. In the future, the batteries should be replaced by the Gens Ace's ones, due to the fact that they are the ideal for the developed MAV, enabling a higher vehicle's operating time. A summary of the characteristics of these batteries is presented in table 4.3. It should also be noted that the mass of the ZOP Power battery is falsely advertised, with the battery weighing 16% more than what was specified (verified when the battery was received).

Manufacturer	Gens Ace [117]	ZOP Power [118]
Model	Bashing	–
Configuration	4S	4S
Capacity (Ah)	5	3.2
Discharge rate (C)	50	75
Weight (g)	395	302.2[1]
Price (€)	52.99 [2]	37.33

[1] Specified by manufacturer. Measured value was 355 g
[2] Shipping not included

Table 4.3: Characteristics of the selected batteries.

4.5 Electronics

This section describes the selection of the different components that compose the electronics of the developed MAV which aren't part of the propulsive system. It should be noted that the autopilot will not be presented in this section, since it is one of the baseline specifications of this work (subsection 4.1.1).

4.5.1 Servos

The developed MAV will implement single axis, tilt rotors, with two opposite rotating rotors mounted on the same tiltable axle, similarly to [27]. The reason for such design is explained further in this

---

[3]The battery discharge rate correlates the maximum current that the battery is able to output to its capacity.

document, on section 4.6. To control the position of two independent tiltable axles, two servos are required, one for each axle. This subsection explains how the servos were selected.

Servos are chosen based on four parameters: torque, rotational speed, mass, and price. For the developed vehicle, the servos were also constrained in the communication protocol, which should be digital, as with the case of the ESCs, in order to have a communication more resilient to noise. They should, also, be able of continuous rotation, being able to rotate 360º. Assuming there is no friction on the tilting mechanism, the torque of the servo should be higher than the gyroscopic moment created by the rotating propellers [43, 119, 120]. To determine the required servo torque, τ_s, equation 4.4 is used:

$$\tau_s = I_{rotor}\omega_s \left|\omega_{rotor_1} - \omega_{rotor_2}\right| \cos(\theta) \tag{4.4}$$

This equation differs from the equation presented in [120], for opposed lateral tilting, because in the developed vehicle's design the rotors will tilt in the same direction. It also differs from the equation presented in [43] because there are two rotors on the same axle instead of just one. As is presented in equation 4.4, the equation depends on four variables: the inertia of a single rotor, I_{rotor} (given by its I_{xx} component), the servo rotational speed, ω_s, the rotational speed of the propellers, ω_{rotor_1} and ω_{rotor_2} (clockwise and counter-clockwise rotation, respectively), and the tilt angle, θ. Analysing the equation, it is possible to determine that the required torque will have its maximum when the propellers are tilted at 0º [89, 121] (perpendicular to the ground) and when one of the motors is at full throttle and the other is stopped.

The desired maximum rotational velocity was stipulated to be of, at least, 30 revolutions per minute (RPM). This means that the servo would take two seconds to fully rotate 360º. To determine the value of the moment of inertia, the propeller was approximated by a solid cylinder, with an equal diameter and mass to the propeller, 254 mm and 20 g, respectively, and with a height of 10 mm, and was considered that the propeller was rotating 50 mm away from the tilt axis. The value of I_{rotor} was estimated to be 0.00021129 $kg \cdot m^2$, as presented in appendix D.3. The maximum rotational velocity of the propeller was assumed to be 12000 RPM, the same as the APC's simulated propeller value [86] and higher than the value given for the maximum motor RPM by the manufacturer performance charts [111]. The maximum servo torque required was determined to be 0.83 Nm, according to equation 4.5, for the previously mentioned situation which corresponds to the peak torque ($\theta = 0º$ and $\omega_{r_2} = 0$).

$$\tau_s = 2.11129 \cdot 10^{-4} \cdot \frac{2 \cdot \pi \cdot 30}{60} \cdot \frac{2 \cdot \pi \cdot 12000}{60} \cdot \cos(0°) \approx 0.83\,N \cdot m \tag{4.5}$$

Usually, servo data only presents the stall torque. A rule of thumb is to look for a servo with a stall torque with, at least, two times the required torque, in order to have a SF and to avoid the servo operation near its stall torque, which can lead to overheating, and to damage of both the servo's gears as its electronics. We looked for a servo that had a stall torque higher than 1.66 Nm and a rotational speed of, at least, 30 RPM. Table 4.4 summarizes the characteristics of the best servos that were found (many more servos corresponded to the characteristics, for example, from Robotis, so to be concise only the best result from each manufacturer is presented). From these servos, the selected was the Feetech STS3215 [122], due to having the lowest price, lowest mass, besides fulfilling all the required parameters.

Manufacturer	AXADD	Feetech RC	Robotis
Model	RW16W [123]	STS3215 [122]	XC430-W240-T [124]
No Load Speed (RPM)	125	52 @ 7.4 V	70
Stall Torque (Nm)	1.65	1.95 (0.5 cont.) @ 7.4 V	1.9
Stall Current (A)	NS [1]	2.5 @ 7.4 V	1.4 @ 12 V
Weight (g)	64	55	65
Price (€)	143.62[2][3][4]	24.89	93.65[3][4]

[1] Not Specified   [2] Unit price from manufacturer's quote for two units
[3] Converted from $ to € using 1$ = 0.86€   [4] Shipping not included

Table 4.4: Summary of the characteristics of some of the found servos.

4.5.2 Battery

Since two batteries will be used in the propulsive system, as mentioned in subsection 4.4.4, it was decided that an additional electronic's battery would be used. The reason for such decision was to avoid the use of bulky DC/DCs and also to avoid the introduction of motors' power noise into the electronics power lane, which would require the use of filters to reduce it. With the use of three batteries, there is a decoupling between the propulsive and the electronics systems (ground is common).

The electronics' battery should be able to supply all the electronics. This implies that it should be able to provide, at maximum, the stall current of two servos plus the current required by the autopilot, Pixhawk 1, the receiver, and any other extra electronics (such as the custom made PCBs, described in the next subsection). To achieve this power requirement, the battery should have a maximum discharge current of, at least, 6 A. This value already considers the use of a SF, since it isn't expected that the servos will be operating nowhere near their stall current. To be able to supply this current (6 A), it isn't necessary the use of a battery with high discharge rates. Given this, it was decided that Li-ion batteries would be used, due to their higher specific energy density when compared to Li-po batteries. Furthermore, it was decided that a 2S battery would be used, since the servos operate at this nominal voltage (7.4 V), meaning that it wouldn't be necessary to use additional DC/DCs to convert the battery's voltage to the servo's voltage. Due to the unavailability of Li-ion batteries in the hobby market, a custom made battery was created, built around two NCR18650B cells [125] and a two-cell 18650 holder, having a capacity of 3.25 Ah, a maximum discharge rate of 6.7 A and only weighing 120 g.

4.5.3 Custom Designed PCBs

The proposed design requires the use of three spatially separated batteries (two for the propulsive system and one for the electronics), which means there is a challenge in the monitoring of the instantaneous current and voltage levels of all batteries. The monitoring of the batteries is required not only to estimate the vehicle's power consumption but also to implement safety functionalities, protecting the

developed MAV from discharged cells, since the state of charge (SoC) can be estimated. Without these safety functionalities, the vehicle could crash, since measures to avoid it can't be implemented in a timely manner. The autopilot used, Pixhawk 1, only has five ADC ports easily usable: two in the "Power" connector, one in the "ADC 6.6V" connector, and two in the "ADC" connector. Having a vehicle that uses three separate batteries, it is desirable to keep track of six signals: three signals corresponding to the voltage levels and three signals for the instantaneous current being "pulled" from each battery. This amounts to one more signal than the available ADC pins. Furthermore, if these analog signals were analysed in the autopilot, the read values wouldn't correspond to the real values, due to the cable harnessing's losses (the propulsive system batteries are distanced by more than 600 mm from the autopilot) and the vulnerability of the analog signals to the noise caused by the motors and ESCs. To address both of these issues, we looked at smart batteries [126].

Smart batteries communicate through I^2C/TWI, implementing a digital protocol called SMBus [127]. This would allow multiple smart batteries to be connected to the same I^2C port available on the autopilot, given that each smart battery is assigned a different slave address. To address the challenge of using three distinct batteries and the issues of using the battery's analog signals, two PCBs were designed, which implement some of the specifications of smart batteries [126] and communicate through SMBus. These PCBs, SmartBat and SmartBat and Router, depicted in figures 4.4(b) and 4.4(c), respectively, report the individual cell voltages and instantaneous current through I^2C/TWI, analyse the SoC of the cells and actuate in case a cell is discharged (sound an alarm). Furthermore, the use of these PCBs plus another custom designed one, the Lateral Router, presented in figure 4.4(a), which acts as cable harnessing router, greatly simplifying the cable harnessing of the developed MAV.

| (a) | (b) | (c) |
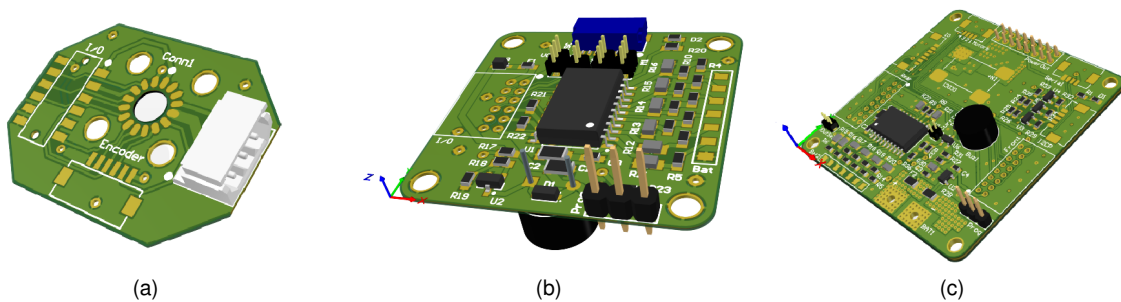
Figure 4.4: Custom designed PCBs: (a) Lateral Router (b) SmartBat (c) SmartBat and Router.

A complete description of the characteristics and capabilities of these custom made PCBs is presented in appendix E. It should be noted that the developed MAV was designed to use two Lateral Routers and SmartBats and one SmartBat and Router.

4.6 Mechanical Design

For an aerial-ground MAV design to be successful, the mass impact of the GAM should be as low as possible and its ground locomotion should be as efficient as possible. Usually, the GAM's lowest mass impact is achieved by passive actuated designs, since the ground locomotion is enabled by the same actuators used for flight, not being impacted by the mass of additional actuators as active actuated

designs are. On the other hand, active actuated designs are able to achieve a higher ground locomotion efficiency when compared to passive actuated designs. This can be justified by the commonly used design of passive actuated multi-modal MAVs, which implement a similar inefficient ground locomotion. Furthermore, it seems that the design of multi-modal MAVs only allows for one type of ground actuation, without the ability of a multi-modal MAV implementing an active or passive ground actuation depending on the application in which it will be used. The developed MAV implements a passive actuated design, due to the lower impact of the GAM's mass in the MTOM, but approaches the problem of the ground locomotion in a different manner to what has been commonly done, solving the ground locomotion's inefficiency problem of these passive actuated designs. Over this section, we will present and explain the inefficiency problem of the usual passive actuated multi-modal MAV design, define how the ground locomotion is enabled in order to have higher efficiency, and present the design decisions, final design and prototype.

Throughout this section, multiple terms that refer to components of the developed MAV will be used. Although the design is only presented in subsection 4.6.6, the components used and their naming are presented in appendix F.

4.6.1   Ground Locomotion

As has been presented in subsection 3.3.1, with the equations of motion for a DDMR (equations 3.24 and 3.25), for a vehicle to be able of longitudinal and lateral motion while on the ground, it needs to be able to produce two forces, F_{u_R} and F_{u_L}, on its right and left side, respectively. Additionally, these forces need to be distanced laterally and longitudinally from the vehicle's CoM by L and d, respectively, as depicted in figure 3.8. Considering a passive actuated multi-modal MAV design, in which there aren't any other actuators other than the ones used for flight (the rotors), a design that allows the rotors and their produced thrust to be responsible for the creation of these forces (F_{u_R} and F_{u_L}) needs to be developed. In fact, as presented in subsection 2.3.2, with the exception of [56], which uses dual shaft motors connected through gears to the wheels, all the reviewed passive actuated multi-modal MAVs use the propellers to drive the vehicle on the ground. This implies that, for the passive actuated multi-modal MAV to be able to move longitudinally and laterally on flat surfaces, a component of the rotors' produced thrust needs to be parallel to the surface where the vehicle moves. In the commonly used passive actuated multi-modal design, the production of these forces is allowed by the way that the MAV is assembled in its structure, allowing it to pitch forward or backwards. These structures are usually a rolling cage [37], more complex cage-like structures [26, 49] or an axle with two freely rotating wheels mounted on its ends [36, 54], with all, generally, sharing the same inefficient ground locomotion design. Usually, it is this pitch angle that allows the vehicle to move on the ground while using only its rotors for actuation. Figures 4.5 and 4.6 depict the usual design approach to passive actuated multi-modal MAVs moving on flat surfaces and on inclined forces, respectively, where θ and γ represent the pitch angle of the vehicle and the slope of the inclined surface, respectively.
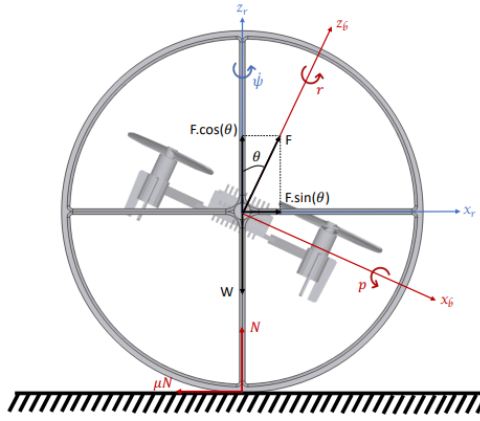
Figure 4.5: Usual approach to passive actuated aerial-ground MAVs moving on a flat surface with the forces represented [128].
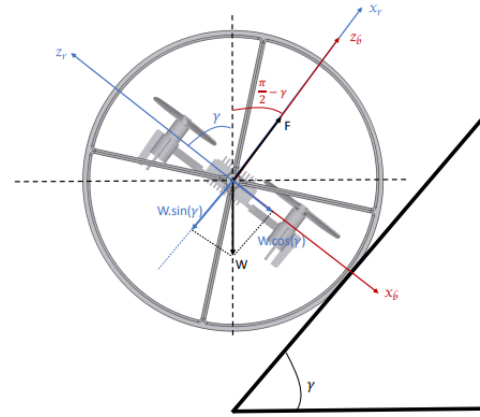
Figure 4.6: Usual approach to passive actuated aerial-ground MAVs moving on an inclined surface with the forces represented [128].

As represented in figure 4.5, the total thrust produced by the rotors can be decomposed into two components: one parallel and the other perpendicular to the surface where the vehicle moves, $T_{\parallel}$ and $T_{\perp}$, respectively. As presented by figure 4.5, $T_{\parallel}$ and $T_{\perp}$ can be determined by using equations 4.7 and 4.6, respectively, where F is the total amount of thrust produced by the rotors.

$$T_{\parallel} = F \sin\theta \qquad (4.6) \qquad\qquad T_{\perp} = F \cos\theta \qquad (4.7)$$

As can be observed from figure 4.5 and is concluded from the equations of motion of a DDMR (equations 3.24 and 3.25), only $T_{\parallel}$ is responsible for the longitudinal and lateral motion of the multimodal MAV on the ground, with $T_{\perp}$ counter-acting the gravity force and reducing the normal force. From these observations, it is possible to reach five conclusions:

- Assuming a constant total thrust being produced by the rotors, the ground speed that the vehicle is able to reach depends directly on its pitch angle. The higher the pitch angle, the higher $T_{\parallel}$ and the speed will be, having a maximum when θ = 90º;

- This conclusion is similar to the previous one, but for a constant pitch angle. The ground speed that the vehicle is able to reach depends directly on the total thrust being produced by the rotors. The higher the total thrust, the higher $T_{\parallel}$ and the speed will be;

- To achieve the highest possible ground locomotion efficiency and range, the MAV should move with a pitch angle of 90º. This conclusion is similar to the first one and was also demonstrated in the second work of HyTAQ [48]. The power consumed by a rotor is directly proportional to thrust by $P \propto T^{\frac{3}{2}}$, as presented in equation 3.5. At low pitch angles, most of the thrust is being wasted on lifting the vehicle, implying that the endurance will be reduced. To keep a given ground speed at this pitch angle, more energy will be required to increase $T_{\parallel}$ when compared with the vehicle moving with a higher pitch angle;

- This vertical component of thrust, $T_{\perp}$, can limit the usability of the vehicle on irregular, bumpy surfaces and on inclined surfaces, which, sometimes (from a certain slope angle), requires the creation of additional downforce, in order to avoid the vehicle flipping over;

- We can further expand the previous observations to the case of locomotion on an inclined surface,

as presented in figure 4.6. In this situation, to have the highest possible ground locomotion efficiency, requiring the maximization of $T_\parallel$, the quadrotor should move at a pitch angle equal to $90°$ minus the slope angle of the inclined surface, γ. This is only possible if the slope angle is known beforehand the locomotion on the inclined surface [128].

The five previous conclusions are closely related, being possible to determine an underlying factor: for a passive actuated multi-modal MAV to implement an efficient ground locomotion, $T_\parallel$ should be maximized and $T_\perp$ minimized. $T_\parallel$ and $T_\perp$ have their maximum and minimum, respectively, at the same pitch angle, $90°$ (only considering angles between $0°$ and $90°$). This implies that the MAV should move on flat surfaces with the rotors parallel to the ground's surface. Moving on inclined surfaces with the rotors parallel to the ground also enables the efficient locomotion without requiring the *a priori* knowledge of the surface's inclination, since $T_\parallel$ is always maximized. This requirement to achieve the highest possible ground locomotion's efficiency can be very difficult to implement in the commonly used passive actuated multi-modal MAV design, being that, to the best of our knowledge, none of the reviewed vehicles implements it nor moves nowhere near this $90°$ pitch angle on flat surfaces.

Given this requirement of the rotors being parallel to the ground's surface where the vehicles move, in order to have the efficient ground locomotion, the developed MAV will implement a dual bicopter design, similar to [27], with two rotors fixed in the same tiltable axle. This enables the vehicle to change the position of its rotors when entering the ground mode, changing them to be parallel with the ground's surface (tilted by $90°$), and use the usual $0°$ inclination position during flight, exhibiting the same behaviour that a usual quadrotor would. Besides, by enabling the rotors to tilt $360°$, the developed MAV should be able to hover and fly at any given pitch angle, similar to [27]. Furthermore, the tilting rotors should enable the vehicle to wall-climb [35] and could improve its flight efficiency [27, 48]. Both of these characteristics could extend the capabilities of the MAV for inspection applications, creating new possibilities for the use of the vehicle.

4.6.2 Wheels

The analysed passive actuated MAVs, in section 2.3.2, fall into three categories, based on the number of wheels in contact with the ground: one-wheeled (cage), two-wheeled, and four-wheeled. Most of the designs analysed use one or two wheels. This is due to the requirement that the MAV needs to tilt (pitch) in order to move on the ground. For a tilt-rotor design, such requirement doesn't impose and so, the developed MAV can use a four-wheel design, which is an inherently more stable design.

The wheel is one of the most important components of the developed MAV, since they are the main component of the ground actuation mechanism. Their design can influence the behaviour that the developed vehicle exhibits while moving on the ground. Different materials will behave differently in different terrains. The design of the wheels could, also, enable the developed MAV to move on water [43, 54]. The wheels should be dimensioned taking into consideration the structure of the vehicle, in order to create a cage-like structure around the propellers, enabling the vehicle to move near humans and structures. Taking into consideration the propeller diameter of 254 mm and considering that the propeller is offset by 50 mm from the tilt axis (SF included), it can be estimated that the tilting propeller

covers an area of 273 mm. Considering that the wheels are the only ones responsible for the cage-like structure, they should have a diameter of, at least, the area covered by the propellers, which corresponds to 273 mm. For the developed MAV, the cage-like structure was dimensioned to cover 325 mm, adding a SF to the distance from the propellers to the ground, enabling the vehicle to move on uneven terrains.

4.6.3 Motor Axis Distance

Although being one of the baseline specifications, the motor axis distance can influence the efficiency of the quadrotor's propulsive system and should be optimized for the MTOM of the vehicle [91, 129]. Usually, this optimization is performed using computational fluid dynamics (CFD) modelling, in order to estimate the best gap between the rotors [91, 129].

Rotor's efficiency is affected negatively when two rotors are too close because their flow affects each other, increasing their power consumption. On the other hand, a gap between the rotors larger than the required increases the vehicle's total mass, leading to a higher power consumption. To determine the relationship between the optimal gap, in mm, and the vehicle MTOM, in kg, the data provided by [91, 129] for a propeller with a pitch of six inches was used, giving an average result between the propeller with a pitch of five inches (the one being used) and a propeller with a pitch of seven inches (which, should, theoretically, produce a higher thrust than the five inches pitch's propeller). This relationship can be calculated using equation 4.8 (from [91, 129]) and it was determined to be 345 mm (rounded to the unit).

$$Optimal\ Gap\ (mm) = 3.1342 \cdot MTOM^2 + 3.1299 \cdot MTOM + 283.01 \tag{4.8}$$

4.6.4 Electronic's Base

The electronic's base is the place on the MAV that is designed to support all the payload (2 kg) and where all the sensors should be mounted. Its size and the location of the electronics mount tubes should be designed and dimensioned taking into consideration that the tilting propellers can collide with an obstacle up to 273 mm away from the tilting axis. This means that the payload can reach up to 220 mm in diameter, as depicted in figure 4.7 (not considering a mechanical structure that lifts the payload).
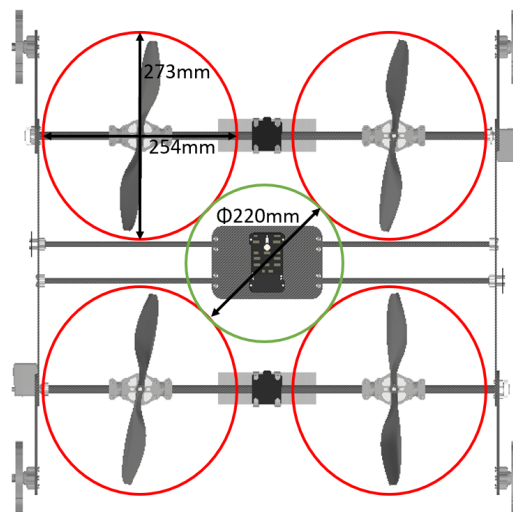
Figure 4.7: Top view of the developed MAV, with the space occupied by the rotors (represented in red) and the space designed for the payload (represented in green).

4.6.5 Materials

The developed MAV was designed taking into consideration the materials commonly used in aerial vehicles [130]. The selected materials were: ABS, used in the 3D printed parts; aluminium 6082, due to its low density, high strength, and easy machinability [130] (on a CNC router), being used for some of the custom parts; carbon fiber reinforced plastic (CFRP), which is lightweight for its strength, offering two to five times the rigidity of aluminium for the same weight, being a commonly used material in aerial vehicles [130]. CFRP's properties makes it the ideal material for the structural parts, being that its use tried to be maximized throughout the design.

4.6.6 Concepts

The final design of the developed MAV was the result of a progressive design evolution. The design process was performed using Autodesk Inventor Professional 2021 [131], which offers a free license for students. In total, three concepts were designed. Each one of the concepts is presented next, being that the final chosen design is presented in 4.6.6.3. The developed MAV was named BogieCopter, due to the resemblance of the different concepts with a bogie (in terms of exterior appearance).

4.6.6.1 BogieCopter 1

The first design created was BogieCopter 1. It started with the design of a simple tilt-rotor quadrotor to which wheels were added to each side of the tiltable motor's arm. Due to the total length of the tubes that support the wheels, a plate was connected between the wheels' support on each side. This was done to avoid the motors' arms easily bending. The final design of Concept 1, presented in figure 4.8, ended up being similar to [57]. The characteristics of Concept 1 can be found in table 4.5 (taken from the CAD model).

Concept 1 Characteristics	
Length (mm)	670
Width (mm)	700
Height (mm)	325
Weight (g)	~ 3055
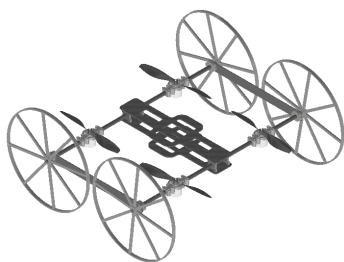
Figure 4.8: BogieCopter 1 design.   Table 4.5: BogieCopter 1 characteristics.

Analysing this concept, it was determined that it presented some advantages and disadvantages. The advantages that can be identified are:

- The wheels cover the propellers in all its 360º, measuring 325 mm in diameter;

- The MAV doesn't have a forward and a downward facing side. This allows the vehicle to fly with any side facing upwards (the motors' arms just need to be tilted in order for the rotors to face upwards). This can be advantageous for inspection applications [27];

- A single battery for the propulsive system can be used, without being required the use of the custom made PCBs, which were referred in subsection 4.5.3.

The disadvantages of this design were many:

- The dimension of the wheels make them unsuitable to be 3D printed locally, which means they would have to be custom made by a third party, driving the costs to an unviable price. It was tested a design where the wheels were printed in multiple parts, but they ended up not having the required strength;

- The need for a wheel support which is mounted on a tiltable axle makes the prototype's mechanical design complex and heavy;

- The side plates, which add resistance to bending, combined with the central plates of the quadrotor mainframe, increase the total mass of the vehicle;

- For the motor's arm to be able of 360° rotation, expensive and heavy slip rings are required, since they need to be able to handle high currents (each motor could require up to 50A) [27].

4.6.6.2 BogieCopter 2

BogieCopter 2 (figure 4.9) is an evolution of BogieCopter 1, which was influenced by the design of [27]. The main question that drove the design was: if the side plates were required, why not make them structural? This meant that the quadrotor's central plates could be changed for ones with lower strength and mass (the electronics mount). It also allowed the use of inexpensive and lightweight slip rings [27], that only need to be able to carry the ESC control signals and the signals for and from the custom made PCBs (small current signals).

This design has a smaller mass than Concept 1, weighing approximately, 5% less, while still being able to rotate the motors' arms 360° although requiring the use of the custom made PCBs. Figure 4.9 depicts Concept 2 and its characteristics can be found in table 4.6 (taken from the CAD model). This concept still didn't address the challenge of the wheels' diameter.
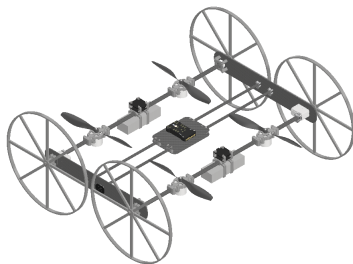
Figure 4.9: BogieCopter 2 design.

Concept 2 Characteristics	
Length (mm)	670
Width (mm)	764.8
Height (mm)	325
Weight (g)	2915

Table 4.6: BogieCopter 2 characteristics.

4.6.6.3 BogieCopter 3

BogieCopter 3 (figure 4.10) tries to solve the wheels' diameter challenge of the two previous concepts. By using smaller wheels, mass was saved (length of the wheel side plate and wheels' diameter were optimized for the assembly to have the lowest possible mass), corresponding to a reduction of,

approximately, 7%, when compared with BogieCopter 2. Also, by changing the position of the wheel supports it was possible to move the servos to the outside of the vehicle (comparing with BogieCopter 2, figure 4.9), allowing a reduction of, almost, 70 mm in the total vehicle width (10%).

The concept lost the advantage of the MAV not having an upwards facing side and the protection of the propellers all over its 360º (when propellers are tilted, they can hit an obstacle that is above them). Even with these disadvantages, BogieCopter 3 was the chosen design, being only referred to as BogieCopter from now on. It should be noted that this concept could be even further improved, with the use of custom-designed parts (for example, the servos could be moved inside the MAV structure), but this would contribute to a more complex design, that would not be as easily manufacturable and accessible to everyone (parts would have to be machined using Mills/Lathes).

Figure 4.10 presents the BogieCopter design and its characteristics can be found in table 4.7 (taken from the CAD model).
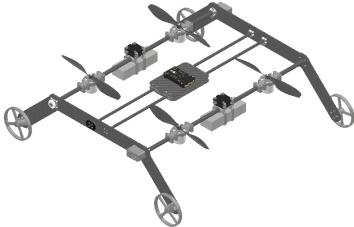
Figure 4.10: BogieCopter 3 design.

BogieCopter 3 Characteristics	
Length (mm)	695
Width (mm)	693.8
Height (mm)	198
Weight (g)	2715

Table 4.7: BogieCopter 3 Characteristics.

4.6.7 Design Verification

Before proceeding to the optimization and stress-strain analysis of the designed parts, both BogieCopter 2 and BogieCopter 3 concepts were analysed in a physics simulator environment, in order to verify that they were able of both aerial and ground locomotion. This would allow for the designs to be corrected if something wasn't working as intended.

4.6.8 Optimization and Stress Analysis

In order to minimize the mass of custom designed parts, to optimize them for the design load cases[4], and verify through simulations that the parts are able to handle the design load cases, an iterative process was used. An example of this process is presented in figure 4.11, in which BogieCopter's wheel support goes through the process, being composed by the following steps:

1. Initial design of the custom part;

2. Constraints and load cases set for the part;

3. Part topology optimization;

4. Redesign of the part based on the topology optimization result. Usually, the result is unpractical and, so, a redesign is made based on the resulted mesh;

5. Stress analysis of the redesigned part, in order to verify that it supports the load cases (should have a safety factor (SF) higher than 2).

---

[4]A design estimation of a set of loads and boundary conditions that the prototype will face.
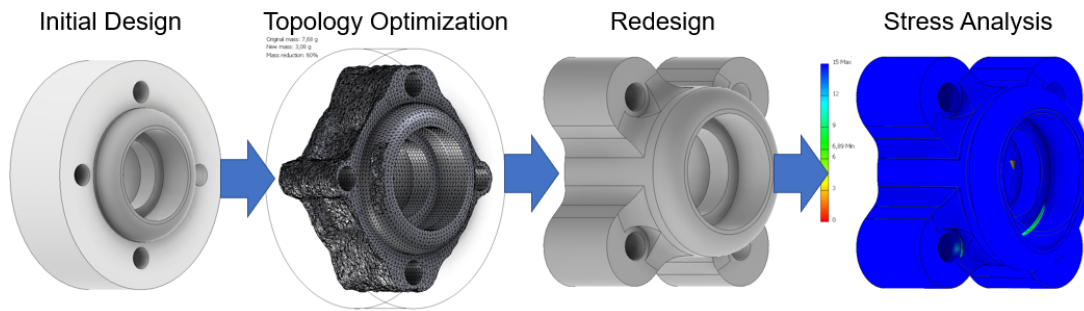
Figure 4.11: Optimization process throughout its different steps. Topology optimization achieved a mass reduction of 60% and the final part has a minimum SF of 6.89 and a 38% lower mass than the initial designed part.

From the stress analysis results, two parts were considered to be the most critical: the wheel shaft and the servo horn. To have the required SF, they should have been machined from aluminium. However, due to the requirement of having to use a lathe or a 4-axis CNC router to manufacture them, which wasn't possible for this work, they ended up being 3D printed.

The 3D printed parts went through yet another optimization process, where the parts were printed and tested afterwards, with real loads. 3D printed ABS parts don't have the same strength as an identical extruded ABS part, being that the obtained results from simulations are for extruded parts. With these real tests, some designs had to be changed (for example the motor supports' design). The 3D printed parts were printed in a Blocks One MK1 [132], with a layer height of 0.1 mm and a cubic infill. Their infill percentage changed depending on if the parts required additional strength or not. The wheel shafts and servo horns were printed using 100% infill and the rest of the 3D printed parts using 40% infill, since it would minimize their mass while still having the required strength.

The optimization of the CFRP parts took a different approach. From the start of the design, the number of parts built from carbon fibre tried to be maximized. This was to achieve the highest possible design strength, while taking its mass into consideration. The motors' arm tubes (CFRP tubes), electronic mount, electronic mount tubes and the structural side plates were designed from readily available CFRP tubes and plates. Carbon fibre is an anisotropic material, not being homogeneous neither isotropic [133], requiring a more complex optimization and stress analysis simulation than metals do, being out-of-scope of this work. To optimize the CFRP tubes, the parts were simulated as if they were manufactured from aluminium and [134] was used to determine the final tube's dimensions, allowing to size the CFRP tubes to have similar properties to those of the simulated aluminium tubes. The thicknesses of the structural plates were selected according to [135]. A thickness of 3 mm was chosen for the structural plates and 1 mm for the electronic mount.

Exploded views of the assemblies are presented in appendix F.

4.6.9 Mass Considerations

Some parts were custom designed and custom machined in aluminium to save mass. This wouldn't be possible without access to a CNC Router, which was free, allowing the parts machined to also be cheaper than off-the-shelf parts (their cost corresponds to the price of the mills and of the material used).

In total, four different parts were custom machined (appendix F presents the names and position of the components): the 6801 bearing support (two used in BogieCopter), the 8 mm clamping hub (four used), the 12 mm clamping hub (two used), and the 12 mm shaft collar (two used). In table 4.8, a comparison between off-the-shelf 8 mm clamping hubs and the custom-designed and machined is presented.

Manufacturer	RobotDigg	Servo City	–
Model	SHF8 [136]	8mm Clamping Hub [137]	Custom 8 mm Clamping Hub
Weight (g)	17.7	8	4.8
Price (€)	1.03[1][2]	6.02[1][2]	5.84[3]

[1] Shipping not included   [2] Converted from $ to € using 1$ = 0.86€
[3] Estimated from tooling and material required for all the custom parts. Includes shipping

Table 4.8: Comparison between available off-the-shelf 8mm clamping hubs and the custom made.

The difference in mass between the custom made and off-the-shelf parts is due to a dimensioning of the custom made part for BogieCopter's load cases, while the off-the-shelf parts are dimensioned for higher load cases. Although being machined in a CNC Router, these parts could be easily adapted to be manufactured by using commonly available tools. In total, the custom parts led to a reduction in mass of, approximately, 53 g, corresponding to, approximately, 2% of the vehicle's total mass. Besides, they also led to a cost reduction of almost 35%, when the cost is compared with the price of the lightest off-the-shelf parts. Although 2% being a small value, it does have an impact on the vehicle's operating time. Considering the efficiency at hover, it corresponds to less 9.4 W required.

The fastener elements were also analysed for an easy vehicle's mass reduction. In the design, the bolts and nuts used are manufactured from steel. However, they could be easily substituted with aluminium/titanium bolts and nuts, since they also offer the required strength, while having a lower mass. Unfortunately, aluminium bolts are not easy to come by (high order volumes required) and titanium bolts are too expensive. The same thing doesn't apply for aluminium nuts, with each M3 DIN 934 nut costing 0.05€, three times as much as a steel nut. The design uses 72 M3 DIN 934 nuts, eight M4 nuts, and eight M6 nuts. Replacing the steel nuts by aluminium ones, 34.7 g can be reduced without any impact in the strength of the MAV. This corresponds to a mass save of 1.3% and less 6.16 W required while hovering.

4.7   Prototype

A prototype was built according to the design of BogieCopter, being depicted in figure 4.12. With the exception of the custom machined and 3D printed parts, the rest of the custom made parts were manufactured using common tools. This includes the CFRP tubes and plates. Due to the required part's and assembly's accuracy, many cut moulds and assembly jigs were fabricated (3D printed), which allowed the parts to be shaped and the prototype assembled with the required accuracy. One of such

assembly jigs is depicted in figure 4.13, which allowed the battery supports to be mounted at the correct orientation and distance from the motors' supports. Figure 4.14 illustrates an overview of the hardware and the cable harnessing used in BogieCopter and table 4.9 presents the total cost of the prototype, divided by the different parts. It should be noted that the 3D printed parts (whose cost is lower than a 1 kg ABS filament roll), autopilot, receiver and transmitter, are not included in this table, since these components weren't bought.

Figure 4.12: BogieCopter's prototype.

Figure 4.13: Simple assembly jig fabricated to assemble the battery supports at the right orientation and distance from the motors support.
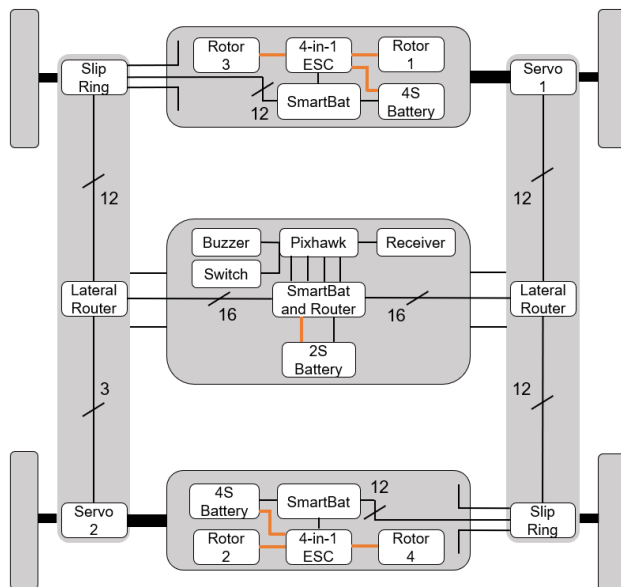
Figure 4.14: BogieCopter's hardware and cable harnessing overview.

Component	Price (€)
2S Battery	19
4S Batteries	74.65
3 mm CFRP plates	123.79[1]
8 mm CFRP tube	18.8
12 mm CFRP tube	35.38
8.5 mm Slip Rings	32.49
Aluminium - Custom Made Parts	32.73
Bearings (6801 and 686)	7.69
Custom Made PCBs	63.89
Fasteners (bolts, nuts and washers)	27.74
ESCs	51.6[2]
Motors	172[2,3]
Propellers	17.8[2]
Propeller Shaft Adapter 5 mm - 8 mm	6.6[2]
Servos	49.78
Tools (crimper, drills, mills, taps, etc)	86.2
Wiring	32.86
Total	853

[1] Enough for two prototypes
[2] Shipping not included
[3] Converted from $ to € using 1$ = 0.86€

Table 4.9: Overview of the prototype's cost.

Chapter 5

Software and Firmware

This chapter focuses on the coding elements of the developed work. It is divided into two sections, software and firmware. The software is relative to the development of a simulation model of BogieCopter 2 and BogieCopter while the firmware is relative to the autopilot code that had to be developed for BogieCopter to be able to fly and to move on flat and on inclined surfaces. In this chapter, developed code to measure power consumptions, in order to have an estimation of the performance of the MAV, is also, briefly, explained.

5.1   Software: Simulator

As mentioned in subsection 4.6.7, simulation models of BogieCopter 2 and BogieCopter were created to be used in RotorS Simulator [138]. This enabled the verification, in a simulation environment, that both concepts were able to fly and move on the ground. Besides, by having the simulation models of these concepts it is possible to develop them through simulations, providing a tool to test different controllers and algorithms.

RotorS [138] is a Robot Operating System (ROS) package, more specifically, a UAV simulator package that runs on top of Gazebo, providing models for some well-known quadrotors, different flight controllers and enabling the test of different path planning algorithms. Gazebo Simulator [139] is a physics engine that reproduces real-life rigid body dynamics and simulates realistic conditions. It enables the use of sensors on a robot, providing realistic feedback to controllers and algorithms, and the simulation of conditions such as wind, waves, friction, etc.
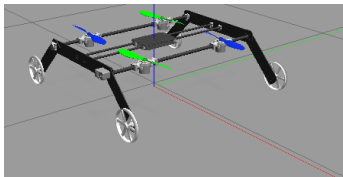
Figure 5.1: RotorS BogieCopter model static on the ground in the Gazebo environment.
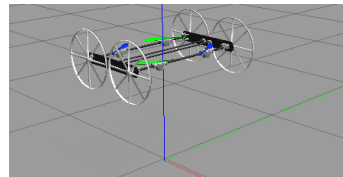
Figure 5.2: RotorS BogieCopter 2 model hovering in the Gazebo environment.

Figures 5.1 and 5.2 show BogieCopter model on the ground and Bogiecopter 2 model hovering, in the Gazebo environment, respectively, running ROS.

5.2 Autopilot Firmware

For the development of this work, it was decided that the capabilities of an existent open-source autopilot firmware would be extended, enabling the developed MAV to both fly as well as to move on flat and inclined surfaces. Since the autopilot hardware used in BogieCopter is a Pixhawk 1, to the best of our knowledge, this limited the firmware to ArduPilot [140] and PX4 [141], which are very similar in terms of capabilities. Between these two, ArduPilot was selected as the starting autopilot firmware, since it is more mature (older), has continuous development since it was created, has a bigger support community than PX4, it is able to run on multiple autopilots, enabling the used autopilot to be easily changed by another (compatible) one, and has demonstrated its capabilities through multiple usual and unusual configurations [142].

ArduPilot firmware is divided by the vehicle type, being that only one type is able to run on the autopilot at a time. This implies that the autopilot firmware needs to be chosen from the available types: AntennaTracker [143] (antenna), ArduCopter [144] (multirotor), ArduPlane [145] (fixed-wing vehicles), ArduRover [146] (ground vehicles and boats) and ArduSub [147] (under-water vehicles). Since the developed platform will behave as a quadrotor during flight, ArduCopter was chosen as the starting firmware for the development of the code.

During the development of this work, Copter-4.0.7 [148] was the latest stable release, being that Copter-4.1.0 was on the initial beta testing phase [149]. Due to its stability, the developed code extends the capabilities of Copter-4.0.7, from now on referred to as, simply, Copter.

Using Copter meant that multiple modifications had to be made to the firmware, including: minor change to the flight code, and the addition of custom made code for the control of the servos, for the battery monitoring from the custom made PCBs, and for the locomotion in flat and inclined surfaces. These three last modifications are presented next.

5.2.1 Servo Firmware

The selected servos, Feetech STS3215 [122], are interfaced through a serial communication protocol identical to the DYNAMIXEL Protocol 1.0 [150]. To enable the interface between Copter, the Pixhawk 1 and the servos, custom code had to be created since Copter doesn't have already this communication protocol implemented. A repository with this code can be found in [151]. The new code was implemented in a new library, named AP_TTLServo, given that the servo's communication protocol is implemented through a TTL interface).

For an easy modification of the used settings and to allow the code to be open to multiple servos that use this communication protocol, several parameters were added, which allow the modification of the parameters without the need to upload a new code to the autopilot.

5.2.2 Battery Monitor Firmware

As mentioned in subsection 4.5.3, one of the challenges that arose from the use of Pixhawk 1 with three batteries was the need to implement battery monitoring that didn't use analog signals. To achieve

just that, three custom PCBs were used, which communicate over I^2C/TWI, implementing a simplified version of smart batteries' specifications [126]. Unfortunately, Copter isn't prepared to have multiple SMBus [127] devices connected, given that it only accepts one device with address (in hexadecimal) 0x0B and in the internal I^2C/TWI bus. To enable the use of multiple I^2C/TWI devices (considering each one has a unique address) and to use the external I^2C/TWI bus (the one available in the Pixhawk I^2C connector), custom code had to be developed. The code created can be found in [152]. Two additional parameters were added to Copter in order to allow the change of the settings without the need to upload new firmware to the board.

5.2.3 Ground Mode Firmware

All the code to enable the locomotion on flat and inclined surfaces had to be custom coded into Copter, since, to the best of our knowledge, nothing similar exists on available autopilot firmwares. This subsection explains the principles behind the ground mode, which enable the MAV to move on flat surfaces and inclined surfaces, and also tackles the problem of locomotion with full payload on high inclination surfaces.

5.2.3.1 Locomotion on Flat Surfaces

The basic principle behind the ground locomotion is that, by having the rotors tilted perpendicular to the surface where the vehicle moves, BogieCopter dynamics are similar to those of a skid-steer ground vehicle. This has already been explained in subsection 4.6.1 and the dynamics for a skid-steer drive system have been determined in 3.3.1.1. Given that the developed MAV is able to create forces distanced from the vehicle's CoM, it is able of longitudinal and lateral motion, being able to move forward, backwards, turn in place (or turn when moving) and brake. For BogieCopter to be able to move forward and brake implies that it is able to accelerate and decelerate or, in other words, it is able to produce forces in opposite directions. If the rotors of the vehicle are tilted in the same direction, this could be easily achieved by changing the direction in which the rotors are spinning, if the same amount of thrust was produced but in opposite direction. Unfortunately, the airfoil of the used propellers is designed in such a way that, when spinning in opposite direction to the designed one, the propellers don't produce anywhere near the thrust they produce when spinning in the designed direction. From this observation, it is possible to reach the conclusion that, to create forces with opposite directions, the forward and the backward rotors should tilt in opposite directions when entering ground mode. Due to the symmetric design of BogieCopter, this means that the servos should tilt in the same direction so that the rotors tilt in opposite directions, as demonstrated in figure 5.3, where θ_A is the tilting angle of the motor's arm; θ_s the tilting angle of the servos, being the absolute value of both values equal; x_B, y_B and z_B are the axis of the body coordinate frame; x_s, y_s and z_s are the axis of the servo coordinate frame. To add some additional protection to the propellers, it was decided that the rotors would tilt $90°$ inwards the MAV structure. Figure 5.4 depicts BogieCopter with the rotors tilted and with the thrust represented, where T is the thrust produced by each one of the rotors, being that the subscript corresponds to the number of

the rotor according to [153].
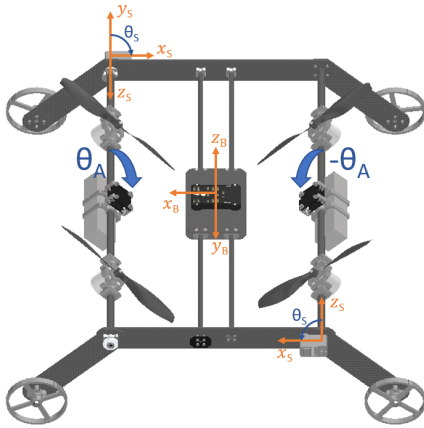
Figure 5.3: BogieCopter tilting the rotors, entering ground mode. Note that the rotors rotate in opposite directions but the servos in the same direction.
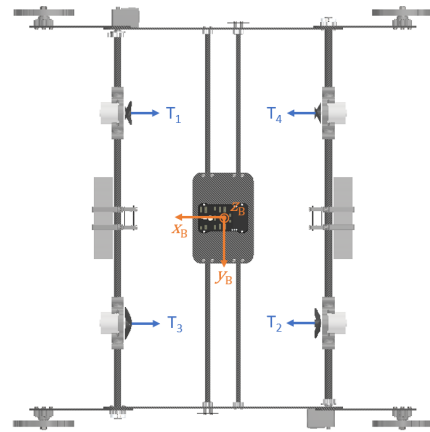
Figure 5.4: Top view of the developed MAV in ground mode, with the rotors tilted inwards the vehicle structure. Forces produced by each one of the rotors represented (rotor numbering follows [153] for a H-shaped vehicle).

From figure 5.4, we can easily understand that the values of F_{u_R} and F_{u_L}, from equations 3.24 and 3.25, are given by the resultant force between T_1 and T_4, and between T_2 and T_3, respectively. Simplifying, on the ground, for the MAV to move forwards (along x_B), T_2 and T_4 should be actuated with the same throttle (which correlates to the propeller's rotational velocity and produced thrust) and should be bigger than the throttle of T_1 and T_3, while to move backwards, T_1 and T_3 should be the rotors actuated. To turn clockwise or counter-clockwise, T_1 and T_2 or T_3 and T_4 should be actuated, respectively. From this observation, we can reach another two conclusions. To have an efficient ground locomotion, when the MAV is moving on a straight line, only a set of rotors should be actuated, T_1 and T_4, or T_2 and T_4, and to brake, only the opposite set of rotors from the ones being used for the locomotion should be actuated.

For BogieCopter to start moving on flat surfaces, assuming perfect conditions, a force higher than the rolling resistance of the wheels plus of the bearings needs to be produced by the rotors. The coefficient of rolling friction for both components is very small [154, 155], as is the total rolling resistance. From this observation, we can determine that, for BogieCopter to start moving, very little thrust needs to be produced. This implies that, for most applications, the thrust during longitudinal motion should be limited, to give better control over BogieCopter. A parameter was added to enable the easy setting of this limit. Although for forward/backwards motion, a high thrust value may not be considered desirable, for braking it is. The braking should be as fast as possible and for that, a high amount of thrust is required momentarily. To detect a brake command, a state machine was created, which detects when the last command was to move in one direction and the current is to move on the opposite, limiting the throttle, momentarily, to another value. These two values, braking throttle limit and braking timer value, can also be set by the operator, in two parameters.

5.2.3.2 Locomotion on Inclined Surfaces

The locomotion on inclined surfaces can be divided into three different categories, depending on the slope of the surface: low slopes, medium slopes, and high slopes. Slopes up to an inclination of $45°$ will be considered low slopes, since the component of the weight parallel to the surface will be lower than 0.707x the weight. High slopes are the ones that require extra downforce, in order to avoid the possibility of the MAV flipping over (walls, for example). It was estimated from the CAD model that the flip-over of the vehicle occurs above $60.9°$, not having been tested experimentally. Slopes between $45°$ and $60.9°$ are considered medium slopes.

To move on low slopes, the required throttle needs to be higher than that used to move on flat surfaces, due to the existence of a component of the gravity force, which acts contrary to thrust, as demonstrated in figure 5.5 (where θ is the inclination of the surface, W is the weight of the MAV, and T is the thrust produced by the rotors). Besides, from a minimum angle, that can be set by the operator, BogieCopter doesn't require the use of the braking with a higher throttle than the throttle limit set for flat surface locomotion, since the gravity will assist in the braking, decelerating the vehicle by itself if no thrust is produced to propel the vehicle forward. From these two observations, a feature was implemented, in which BogieCopter automatically detects the slope angle, adjusts the throttle limits accordingly and disables the braking (this is only possible due to the MAV's design). Three new parameters were added to the code to enable these functions. Besides the additional functionality, the lateral locomotion on low slopes is equal to that on flat surfaces. It should be noted that, although the MAV will be able to climb medium slopes with only these modifications, new functionalities were added, in order to increase the factor of safety (FoS) of the thrust that the vehicle is able to produce while climbing slopes, guaranteeing it is able to climb any slope, with the designed payload.
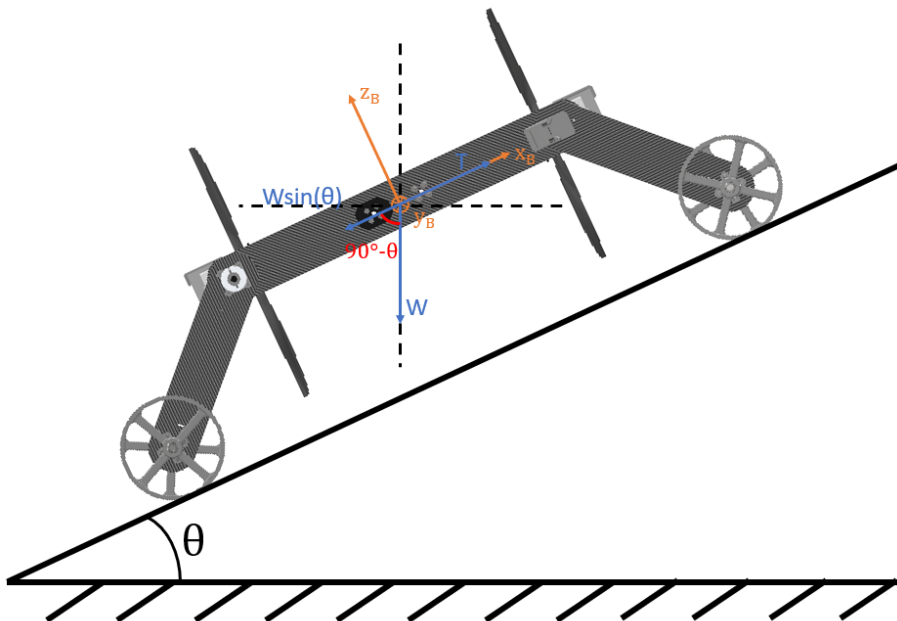
Figure 5.5: BogieCopter climbing low slope, with forces represented (normal force and friction not represented).

On medium slope surfaces (above 45° slopes), the weight component parallel to the surface corresponds to more than 0.707 of the total weight. Considering that in the locomotion on low slopes only two rotors are used, there isn't a high FoS between the thrust that the rotors are able to produce (maximum 2 kg each) and the required thrust (MTOM of 4 kg). At the inclinations of medium slopes, it is almost guaranteed that braking isn't required, since the weight component will act as the brake. A power mode was created, in which the four rotors are tilted in the same direction and used to create the thrust required to climb the slope, as represented in figure 5.6
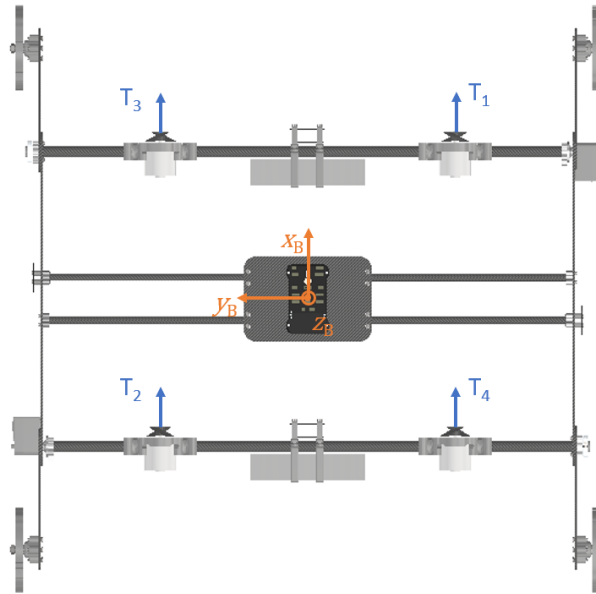
Figure 5.6: BogieCopter with the four rotors tilted in the same direction, for a climb with a higher factor of safety, guaranteeing the ability to climb medium slopes with the required payload.

The use of the power mode (four rotors to move on surfaces) should be used with caution. First, the braking capability of the drone once it finishes climbing the inclined surface will be nonexistent, since the rotors will take time to move back to their "normal" position (tilted inwards the vehicle), in which BogieCopter is able to brake. Second, the turning of the MAV changes in order to account for the different position of the rotors (T_1 and T_4, and T_2 and T_3 used to rotate counter-clockwise and clockwise, respectively). The vehicle won't be able to turn in place and turning while climbing the inclined surface isn't recommended, due to the delay of the tilting mechanism (supposing that the MAV turns 180°, it will accelerate downwards the ramp and not upwards until rotors change the tilting direction). For these reasons, the power mode is enabled by a switch in the radio transmitter. Also, this mode is only recommended for medium slopes, since the rotors will be operating as co-axial rotors, due to their distance [60], which have higher power requirements than single rotors, as demonstrated in equation 3.11.

To move on high slopes (above 60.9°), the additional creation of downforce is required in order to avoid the possibility of BogieCopter flipping over. This implies that a component of thrust perpendicular to the surface and directed towards the surface is required. To achieve this, the rotors should be tilted more than 90°, towards the surface, as depicted in figure 5.7. This is what enables the vehicle to climb walls [35]. To move on and climb these slopes, the turning of the MAV is required to be equal to that in

power mode, with the same challenges. Furthermore, the braking capability will be nonexistent, when moving back to flat surfaces, due to the position of the rotors.
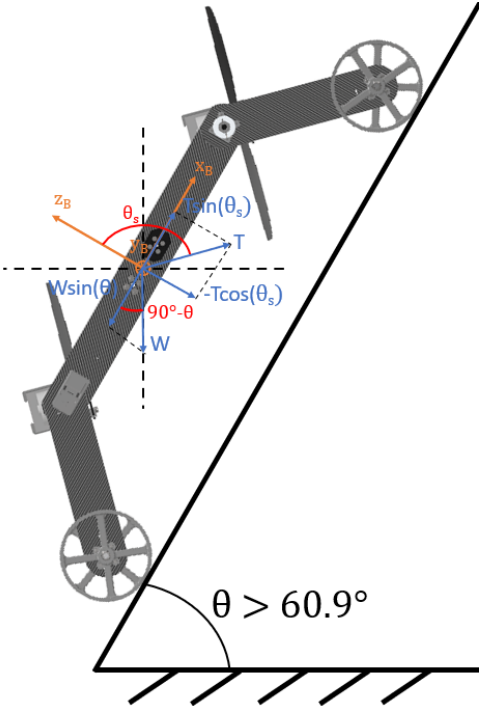
Figure 5.7: BogieCopter climbing a high slope, requiring the creation of downforce for the MAV not to flip-over. The rotors should tilt more than 90 ° to achieve that.

5.2.3.3 Transmitter Inputs

Another important step in the development of the firmware was to assign functions to the motion sticks of the radio transmitter and the channels of the receiver. The radio transmitter used is a Spektrum DX8 [156], which is a Mode 2 radio transmitter, having the throttle gimbal on the left side. This and the other stick motions are represented in figure 5.8.

Figure 5.8: Spektrum DX8 Mode 2 radio transmitter [156], each stick motion follows the standard: (1) Throttle (2) Yaw (3) Pitch (4) Roll (5) Flaps Gyro (6) Aux 2 GOV.

Usually, aerial vehicles assign the functions throttle to stick motion 1 (S1), yaw to S2, pitch to S3 and roll to S4. In the case of ground locomotion, we want to be able to control the longitudinal motion

(forward/backwards) of BogieCopter but also the no-input state, where none of the rotors is actuated for the longitudinal motion, with the vehicle maintaining its velocity (on ideal conditions, an important characteristic of ground vehicles). This implies that the resting position of the gimbal used for the stick motion of the throttle should be in its middle position. On mode 2 transmitters, that is only possible on the gimbals used for S2, S3 and S4, due to their spring mechanism construction. To maintain the control as similar as possible to the flying control, with the throttle being controlled by a vertical motion and not a horizontal motion, S3 is used as the throttle control, enabling three commands: forward and backwards motion, and maintain velocity. Avoiding the use of the same gimbal for throttle and turning control, implies that S2, during the ground mode, changes to control the yawing of the vehicle. To some degree, in the autopilot's firmware during ground mode, a mode 1 transmitter (throttle on the right side) is simulated (only some characteristics implemented). Due to the way that Copter is coded, this also means that in ground mode, after arming the vehicle, S1 should be put in its middle position, in order to avoid the disarming of the MAV. Having changed control channels of the transmitter only during ground mode required a modification of the flight code, in order to avoid that the vehicle enters flight mode while S1 is not in the bottom position.

Besides changing the functions of S2 and S3 during ground mode, additional assignments were given to the stick motion of 5 and 6 on ground mode. S5 changes the turning of the skid-steer vehicle while it moves backwards. Since a skid-steer vehicle behaves similar in any direction of movement, for some operators, it is beneficial that the turning direction remains constant independently of the direction of the longitudinal motion (a right motion of S2 should always represent a clockwise turn in these setting). This functionality is enabled by moving S5 to its lower position. The stick motion 6 enables the power mode, changing the tilting of the rotors depending on their position. In the middle position, the rotors are tilted accordingly to the normal mode while in the top position and bottom position the rotors are tilted forwards and backwards, respectively, enabling the power mode.

5.2.3.4 Firmware Overview

The developed firmware for the ground mode implements similar functionality to ArduRover's manual mode [157], with all the additional functionalities previously mentioned throughout this subsection. A motor mixing function was implemented, that enables the translation between the transmitter commands and the motors' actuation. The control of BogieCopter while in ground mode should be similar to that of a ground vehicle. A simplified flowchart of the developed firmware is presented in figure 5.9.
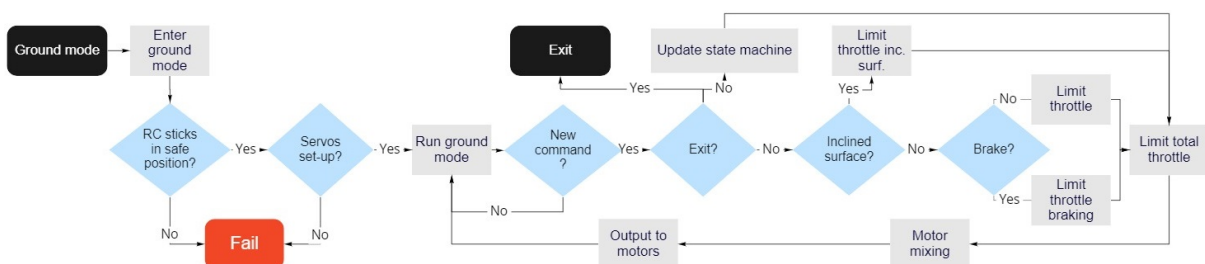
Figure 5.9: Simplified flowchart of the ground mode firmware.

The developed ground mode firmware can be found in the following repository: [158].

Chapter 6

Results and Validation

This chapter focuses on the validation of BogieCopter's design and capabilities. It is divided into four sections. The first section is focused on the developed vehicle's mass, with the total mass and the ground actuation mechanism's (GAM's) mass of the vehicle being analysed. In section 6.2, the results from static thrust tests performed with the selected rotor are compared with results from tests realised with other rotors, in order to validate or select a better rotor for the MAV. In section 6.3, the numerous real tests that were conducted with BogieCopter are described and images from these tests are presented. In the last section, section 6.4, a comparison between the power consumptions of the MAV at different operating states is given.

6.1 Prototype Mass

The final BogieCopter prototype was weighed, without any payload, and its mass was determined to be 2.7 kg $\pm$ 0.1 kg. This corresponds to a mass difference of 35% $\pm$ 5% when compared with the intended design mass. This difference was impacted by two factors: the use of over-dimensioned structural components (CFRP plates and tubes), which weren't properly optimized for the design load cases, as mentioned in subsection 4.6.8, and a wrong assumption for the value of the relation between the vehicle mass and the payload (subsection 4.3.2, equation 4.1). In fact, if the value considered was closer to the one for a similar-sized multi-modal MAV, such as Drivocopter [5], whose relation value corresponds to 1.914 (considering the mass from the active GAM as payload), the final vehicle mass would be 41% lower than the estimated design mass. Considering the MTOM of 4 kg and the T/W ratio of 2, this vehicle's mass limits its payload capacity to 1.3 kg. This payload is still high enough for most inspection applications (a RGB and thermal camera's sensor plus a LIDAR may only require 1 kg of payload capacity, according to tables A.1 and A.2). Analysing the characteristics of the multi-modal MAVs reviewed in section 2.3 (summarized in table 2.2), to the best of our knowledge, BogieCopter has the highest payload capacity for a multi-modal MAV (higher is better) and presents the lowest relation between vehicle mass and payload (lower is better), considering a T/W ratio of 2. In reality, Drivocopter [5] has a lower relation between vehicle mass and payload but its T/W ratio is unknown, having been excluded from this comparison due to the lack of data.

One of the biggest disadvantages of a multi-modal MAV is the mass added by the GAM. This mass has a negative impact on the overall vehicle's flight operating time, increasing the required power for flight (as demonstrated by equation 3.5) and reducing the MAV's usability in different applications. Due to this, the reduction of the GAM's mass was one of the design goals. Each wheel assembly (appendix F.4) was weighed and its mass was determined to be 82.2 g $\pm$ 0.1 g. This corresponds to a total GAM's mass of 328.8 g $\pm$ 0.4 g, representing 12.1% of the total vehicle's mass and 8.2% of the MTOM. To the best of our knowledge, BogieCopter is the MAV with the second lowest percentage of GAM's in its MTOM, surpassed only by the mono-wheel design of Gemini [44, 45]. However, the developed vehicle doesn't require any actuation to be static on flat surfaces, which means there is no energy consumption, whereas Gemini consumes 106 W, a value that corresponds to 0.6x the energy it requires while it is moving. This downside of Gemini's design can impact its operating time negatively. For example, if we consider that the MAV is required to perch for extended periods of time, as in some inspection and surveillance applications, the inability to be static without requiring actuation is a disadvantage.

Figure 6.1 presents an overview of BogieCopter's mass distribution for its main subsystems. We can verify that the payload represents 32.1% of its MTOM, a very high value for MAVs.
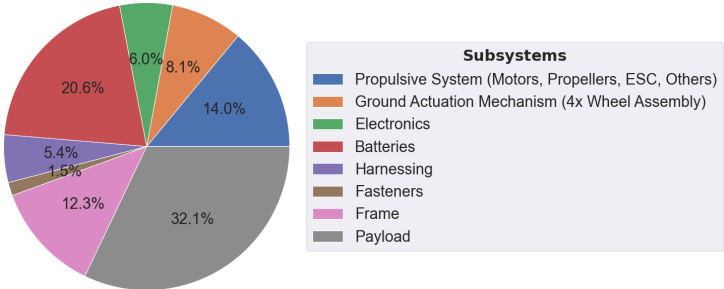
Figure 6.1: Overview of BogieCopter's mass distribution for its main subsystems.

6.2 Rotor Test

As mentioned in subsection 4.4.1, rotors' static thrust tests were conducted in a custom-adapted thrust stand (described in appendix G). The objectives of these tests were to determine the performance of the different rotors, by determining the thrust, power and efficiency of the rotors in relation to the applied throttle and to select the best rotor for the design. Furthermore, the relationship between throttle and thrust has to be known in order to optimize the autopilot firmware.

The static thrust tests were performed using four different propellers (identified in subsection 4.4.1), APC 10x5E, APC 10x7E, HQ Prop 10x6x3, and Dynam 10x7x3 and four different motors (three of them identified in subsection 4.4.2): Dualsky ECO2814C-V2 and ECO2820C-V2, Racerstar BR2814, and T-Motor AT2814. Dualsky ECO2820C-V2 [107], although not being a possibility for BogieCopter during the design phase, due to its higher mass (138 g) could be a possibility for a future improvement if its performance surpasses the downsides from the increased mass (it is able to handle a higher maximum current than ECO2814C-V2 while having a similar performance). The static thrust tests were performed at the nominal voltage of the propulsive system's batteries used, 14.8 V, and with the motors at room temperature at the start of the test (27-28ºC). Two tests were conducted for each rotor, with the throttle

being increased by 5% after remaining at the throttle level for five seconds. The motors' specified maximum power and current were never reached, in order to protect the motor from damage, resulting in some motors not exceeding a certain throttle level.

To facilitate the analysis of the data, four different plots are presented, one for each motor with all the propellers. To keep the plots clean, only the efficiency and thrust are presented, given that the total power can be estimated from these parameters. Besides, the efficiency and thrust are more important for the selection of the rotor. Figures 6.2(a), 6.2(b), 6.2(c), 6.2(d) present the efficiency and thrust versus throttle for the rotors with the AT2814, BR2814, ECO2814C-V2, and ECO2820C-V2 motors, respectively. For a broader comparison of the rotors' performance, figures 6.3(a), 6.3(b), 6.3(c) present the power and thrust versus throttle, and the efficiency versus thrust for all the analysed rotors, respectively. It should be noted that, in these three figures, the lines representing the performance of the rotors with the selected motor (AT2814) are thicker and, for better visualization, the efficiency plot only starts at a thrust of 300 g. It should also be noted that in the case of figures 6.2 and 6.3, the plot lines represent average values for the two test runs.
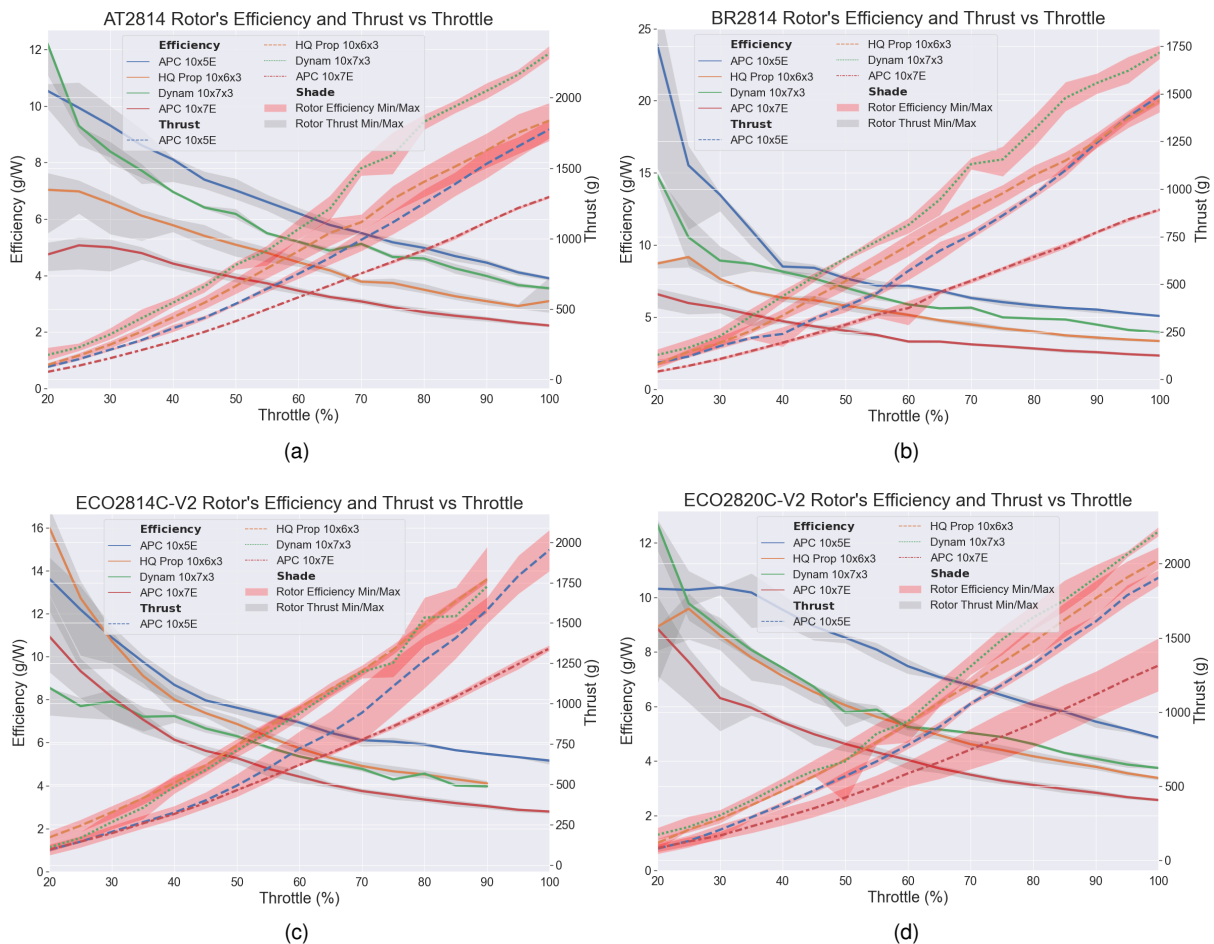
Figure 6.2: Thrust and efficiency vs throttle for each rotor (line represents average value) with the motors: (a) T-Motor AT2814 (b) Racerstar BR2814 (c) Dualsky ECO2814C-V2 (d) Dualsky ECO2820C-V2.

As can be concluded by analysing figure 6.2(b), none of the analysed propellers can provide the required maximum thrust of 2 kg for the BR2814 motor. From figures 6.2(a), 6.2(b), 6.2(c), and 6.2(d) it is

possible to verify that the rotors with the APC 10x7E couldn't achieve the required maximum thrust. This observation goes against the theory [91, 129] and the data provided in [107], being that the best explanation for this result is that the APC 10x7E propeller used for the test was defective. From figure 6.3(c), it is possible to verify that from ~400 g to ~1.6 kg of thrust, the most efficient rotor is the ECO2820C-V2 with the APC 10x5E. Unfortunately, this rotor isn't able to produce the required maximum thrust and has a lower efficiency when the motor is combined with the other tested propellers, making it unviable (figure 6.2(d)) for the MAV. Having excluded the ECO2820C-V, it is possible to verify and conclude, from figure 6.3(c), that the rotor tested with the highest efficiency is the ECO2814C-V2 motor. Analysing figure 6.2(c), it is possible to verify that this motor with the APC 10x5E was able to produce the required maximum thrust of 2 kg (produced a maximum of 2.078 kg) while consuming, on average, 378 W. This value is within the maximum power restrictions of the motor, which was the initial reason to exclude it, given the motor's manufacturer test data [107]. Being able to produce the required maximum thrust and having one of the best efficiencies versus thrust makes this the ideal rotor for BogieCopter, enabling it to achieve the highest possible operating time. Analysing figure 6.2(a), it is possible to verify that the maximum thrust that the rotor chosen for BogieCopter (AT2814 with APC 10x5E) was able to produce, in the static thrust tests, was 1843 g, which is significantly lower than the design maximum thrust. The selection of this motor was based on the motor's manufacturer data [111], which demonstrates that the motor is able to produce a maximum thrust of 2274 g, with the APC 10x5.5 propeller. Taking into account the formula given in [91] and reproduced in equation 6.1, it was determined that the difference in thrust, F_C, from a propeller with a pitch (P) of 139.7 mm to a propeller with a pitch of 127 mm was, approximately, -48 g, resulting on a maximum produced thrust of 2226 g by the rotor. Even when considering a SF of five for the difference in thrust between the propellers, the value estimated for the maximum thrust would still be higher than the required 2 kg. Static thrust tests should be conducted, in the future, with the AT2814 and APC 10x5.5 to verify the motor's manufacturer data.

$$F_{C-10} = (P - 127) \cdot 0.037 \tag{6.1}$$

Still considering the 4 kg MTOM, this result for the used rotors' maximum thrust impacts negatively the BogieCopter's T/W ratio, reducing it to 1.843. This value still provides a high enough SF to the produced thrust, meaning that the developed MAV is able to operate in windy conditions. On the other hand, considering a T/W ratio of 2, BogieCopter payload capacity is reduced to 986 g. From figure 6.3(c), it is possible to verify that the used motor (AT2814) with the Dynam 10x7x3 propeller was able to produce a thrust higher than the required maximum thrust and achieved a higher efficiency while producing any given thrust when compared with the APC 10x5E. This observation implies that, if the used motor isn't replaced for the more efficient ECO2814C-V2, the propeller could be. By changing the used propeller, besides BogieCopter benefitting from the increased rotor's efficiency, it would gain the benefits of using a three-blade propeller on tilt-rotor designs, which have a more symmetric mass distribution, leading to lower rotor induced vibrations [89]. Although not being an objective, from all the plots we can verify that the rotor with a three-blade propeller was able to produce a higher thrust than with a two-blade propeller, as demonstrated in equation 3.8, and, sometimes, even with a higher efficiency (for example, the AT2814 with the Dynam 10x7x3 versus the APC 10x5E), contrary to the results presented in [60].

(a)

(b)

65
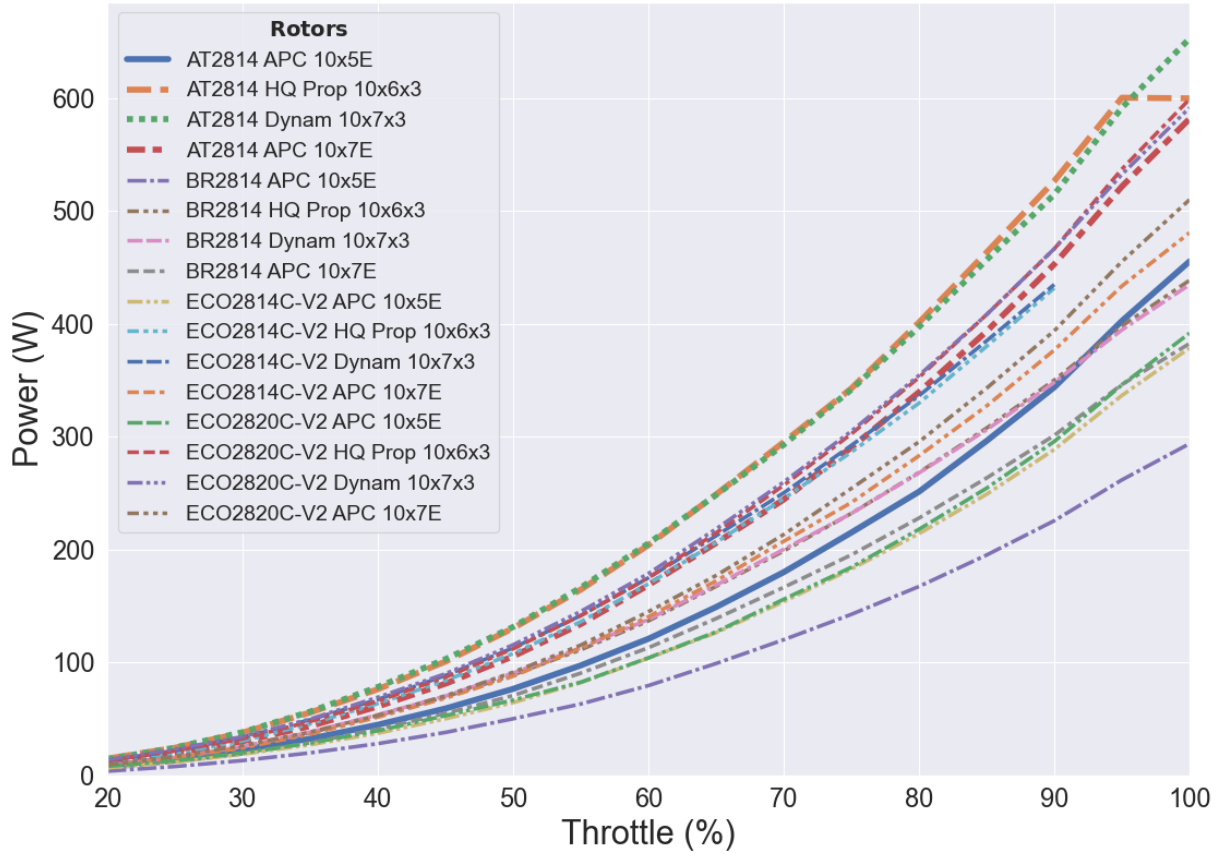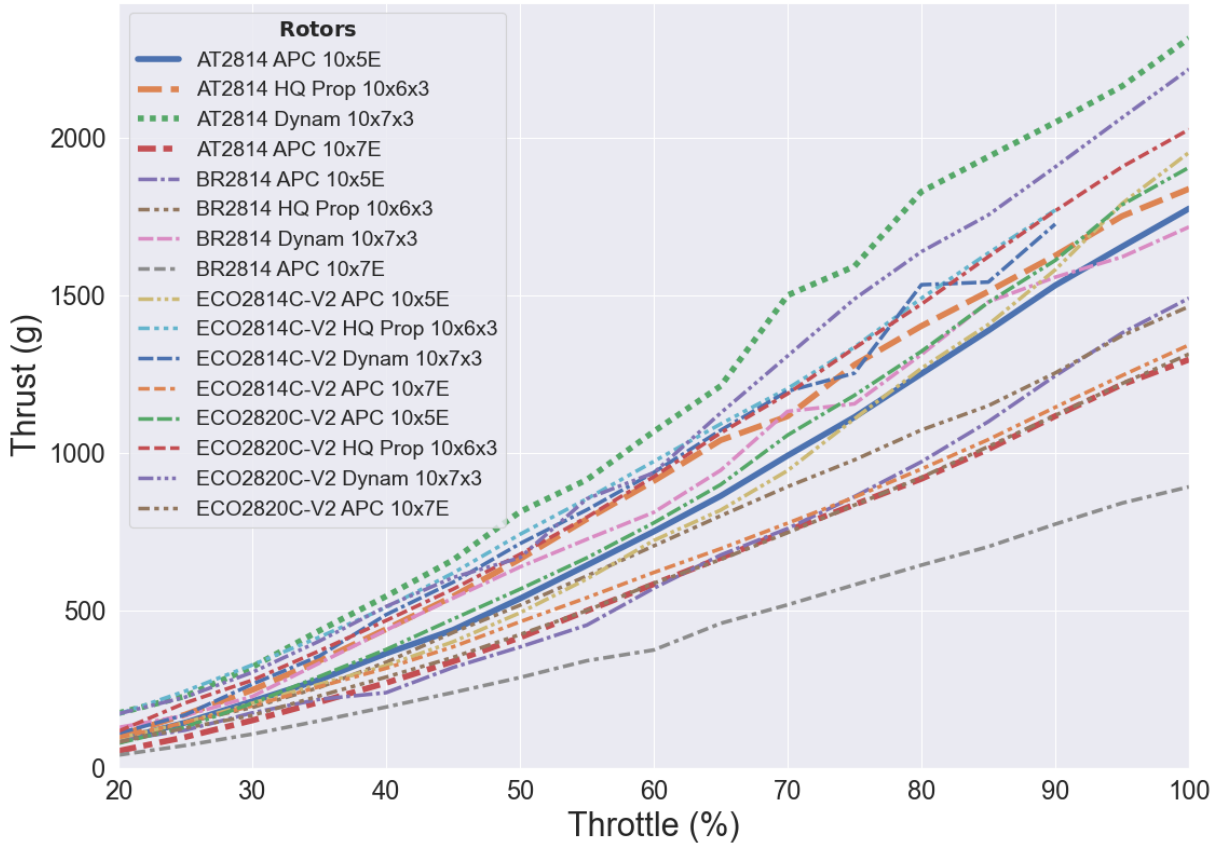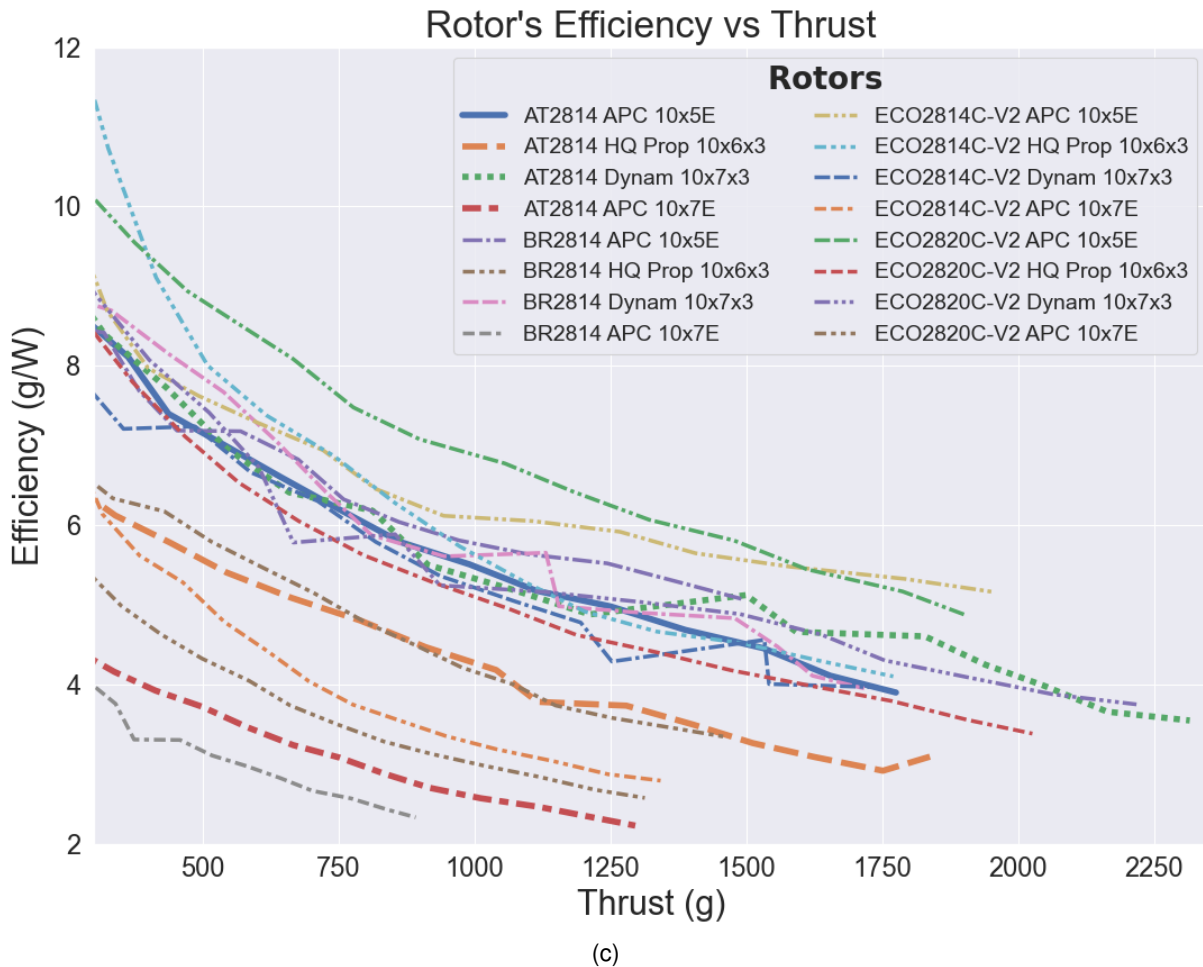
Figure 6.3: Comparison between the performance of the different tested rotors (lines for the rotor with the selected motor are thicker and lines represent average valus) (a) Power in relation to throttle (b) Thrust in relation to throttle (c) Efficiency in relation to thrust.

6.3 Locomotion Tests

Having BogieCopter's prototype built, the next steps were the design validation, achieved through the realisation of multiple tests, exploring the capabilities of the vehicle in the different modes of locomotion, and the improvement of the developed firmware, enabled by the tests' results. The tests here presented were conducted after a thorough verification that the autopilot was working properly, which was performed without any propeller on the MAV (for safety reasons). This section is divided among the different types of tests that were performed.

6.3.1 Aerial Locomotion

The first tests performed were flight tests, given that the aerial locomotion didn't require the use of any custom firmware, since BogieCopter behaves just like a normal quadrotor in flight. ArduCopter [144], as presented in section 5.2, is a well-established firmware, having already demonstrated its capabilities throughout multiple designs [142] and would, therefore, establish a baseline for the performance of the prototype. If the developed MAV wouldn't be able to fly with the original firmware, something would

be wrong and required correction. This wasn't the case, and from the first flight test, BogieCopter demonstrated to be a very stable flying platform. A set of pictures from such test are presented in figure 6.4, which depict the MAV from arming (figure 6.4(a)) up to landing (figure 6.4(f)).
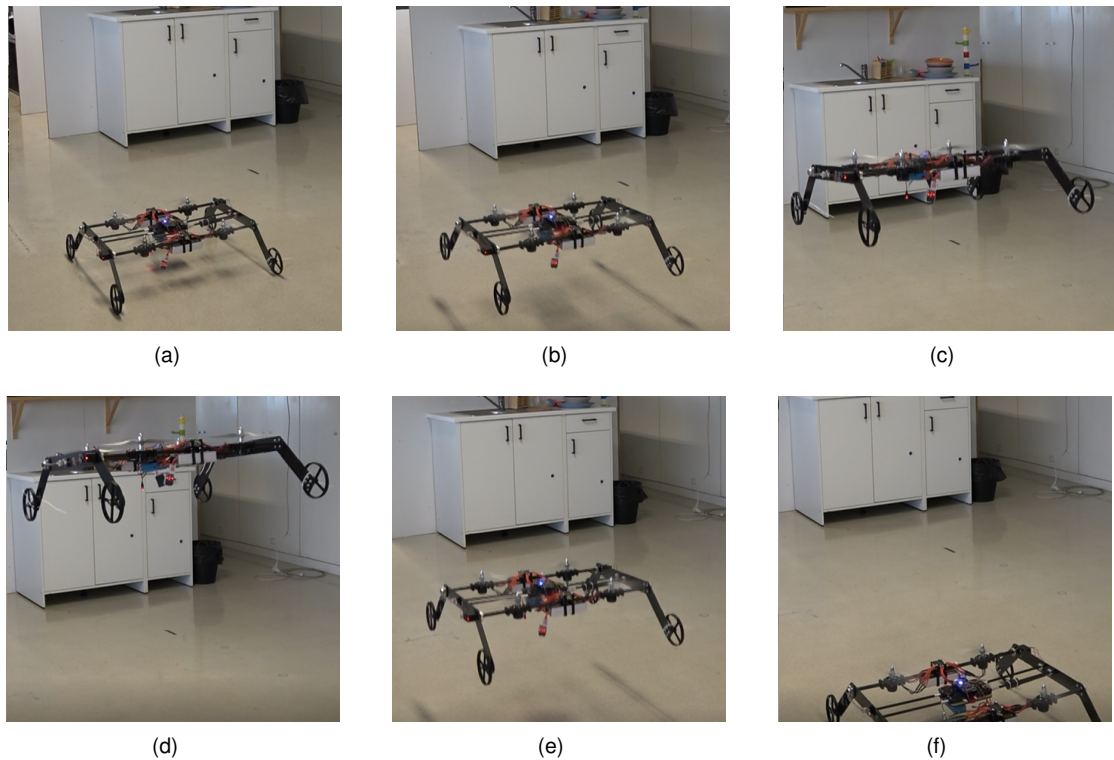
Figure 6.4: BogieCopter flight test, throughout its multiple phases: (a) MAV armed (b) Climbing (c) Hovering (d) Moving backwards (e) Descending (f) MAV landed.

6.3.2 Ground Locomotion on Flat Surfaces

Having validated BogieCopter's ability to fly, the next set of tests were conducted using the custom firmware. Initially, only the longitudinal motion of the vehicle while on flat surfaces was evaluated. The goal was to assess the stability of both the vehicle and the firmware. Figure 6.5 depicts one of such tests, in which the ability of the vehicle to accelerate and decelerate was evaluated. BogieCopter started to move just before the first carpet (represented in figure 6.5(a)), moving up to the third carpet (represented in figure 6.5(c)), where it would brake. The distance between these two carpets was 441 cm.
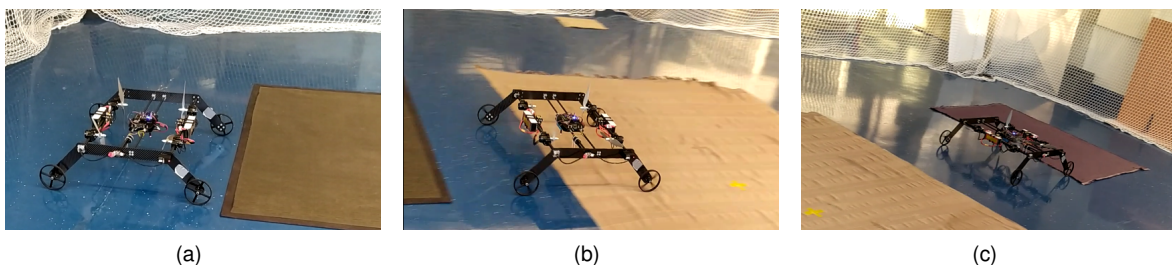
Figure 6.5: Longitudinal locomotion test, with the starting point ((a)) distancing 441cm from the finishing point ((c)): (a) Starting point of the test, just before the first carpet (b) BogieCopter passing through the middle carpet (c) Finishing point of the test, just before the third carpet.

During the test depicted in figure 6.5, it was possible to verify that the MAV started moving when a

throttle as low as 10% was commanded. By keeping the throttle at constant levels, BogieCopter was able to reach speeds of ∼1 m/s and ∼4.1 m/s, with the throttle at 10% and 35%, respectively. These tests not only demonstrated the ability of the MAV to move longitudinally but also demonstrated its ability to be controlled at different speeds.

Although not initially intended during these longitudinal motion tests, the impact resistance of BogieCopter, while moving on the ground, was validated. During the tests performed without the firmware which implemented the braking state machine, as described in 5.2.3.1, the MAV wasn't able to brake in time and ended up colliding with the wall. This collision is presented in figure 6.6. Although the force of impact, BogieCopter didn't suffer any damage, with the collision (and impact) being reproduced several times afterwards, validating its resistance to ground collisions.

| (a) | (b) | (c) | (d) |
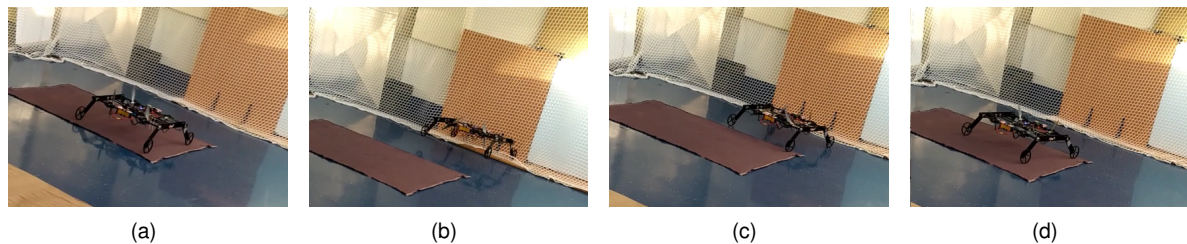
Figure 6.6: BogieCopter hitting the wall at around ∼4.1 m/s: (a) BogieCopter not braking in time, going towards the wall (b) Strong impact against the wall, with the MAV coming off of the ground (b) BogieCopter being pushed off of the wall (b) Stopping after collision.

Having validated the longitudinal locomotion of the vehicle, the next tests conducted evaluated its lateral locomotion's capability. As mentioned in 5.2.3.1, BogieCopter should behave just like a normal skid-steer vehicle on the ground, being able to turn in place. A simple test was conducted to demonstrate this capability, being depicted in figure 6.7. It is possible to verify the developed MAV turning 270° without moving longitudinally (turn in place).

| (a) | (b) | (c) | (d) |
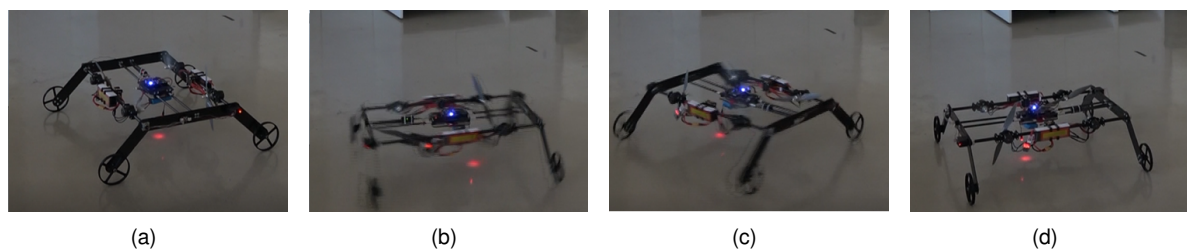
Figure 6.7: BogieCopter turning in place: (a) Starting the turn (b) ∼90 ° (c) ∼200 ° (d) Finishing ∼270° turn.

Having determined that the individual components (longitudinal and lateral motion) of the ground mode were working as intended, multiple tests that combined these characteristics were performed.

One of such tests was the movement in a simulated confined space, demonstrating the ground mode's capabilities of the developed multi-modal MAV. Figure 6.8 shows BogieCopter moving on a confined space, a long narrow wheel-chair ramp, with the dimensions of the test circuit represented in figure 6.9. From figure 6.9 and the dimensions of BogieCopter (4.6.6.3), it is possible to verify that the maximum clearance between the MAV and the walls was 0.15 m (assuming an equal distance to the

walls from any side of the vehicle). At this clearance level, it wouldn't be safe to fly the MAV but it is safe to drive it on the ground (the MAV is able to resist ground collisions and surpass them, as demonstrated by the previous tests). It should be noted that the ground of the test circuit wasn't flat, having some minor slopes, with, approximately, 4.2° of inclination, with BogieCopter demonstrating being able to overcome them.
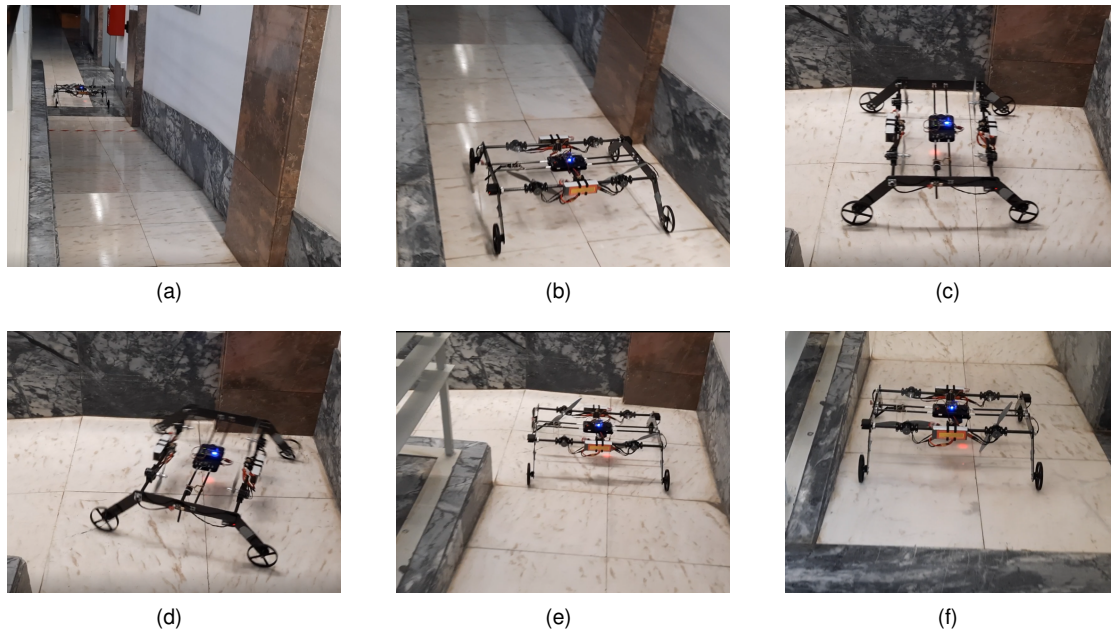
Figure 6.8: Test on a simulated narrow and confined space, a long narrow wheel-chair ramp (noticeable the 4.2° slopes in figure 6.8(a)): (a) Starting point of the confined test circuit (b) BogieCopter moving forward (c) Arriving at the turning point (d) (e) Turning (f) Arriving at the finish line of the confined test circuit.
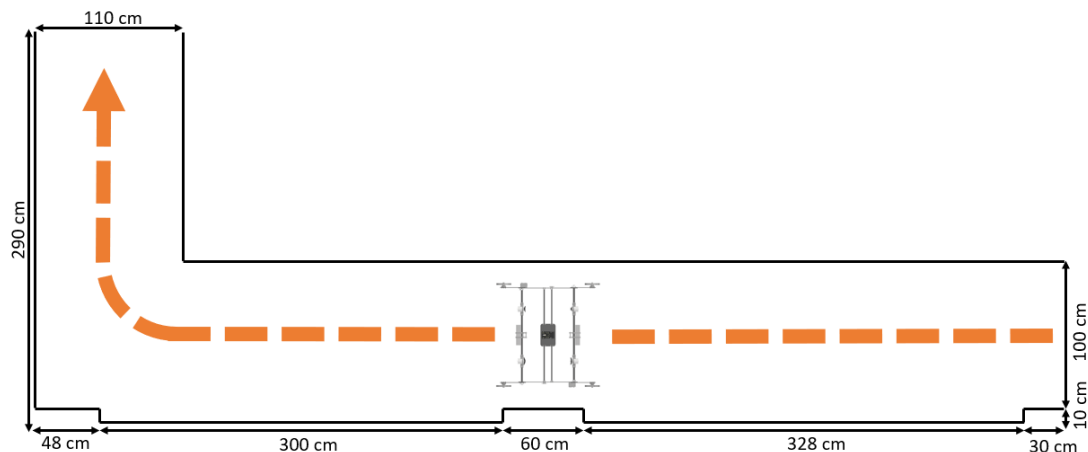
Figure 6.9: Dimensions of the confined test circuit, at scale, depicting the developed MAV and the path to be followed (represented in orange).

Multiple tests were conducted to validate BogieCopter's capabilities to move on multiple different ground terrains. One of such tests was the locomotion on rocky soil ground, which is depicted in figure 6.10. Due to the nature of the terrain, it had some slopes, with the biggest one having an inclination of 5°. The developed MAV was able to overcome them easily and was, also, able to move over small grass, with, sometimes, the propellers hitting and cutting them, without causing any damage to the vehicle.

69

Figure 6.10: BogieCopter moving on rocky soil ground: (a) Test starting in a sidewalk (b) Longitudinal motion (c) Turning (d) Climb of small slope ($\sim 5°$).

6.3.3 Multi-modal Capability

BogieCopter is a multi-modal vehicle, being able to fly and move on the ground. The previously performed and presented tests validated its capabilities to fly and to move longitudinally and laterally on flat surfaces but didn't validate its multi-modal capabilities (the ability to change the locomotion mode). Several tests were performed in order to validate this ability, with one of such tests depicted in figure 6.11. The developed vehicle moves on the ground, due to the higher efficiency of this locomotion, and, when faced with an obstacle (in this case, stairs), which doesn't allow the vehicle to continue to follow its path, transitions to flight mode, in order to overcome the obstacle. Once the obstacle is surpassed, the vehicle transitions back to ground mode, proceeding with its path in the more efficient locomotion mode.
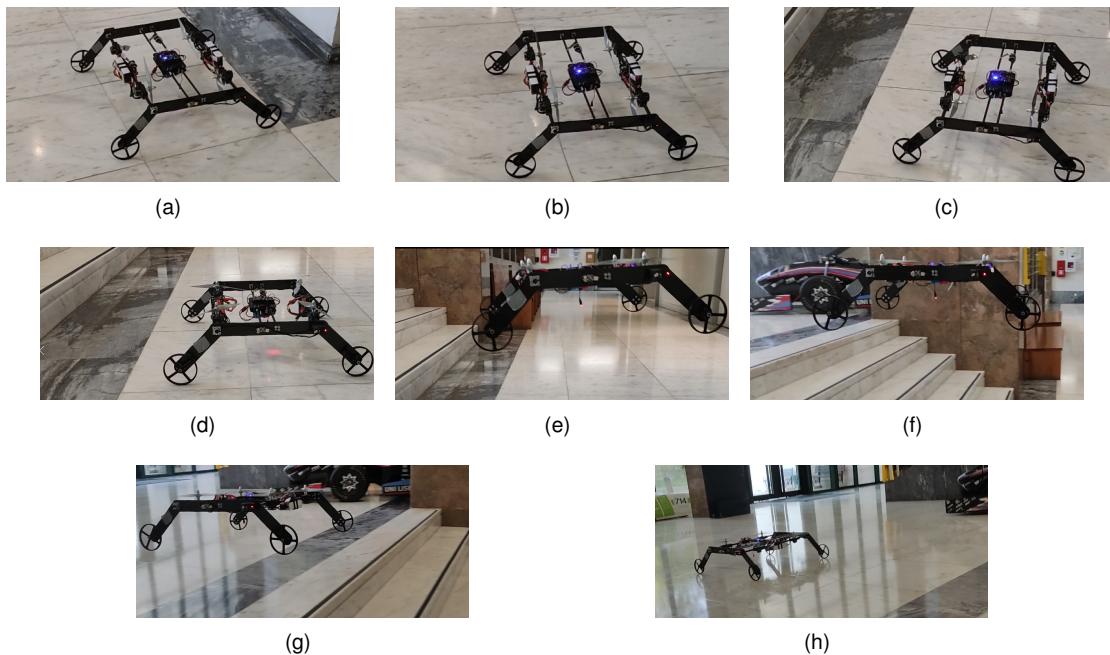
Figure 6.11: BogieCopter multi-modal test: (a) BogieCopter in ground mode (b) Moving on the ground (c) Reaching an obstacle - stairs (d) Transition to flight mode (e) (f) Fly over obstacle (g) Landing (h) Transitioning back to ground mode.

6.3.4 Ground Locomotion on Inclined Surfaces

In the literature reviewed and the state-of-the-art multi-modal MAVs explored in section 2.3, it is possible to verify that the problem of locomotion on inclined surfaces is rarely explored. To the best of our knowledge, only Shapeshifter [51, 52] explores the problem theoretically and NINJA UAV [54] experimentally, by showing the MAV climbing stairs. In this subsection, BogieCopter's ability to move on

inclined surfaces will be demonstrated, providing evidence that passive actuated multi-modal MAVs are able to move on inclined surfaces.

As has been presented previously in subsection 4.6.1 and following [128], locomotion on inclined surfaces for the usual approach to passive actuated multi-modal vehicles requires an *a priori* knowledge of the slope angle. BogieCopter design addresses this issue, being able to move on inclined surfaces without requiring knowledge of the slope angle. In fact, as in the flat surface locomotion, BogieCopter behaves similar to a normal ground vehicle, being very easy to control.

A set of tests were performed to validate the performance of BogieCopter on inclined surfaces. Three types of inclinations were tested, with slope angles of $14°$, $22°$, and $33°$. These were the inclined surfaces that were readily available in skate parks, being that the developed MAV should be able to climb lower or steeper slopes, with the limitation that from a certain slope angle, the vehicle requires additional downforce to not flip over, as described in 5.2.3.2. Unfortunately, this inclined surface's maximum angle couldn't be determined experimentally. Figures 6.12, 6.14, 6.16, and figures 6.13, 6.15, 6.17, depict BogieCopter in normal mode and power mode, respectively, climbing inclined surfaces with $14°$, $22°$, and $33°$, validating its capability for locomotion on inclined surfaces.

Figure 6.12: Climb of a $14°$ slope in normal mode.
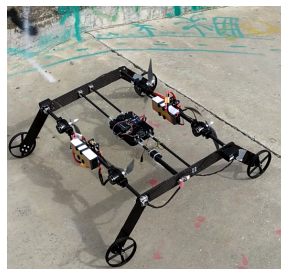
Figure 6.13: Climb of a $14°$ slope in power mode.

Figure 6.14: Climb of a $22°$ slope in normal mode.

Figure 6.15: Climb of a $22°$ slope in power mode.

(a) (b) (a) (b)

Figure 6.16: BogieCopter climbing a $33°$ slope in normal mode (a) Start climbing (b) Moving on inclined surface.
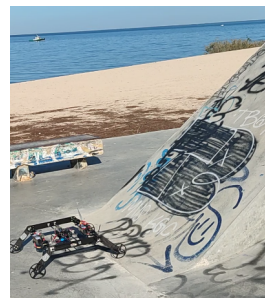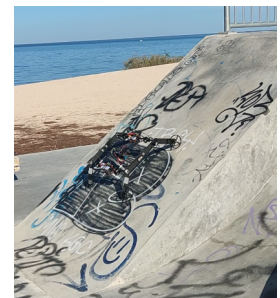
Figure 6.17: BogieCopter climbing a $33°$ slope in power mode (a) Start climbing (b) Moving on inclined surface.

6.3.5 Wall-Climbing

As mentioned in subsection 4.6.1 and in 5.2.3.2, the design of BogieCopter, similarly to [35], enables it to wall-climb. For wall-climbing, the propellers should be tilted towards the wall, in order to create the required downforce that enables the MAV to stick to the wall. A simple test was performed to test this hypothesis, with the results presented in figure 6.18. The test was conducted in a skate park, which

had a 2 m vertical wall with a platform on its top, enabling a rope to be attached to secure the MAV. During the test, BogieCopter's propellers were tilted at 135°. As it can be concluded from figure 6.18, BogieCopter was able to successfully stick to the wall and climb it. The code used for this test can be found in [159].

| (a) | (b) | (c) |
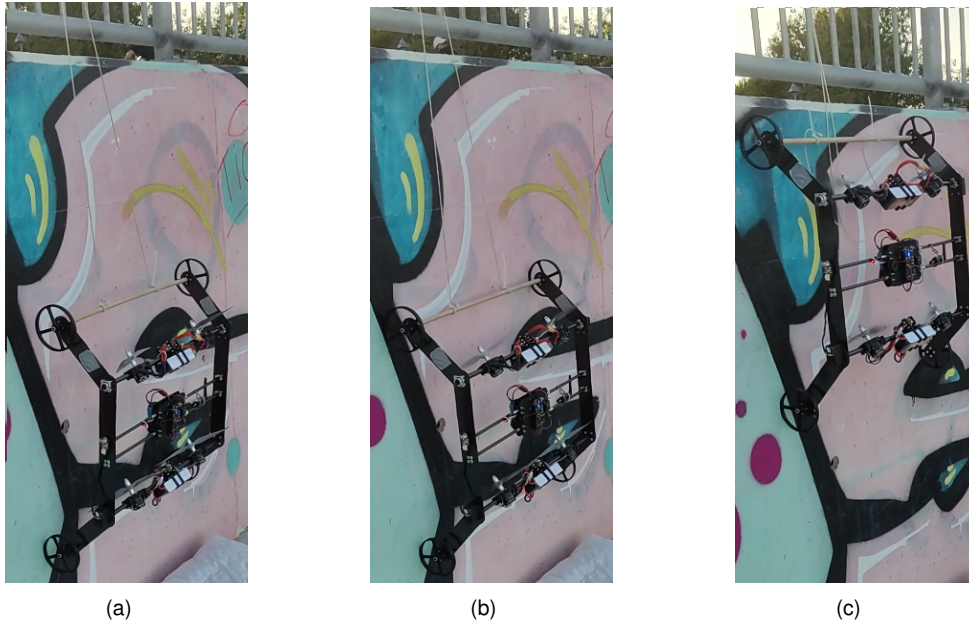
Figure 6.18: Wall-climbing test: (a) BogieCopter being held by a rope - rope in tension (b) BogieCopter sticking to the wall (b) BogieCopter climbing the wall - rope is loose.

6.4 Power Consumption

During the tests conducted with the developed MAV (section 6.3), data such as throttle, instantaneous current and battery voltage was logged, in order to allow multiple data comparisons. Although not being previously mentioned, two tests with a payload of 2 kg were also conducted, for the ground mode on flat surfaces and flight mode. Figure 6.19 depicts BogieCopter with the payload, two 1 kg weights.

Figure 6.19: BogieCopter with two 1 kg weights, simulating a 2 kg payload.

One of the comparisons that this data enables is between the instantaneous power consumption of the different operating states (the ones with most interest) and is presented in figure 6.20(a). The other comparison that can be performed is relative to the required throttle. Given that there is a directly proportional relationship between throttle and thrust, a comparison between the required throttle to maintain a certain operating state, during the experiments, with the theoretically required throttle, given by the mass of the vehicle during the test and the data from the static thrust tests, is possible. This comparison is presented in figure 6.20(b).

From figure 6.20(a), it is possible to conclude that, as expected, the mode requiring the least average power was the locomotion on flat surfaces at 1 m/s, requiring 29.8 W. This value is ∼28.8x lower than the required power for flight. Even considering BogieCopter moving with a 2 kg payload on a flat surface at 1 m/s, the value for the power has doubled to 58.6 W, still being ∼14.7x lower than flying without any payload or ∼25.5x lower than flying with a 2 kg payload. Additionally, as expected, moving at 4.1 m/s requires more energy than moving at 1 m/s, requiring almost 5.7x more energy. Considering the current batteries being used by BogieCopter, this corresponds to a travelling distance of ∼11.5 km and ∼8.2 km while moving on flat surfaces at 1 m/s and 4.1 m/s, respectively. These values could be further increased when using the batteries recommended in subsection 4.4.4. When dealing with slope angles up to 33°, flying still requires more energy, with BogieCopter having, approximately, a 1.85x lower power consumption while remaining in a 33° inclined surface than when hovering. Climbing an inclined surface higher than 33° should, also, spend less energy than flying over it. One of the unexpected results was the energy required to climb a 22° inclined surface in normal mode, which should have been closer to the value attained for the power mode. The only reason for this, as can be visualized by the comparison between the supposed and the test throttle, in figure 6.20(b), was that the MAV gained enough speed just before the slope for not require more energy (throttle) while climbing it. Through the multiple tests conducted on the 22° slope, the same results were attained, meaning that the slope in the inclined surface's base should be lower than the 22°. The higher power required to climb the inclined surface in the power mode compared to the power for the normal mode is justified by the fact that the rotors behave as a co-axial rotor (their distance isn't enough to avoid the interaction between their flows), requiring more energy and being less efficient [53, 60]. For the 33°, the power required for both modes is almost the same and for higher slopes, the power mode is expected to require less energy, since the rotors in the normal mode will present a lower efficiency at the required thrust level and the rotors for the power mode will be operating at a lower throttle level and at a higher efficiency level. The highest power achieved by an operating state was for the wall-climb. It wasn't expected this value to be ∼1.77x higher than the required power for hovering without payload, but as mentioned in [35], this could be related to a non-optimized tilt of the rotors. During the course of this work, it wasn't possible to optimize the rotor's tilt and it should be in the future.

From figure 6.20(a), it is possible to conclude three things. As expected, the throttle for the power mode is lower than the throttle for the normal mode, since four motors are being used instead of two. The value of the throttle for the 22° inclined surface at normal mode is way lower than the expected (a difference higher than 10% wasn't expected), with the reason having been presented previously. The last conclusion is that the throttle, in all the compared operating states, was lower than the throttle estimation enabled by the static thrust tests' data. This can be justified by two factors: since the MAV is operating in close proximity with the ground surface, it could have been affected by ground effect, although its effect should be minimal with BogieCopter's design [160–162], and the batteries used were fully charged, having a higher voltage than the nominal one, leading to a higher thrust for each given throttle. This last factor should be the one that impacted the most the difference in the required throttle's values.
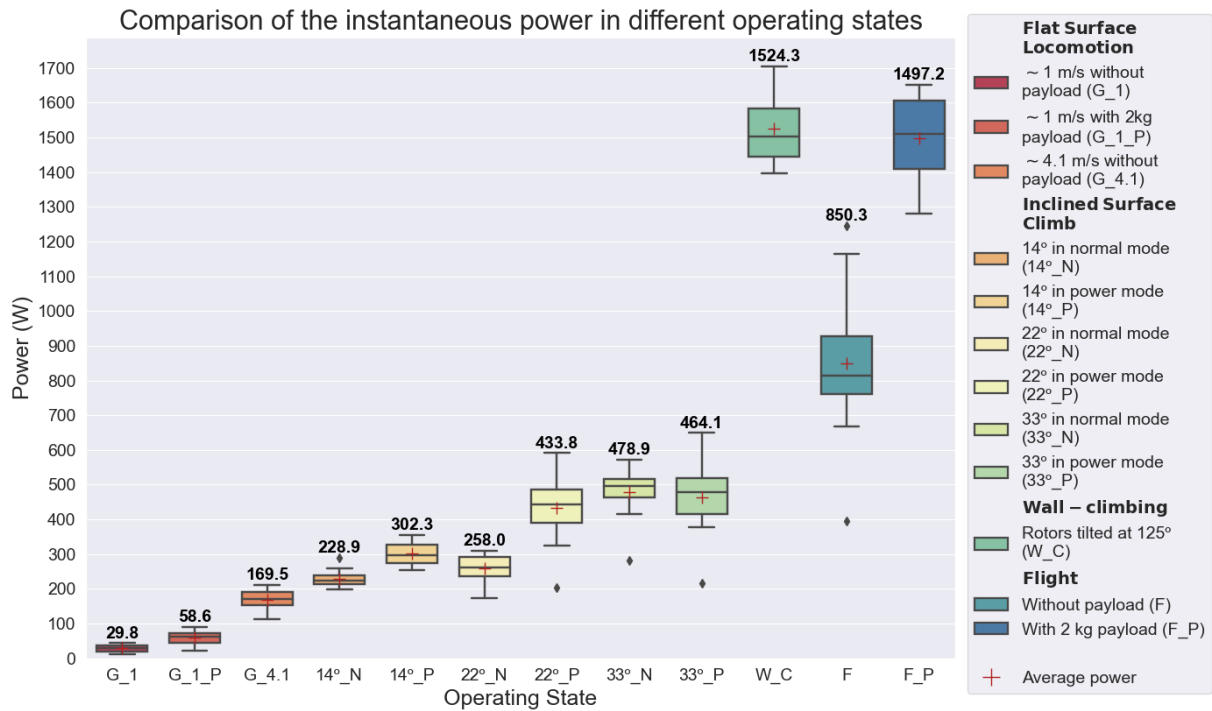
(a)
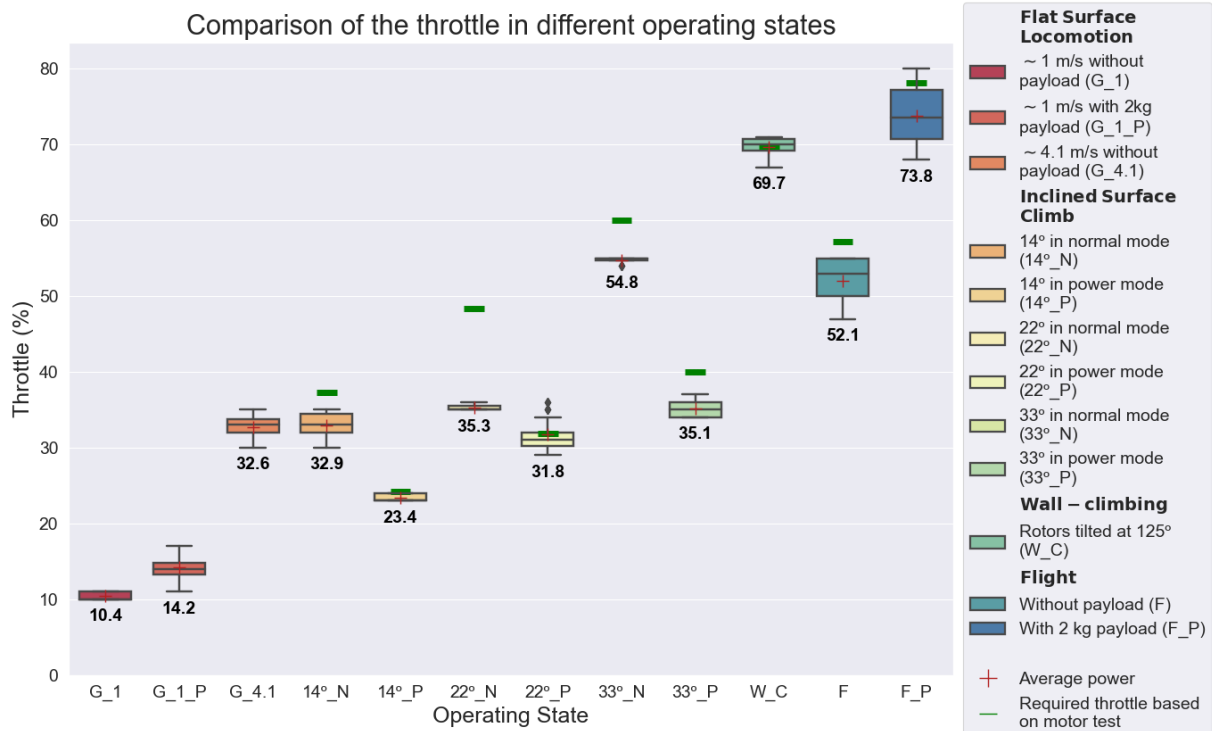
(b)

Figure 6.20: Comparisons enabled by the test's logged data. The values above and under the plots correspond to the average value to maintain the operating state (power and throttle, respectively) (a) Comparison between the power consumption in different operating states (b) Comparison between the required throttle in different operating states, showing the required throttle based on values from the rotor's static thrust tests.

Chapter 7

Conclusions

In this work, the design, development and testing of a novel passive actuated multi-modal MAV are described. BogieCopter addresses the issues identified in the reviewed multi-modal passive actuated MAVs, being a mechanical simple, efficient and cost-effective solution for many different applications, such as inspection. The use of a tilt-rotor system decouples the flight control from the ground control, leading to a simpler controller design, with the vehicle exhibiting a similar behaviour to skid-steer ground vehicles, during ground locomotion. The design of BogieCopter also enables it to hover at any given pitch angle [27] and to wall-climb, enabling new possibilities for the locomotion of the vehicle. The ability of BogieCopter to move on flat surfaces, inclined surfaces, walls, and to fly is demonstrated, and the power consumptions in each operating state are presented. A simulation environment is also presented, allowing a more efficient development of future controllers and path following algorithms.

7.1 Achievements

Literature and State-of-the-Art reviewed: The literature and state-of-the-art review revealed that multi-modal MAVs is a growing area of interest. Most of the analysed passive actuated MAVs follow the same inefficient design and don't present enough payload capacity for many inspection applications. Essential information required to use the MAV in different applications is, also, not presented. To the best of our knowledge, the comparison realised in this work is the most vast in the multi-modal MAVs literature;

Design Procedure: A design procedure for the development of a multi-modal MAV was presented, describing the steps required to select the components of the vehicle and enabling the reader to follow them to build its own MAV;

Custom components: Custom mechanical and electrical components were designed and developed, in order to solve encountered challenges during the design. One of such components are the custom designed PCBs, which can be used in other vehicles using more than two batteries or, even, to implement a simple control of the SoC of multi-cell batteries, enabling the creation of smart batteries in a cost-effective manner;

75

Design: A novel platform was designed, BogieCopter, which uses the same four actuators used for flying for its multiple modes of operation, without requiring the addition of complex and heavy actuators. BogieCopter has enough payload capacity for most applications that use MAVs, having a MTOM of 4 kg and a payload capacity of 1.3 kg or 986 g, considering a T/W ratio of 1.843 or 2, respectively. The vehicle is able to achieve a total hovering flight time of, approximately, eight minutes. Furthermore, the vehicle is able to resist ground impacts and its design opens up the possibility of using it as an active actuated multi-modal MAV (by using the servos);

Simulator: Simulation models and flight controllers for two BogieCopter concepts were also developed, easing the future development and test of controllers for the prototype;

Firmware: Firmware for the interface of different components and actuation modes was developed. This firmware addresses some limitations of the Ardupilot firmware, such as the inability of using more than one I^2C/TWI battery monitor and adding support for servos that implement a communication protocol similar to DYNAMIXEL Protocol 1.0;

Rotors identification: Multiple rotors have been tested in a custom adapted thrust stand, enabling the validation and/or choice of the best rotor for the vehicle. This data adds up to the readily available data online, easing the selection process of future rotors;

Validation: BogieCopter was validated through multiple flights, ground locomotion on flat and inclined surfaces, wall climbing, and multi-modal tests. Contrary to previous works, the capability of the vehicle to move on inclined surfaces was demonstrated. BogieCopter's ability to wall-climb was also demonstrated, creating new possibilities for the use of the vehicle. A comparison between the power required for the different operating states was also presented and was demonstrated that moving on the ground is more efficient than flying. In fact, moving on flat surfaces with a 2 kg payload, at 1 m/s, requires 25.5x less energy than flying with the same payload. The minimum energetic requirement was achieved while moving on flat surfaces at 1 m/s, without any payload, requiring only 28.8 W to maintain this operating state. BogieCopter's ability to climb slope angles up to 33° was also demonstrated. The vehicle is able to reach speeds of up to 4.1 m/s, while moving on the ground with the throttle limited at 35%, being that superior velocities should be possible to attain with higher throttle levels. The tests performed with the developed MAV show the possibilities that the vehicle has for many different applications, such as inspection.

7.2 Future Work

Throughout this work, although the success of the proposed design, which was able to surpass all the tests performed, some details were identified, in order to improve the current design and to add more functionalities to the vehicle. These details are exposed next.

Batteries: The batteries that were identified during the design for BogieCopter were out of stock, with alternative batteries having been used, although not being ideal for the design. The change of the current batteries for the selected ones should improve the operating time of the vehicle;

Rotors: As was concluded from the static thrust tests, the current rotors don't have the best performance. A simple improvement would be to change the motors or the propellers of the vehicle for the most performant ones identified;

CFRP components: The CFRP components weren't optimized for the load cases, due to carbon fibre being an anisotropic material, requiring a more complex optimization process. With the optimization process used, the CFRP materials ended up being over-dimensioned. With the optimization of these components, the mass could be reduced in the prototype, increasing its payload capacity. For example, the side plates could be manufactured from a composite structure of CFRP and structural foam instead of the solid CFRP structure that was used;

Electronics mount plates: At the moment, the electronics mount plates are 3D printed although they were designed to be made out of CFRP. Changing these components for the designed one's (manufactured out of CFRP or even the composite CFRP and structural foam material) should decrease the total mass of the vehicle;

Weak points: Two weak points were identified in the structure of BogieCopter, the wheel's shaft and the servo horn. These components were 3D printed. Replacing these components for similar manufactured out of aluminium should increase the overall strength of the design;

Active actuation: The use of 360º turnable servos opens up the possibility of also using them as an active actuation for the wheels. This hasn't been explored in this work;

Wheel Design: Studies of different wheel designs could be realised, in order to determine the best material and the best shape for the wheels. Also, the design of the wheels can open up the possibility for BogieCopter moving on water;

Water locomotion As mentioned previously, the wheel design can open up the possibility of BogieCopter to move on water. This would require the use of waterproofed components, which isn't the case at the moment, and an analysis of the dynamics, which should be similar to the ground locomotion, given the many airboat's designs that explore this principle;

Wall-climbing: Further studies on the capabilities of wall-climb of BogieCopter can be performed, in order to improve its efficiency and capabilities;

Hovering at different pitch angles: The use of tilt rotors on BogieCopter should enable it to hover and fly at any given pitch angle. This possibility could be explored;

Efficient Forward Flight: The capabilities of the vehicle during forward flight could be expanded, implementing a more efficient forward flight, which is granted by the use of tilt-rotors. A wing structure could be designed for the central structure of BogieCopter, which would create lift and reduce the required energy to fly;

Aerodynamic analysis: An aerodynamic analysis (CFD) could be conducted, in order to determine aerodynamic losses and improve the design, by optimizing the components that produce the most aerodynamic interferences;

Controllers: At the moment, no ground position or ground speed controller has been designed for BogieCopter. The controllers implemented in ArduRover could be, potentially, used on the developed vehicle for the ground mode but not without the addition of sensors, such as GPS, wheel encoders and/or optical flow sensors;

Autonomy: At the moment, BogieCopter doesn't implement any autonomy level. Simple levels of autonomy could be implemented, such as automatic take-off and land, which ArduCopter already implement, requiring only the addition of Time-of-Flight (ToF) sensors. Further levels of autonomy, up to and including full autonomy, can be explored;

Path following controller: Having a multi-modal vehicle, an energy aware path following controller/ algorithm can be developed. This controller would take into account the power requirements of the different operating states and would optimize the path in order for the lowest amount of energy to be spent while following the path;

Tests: Overall, more vehicle's tests can be performed. These could address the questions created in other works done in the multi-modal MAVs area and, hopefully, conclude that BogieCopter has the best design. Furthermore, the vehicle could be tested in real inspection scenarios;

Test bench: A test environment could be developed to test the different locomotion modalities of BogieCopter, with the required safety harness to protect the vehicle. During this work, public spaces such as parking lots or skate parts have been used to test some of the capabilities of BogieCopter, which limited some of the results that could be attained. A test bench would allow a more extensive test of the developed MAV, besides allowing the test of all modalities in a research facility.

Appendix A

Payload

To estimate the required payload's mass, a market search was performed, in order to determine the most commonly used, currently in production, RGB and thermal (IR) camera's sensors, and LIDARs. These sensors are the most used for inspection applications, as presented in section 2.2. In the case of the RGB and IR camera's sensors, only compact sensors, which include both cameras in a single unit, were looked for. Section A.1, table A.1, presents the RGB and IR camera's sensors identified and section A.2, table A.2, presents the LIDARs identified. It should be noted that the sensors identified don't represent all the offer available and its intended purpose is only to enable an estimation of the payload's mass associated with these sensors.

A.1   RGB and Thermal Cameras Sensors

Manufacturer	DJI	FLIR	WORKSWELL	Yuneec	
Model	Zenmuse H20T [163]	VUE® TZ20-R [164]	WIRIS Security [165]	CGOET/X [166]	E10Tv [167]
Gimbal	Yes	Yes	No	Yes	Yes
RGB Camera Resolution	20 MP	NS[1]	1920x1080 px	2.13 MP	2.13 MP
IR Camera Resolution (px)	640x512	640x512	800x600	160x120	640x512
Weight (g)	828 ± 5	640	< 720	326	384

[1] Not Specified

Table A.1: Identified (currently in production) sensors with RGB and thermal cameras.

A.2 LIDARs

Manufacturer	Livox	Velodyne	
Model	MID-70 [168]	Puck [169]	Puck LITE [170]
Horizontal FoV (º)	70.4	360	360
Measurement Range (m)	up to 260	100	100
Weight (g)	580	∼830	∼590

Table A.2: Identified (currently in production) LIDARs.

A.3 Payload Estimation

Analysing tables A.1 and A.2, it is possible to determine a maximum mass budget of 840 g and 600 g for the RGB and thermal camera's sensor and for the LIDAR, respectively, corresponding to a total maximum payload of 1440 g. Considering a safety factor, which will enable the use of a computer on-board for computationally demanding applications, includes the mass of wiring and of the mechanical structures required to use the previously mentioned sensors and accounts for the mass of any extra sensor, the maximum total payload can be estimated to be 2 kg.

Appendix B

Propellers

This Appendix describes the propeller selection from the data outputted by the custom script created to constrain the number of possible propellers. Figure B.1 presents the outputted data.

B.1 Data of Possible Propellers

105x45.dat

	RPM	Thrust (kg)	Power (W)	Efficiency (g/W)
Hover	9000	1,2065557	156,59697	7,704846908
Max Thrust	12000	2,2089948	447,41992	4,937184795

10x3.dat

	RPM	Thrust (kg)	Power (W)	Efficiency (g/W)
Hover	10000	1,15212462	149,1399744	7,725122821
Max Thrust	13999	2,340536629	432,5059258	5,411571241

10x38SF.dat

	RPM	Thrust (kg)	Power (W)	Efficiency (g/W)
Hover	8000	1,1838761	164,05397	7,216381734
Max Thrust	11000	2,2724978	447,41992	5,079116186

10x4.dat

	RPM	Thrust (kg)	Power (W)	Efficiency (g/W)
Hover	9000	1,165732391	164,0539718	7,105785845
Max Thrust	12000	2,131884139	432,5059258	4,929144347

10x45MR.dat

	RPM	Thrust (kg)	Power (W)	Efficiency (g/W)
Hover	8000	1,0477984	126,76898	8,265416265
Max Thrust	11000	2,0366297	410,13493	4,9657554

10x45MRF-RH.dat

	RPM	Thrust (kg)	Power (W)	Efficiency (g/W)
Hover	8000	1,061406146	134,225977	7,907606038
Max Thrust	11000	2,050237512	350,4789398	5,849816578

10x46SF.dat

	RPM	Thrust (kg)	Power (W)	Efficiency (g/W)
Hover	8000	1,0160469	126,76898	8,014949106
Max Thrust	12000	2,3314648	454,87692	5,125484872

10x47SF.dat

	RPM	Thrust (kg)	Power (W)	Efficiency (g/W)
Hover	7000	1,002439138	134,225977	7,468294591
Max Thrust	10000	2,104668597	439,9629245	4,78374081

10x58EP(F2B).dat

	RPM	Thrust (kg)	Power (W)	Efficiency (g/W)
Hover	8000	1,070478	141,68298	7,555445445
Max Thrust	11000	2,081989	499,61891	4,167154043

10x5E.dat

	RPM	Thrust (kg)	Power (W)	Efficiency (g/W)
Hover	9000	1,260986789	171,5109706	7,352222336
Max Thrust	12000	2,317857011	521,9899104	4,440424929

10x6-4.dat

	RPM	Thrust (kg)	Power (W)	Efficiency (g/W)
Hover	7000	1,2383072	171,51097	7,219988121
Max Thrust	9000	2,0593094	350,47894	5,875700722

10x6E.dat

	RPM	Thrust (kg)	Power (W)	Efficiency (g/W)
Hover	8000	1,052334298	141,6829757	7,427387047
Max Thrust	11000	2,036629741	499,6189142	4,076366373

93x3.dat

	RPM	Thrust (kg)	Power (W)	Efficiency (g/W)
Hover	11000	1,1611965	164,05397	7,078136873
Max Thrust	15000	2,2407463	454,87692	4,926049663

95x45.dat

	RPM	Thrust (kg)	Power (W)	Efficiency (g/W)
Hover	10000	1,043262451	141,6829757	7,363357849
Max Thrust	13999	2,118276368	507,075913	4,177434411

95x5MR.dat

	RPM	Thrust (kg)	Power (W)	Efficiency (g/W)
Hover	9000	1,1566605	164,05397	7,050487901
Max Thrust	12000	2,1092045	507,07591	4,1595439

9x3.dat

	RPM	Thrust (kg)	Power (W)	Efficiency (g/W)
Hover	11000	1,075013917	149,1399744	7,208087042
Max Thrust	15000	2,068381207	417,5919283	4,95311587

9x37SF.dat

	RPM	Thrust (kg)	Power (W)	Efficiency (g/W)
Hover	10000	1,0024391	141,68298	7,075226455
Max Thrust	14000	2,0275579	447,41992	4,531666537

Figure B.1: Propeller data, constrained by the custom script. The specifications were constrained from the propeller file (<propeller Name>.dat). Efficiency with background green color represent the efficiencies that respect the optimal design efficiency.

B.2   Selection Process

As can be seen in figure B.1, the propellers that respect the optimal efficiency for both hover as maximum thrust are the APC 10x3, APC 10x3.8SF, APC 10x4.5MRF-RH, APC 10x4.6SF, and the APC 10x6-4. Unfortunately, the APC 10x3, 10x4.6SF and 10x6-4 only exist in counter-clockwise shape, the APC 10x4.5MRF-RH is a folding propeller (being excluded for this reason) and the APC 10x3.8SF was out of stock. Since there wasn't a propeller available with an efficiency at maximum thrust higher than 5 g/W, the propellers in figure B.1 were further constrained to have a simulated maximum thrust higher than 2.2 kg (adding a 10% safety factor to the design maximum thrust). The propellers APC 10.5x4.5, APC 10x5E, and APC 9.3x3 respected the constraints. Once again, the APC 10.5x4.5 and 9.3x3 don't exist in counter-clockwise and clockwise shape, being the final propeller selected the APC 10x5E.

Appendix C

Comparison between T-Motor Motor's Efficiencies

C.1   Efficiency Comparison

From the data provided by T-Motor [110, 111], it is possible to verify that the AT2814 is, overall, more efficient than the AS2814 motor, being, approximately, 10% more efficient producing any given thrust. Being 10% more efficient means that the operating time of a MAV using the AS2814 motors could be increased by 10% by only changing the motors to the AT2814. The data from the manufacturer is plotted in figure C.1, easing this comparison. The data is based on the data for the APC 10x5.5 propeller, which is similar to the propeller being used in the developed MAV.
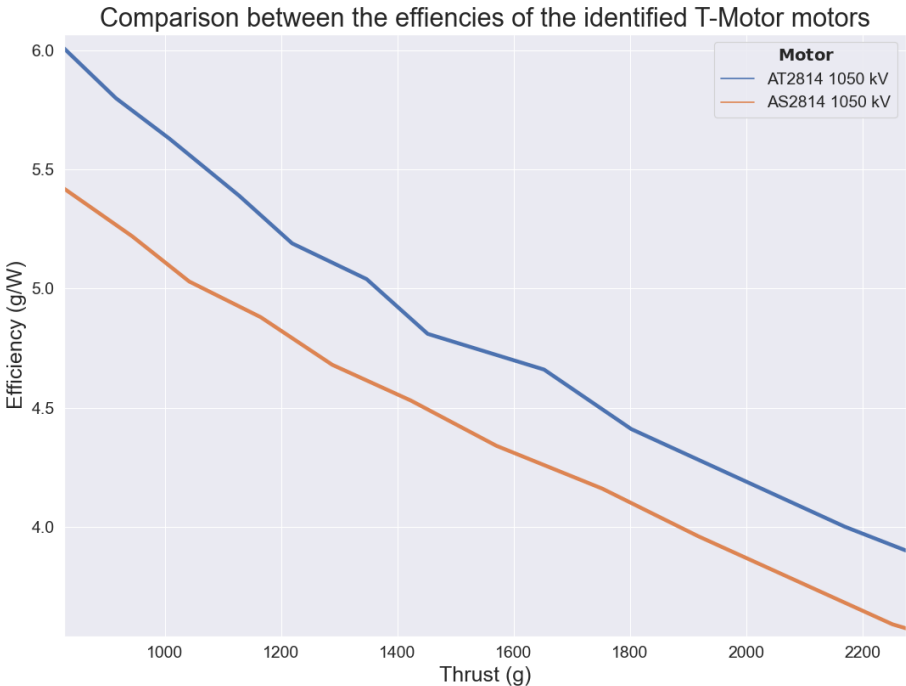
Figure C.1: Comparison between the efficiency of the AT2814 and AS2814 motor, while producing any given thrust (data from manufacturer specifications for an APC 10x5.5 propeller).

Appendix D

Determination of Propeller's Moment of Inertia

D.1 Approximation by Cylinder

The moment of inertia of a propeller can be approximated by the inertia of a solid cylinder. Figure D.1 depicts the cylinder, with its dimensions represented. These are used to determine equations D.1 and D.2, representing the cylinder's moment of inertia along the Z, and the X and Y axis, respectively, where m is the mass of the cylinder. The moment of inertia of the propeller in its rotating axis is equal to I_Z.
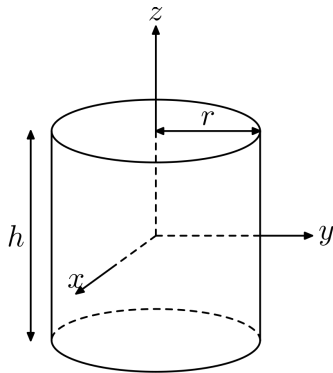
$$I_Z = \frac{1}{2}mr^2 \qquad \text{(D.1)}$$

$$I_X = I_Y = \frac{1}{12}m(3r^2 + m^2) \qquad \text{(D.2)}$$

Figure D.1: Cylinder's dimensions used to determine the moments of inertia of a solid cylinder.

D.2 Parallel Axis Theorem

The moment of inertia that can be determined by using equations D.1 and D.2 considers that the component is rotating about its CoM. In the case of the rotor, we will consider that the centre frame is along the tilt axis (Y-axis is aligned with the tilt axis), being that the propeller is separated in its Z-axis

from this centre frame. To determine the correct moment of inertia, the Parallel Axis Theorem needs to be applied [171]:

$$I = I_0 + md^2 \tag{D.3}$$

Where d is the distance between the propeller CoM and the tilt axis, along which the rotor tilts.

D.3 Propeller's Moment of Inertia

Considering that the propeller has a diameter, $\frac{r}{2}$, a height, h, and mass, m, of 254 mm, 10 mm and 20 g, respectively, and it is distanced, d, 50 mm from the centre frame along the Z-axis (Y-axis aligned with the tilt axis), we can approximate the moment of inertia of the propeller by using equations D.1 and D.3:

$$I = \frac{1}{2}mr^2 + md^2 \tag{D.4}$$

By using equation D.4 we can determine the propeller's moment of inertia to be:

$$I = \frac{1}{2} \cdot 0.02 \cdot 0.127^2 + 0.02 \cdot 0.05^2 = 0.00021129 \, kg/m^2 \tag{D.5}$$

Appendix E

Custom Made PCBs

E.1 Introduction

The design of BogieCopter creates one challenge inherent from the use of three batteries. The autopilot used in BogieCopter, Pixhawk 1, only has five easily usable ADC inputs. Having three batteries, it is necessary to control six states, the current and voltage of each battery, in order to determine if the batteries are running out of charge and actuate in case they are. Also, if the battery current and voltage could be communicated digitally to Pixhawk 1, that would be a plus, since the current and voltage could be measured close to the source, avoiding losses in the cable harnessing. Furthermore, digital communication protocols are less prone to interference by noise, which the motors' and ESCs' switching can cause. Considering the use of custom made PCBs, the battery current and voltage can be estimated close to the batteries, avoiding the losses in the cable harnessing. In total, three custom PCBs were designed: the SmartBat, and SmartBat and Router, which will enable the creation of simple smart batteries, and the Lateral Router, which is nothing more than a simple cable harnessing router between the motors' arms, the servos and the electronics mount.

E.2 Lateral Router

The Lateral Router is a simple PCB, which has the possibility of having three connectors. It connects the slip ring in the motors' arms, the servo and a wheel encoder to the SmartBat and Router PCB, which is located in the electronics mount. Its use simplifies the cable harnessing, reducing the number of cables used (ground from the different components is connected here, for example) and simplifies the assembly and disassembly of BogieCopter. Figure E.1 depicts the Lateral Router PCB. Due to its simplicity, the schematics aren't presented.
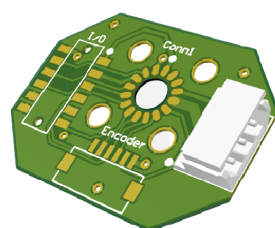
Figure E.1: Lateral Router PCB.

E.3 SmartBat

As has been mentioned in E.1, the objective of SmartBat is for it to work as a simple hardware of a smart battery. A smart battery can be described as a battery equipped with specialized hardware that provides present state, calculated and predicted information to its SMBus [127] Host under software control [126]. Smart batteries have a lot of capabilities, from the estimation of instantaneous current up to the estimation of state of charge (SoC) [126] (the battery in a laptop is a smart battery), but for this work we are only interested in a subset of this capabilities, enabling the creation of a simpler and less expensive solution. We are interested in the estimation of the instantaneous current and voltage, in order to allow the power comparison between different operating states and also to protect BogieCopter from batteries that are running out of charge. In fact, if the battery runs out of charge during flight, the MAV can stop flying and crash. By knowing that batteries are running out of charge in a timely manner, precaution measures can be taken, such as landing the vehicle. Since the batteries used in the propulsive system are multi-cell batteries (with the cells in series), the SoC needs to be estimated from the individual cell voltage. This has to do with the fact that a single cell can run out of charge faster than the rest of the cells in the battery, due to unbalances in the internal resistance of the cells. That's why, in systems with high power requirements (high current) that use multi-cell batteries, such as an aerial vehicle, battery cell alarms are used (such as the one presented in figure E.2), to let the operator know that, at least, one of the cells is running out of charge.

Figure E.2: Battery cell tester and alarm.

E.3.1 Hardware

It is required that the instantaneous current being withdrawn from the battery and the individual cell voltages are measured. To measure the current, a current sense circuit is required. Fortunately, most ESCs already implement this circuit (one of the requirements of the selected ESC was that it had to have this circuit), being that it is only required to convert this analog value into a digital one. Relatively to measuring the individual cell voltages, the ESCs don't implement a circuit for this application, being that it is required to implement it in the custom PCB, SmartBat. The measurement of the analog cell voltages can be performed with multiple circuits, each one having its own advantages and disadvantages. For the custom made PCB, a resistor voltage divider is used, given that it is the least complex and more cost-effective circuit [172]. Despite these advantages, measuring the voltage with a resistor voltage divider presents one of the highest inaccuracies, requiring high precision resistors [172]. For these PCBs, inaccuracies up to 10 mV are acceptable (using 0.1 % resistors).

For BogieCopter to remain a platform that could be easily upgraded and adapted, it was decided

that SmartBat should be able to measure the individual cell's voltage of up to a 6S battery (six cells in series). This required the use of a microcontroller with, at least, seven ADC inputs (six for the voltages and one for the current). Also, the microcontroller should have, at least, one I^{2}C/TWI interface, in order to implement some of the specifications of the SMBus protocol [127]. To keep the firmware development as simple as possible, a microcontroller compatible with Arduino was used [173], the ATtiny1616 [174]. Besides, this microcontroller was used due to the capabilities it offers while being manufactured in a package that is easily hand-solderable.

SmartBat has a buzzer and a LED, in order to warn the operator when one of the battery cells is running out of charge (the minimum cell's voltage can be specified by the operator). It also acts as a simple router between the ESC and the slip ring, only outputting two out of the four motor control signals from the ESC (which can be changed by jumpers). The total spacing between the mounting holes of the SmartBat was limited by the spacing in the used ESC, which corresponds to 30.5 mm. The board weighs 8.4 g, which includes the cable to connect the PCB to the battery balancing connector. This mass is lower than the mass of a battery cell tester and alarm, which weighs 12 g. Figure E.3 depicts the designed SmartBat PCB. A complete schematic of SmartBat's circuit is depicted in figure E.6 and the PCB layout is presented in figure E.7.
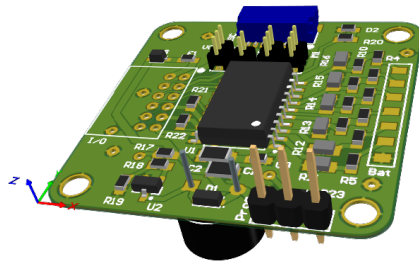
Figure E.3: SmartBat PCB.

E.3.2   Firmware

The firmware of SmartBat was developed using Arduino [173], enabling a quick development. Simplifying, the firmware determines the instantaneous current and the individual battery cell's voltage, outputs the data through I^{2}C/TWI, and sounds an alarm and turns on a LED if one of the cells has a voltage lower than a specified voltage (by the operator) or if an alarm signal is set by the operator. It should be noted that, although SmartBat and SmartBat and Router PCBs are physically different, their code is almost the same, only changing the current multiplying factor used. The code created for the custom made PCBs can be found in [175].

E.4   SmartBat and Router

As the name implies, the SmartBat and Router is a SmartBat with additional capabilities. As with the Lateral Router, SmartBat and Router is also responsible for the routing of the harnessing. It has two input connectors, which are connected to the Lateral Routers (slip ring, servo and encoder signals), and

outputs signals to the Pixhawk 1 through multiple connectors (one for each type of used connector in the Pixhawk 1). It also has additional connectors to extend its capabilities and enable its use in upgraded versions of BogieCopter (such as additional I^{2}C connectors and connections for power outputs). In the next subsection, the additional circuitry of SmartBat and Router is presented, being that for the basic functionality refer to SmartBat (E.3).

E.4.1 Hardware

One of the fundamental differences between SmartBat and SmartBat and Router is that, the latter, doesn't interface with an ESC, meaning that a custom designed current sensing circuit needs to be implemented. The current sensing circuit is as simple as a current sense resistor and current shunt monitor, in this case, an INA139 [176]. An example of a current sense circuit using the INA139 is depicted in figure E.4. Taking into consideration that BogieCopter should be upgradeable and should take into consideration the use of multiple additional sensors, the current sense circuit and the PCB were designed to be able to handle a maximum current of 30 A. To be able to handle this current, SmartBat and Router uses a four-layer design. This current capacity gives plenty of room for SmartBat and Router to be able to handle the power requirements of additional circuits. Furthermore, it includes a 5 V and a 3.3 V DC/DCs (switching and linear, respectively) that are able to handle 3 A and 750 mA, respectively. All these voltages are routed to a connector for easy access and assembly of extra power harnessing.

In SmartBat and Router, a level shifter was also implemented. The level shifter main purpose is to modify the voltage of signals, in this case, from the I^{2}C signals. Pixhawk 1 uses 3.3 V for the I^{2}C signals and the custom boards use 5 V. While the custom boards can interface with the voltage levels of Pixhawk 1, the interface of Pixhawk 1 with the 5 V signals of the custom boards could damage it. The use of the level shifter avoids this damage and enables the reduction of the number of boards used (if SmartBat and Router didn't have the level shifter an additional board had to be used).

SmartBat and Router were dimensioned in order to be easily assembled on top of a Pixhawk 1 autopilot (taking into account the use of spacers), measuring 58x58 mm and weighing 23.7 g. Figure E.5 presents the PCB design of SmartBat and Router, figure E.8 illustrates the schematic of the PCB and E.9 depicts the PCB's layout.
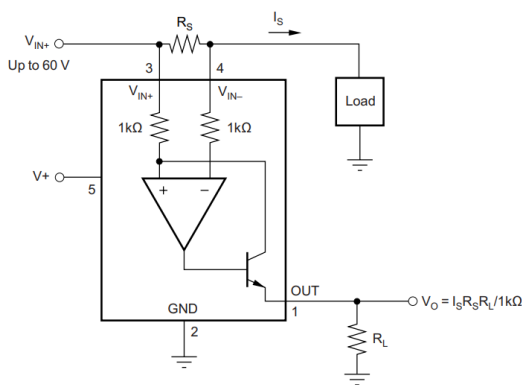
Figure E.4: Typical current sense circuit using the INA139 [176].
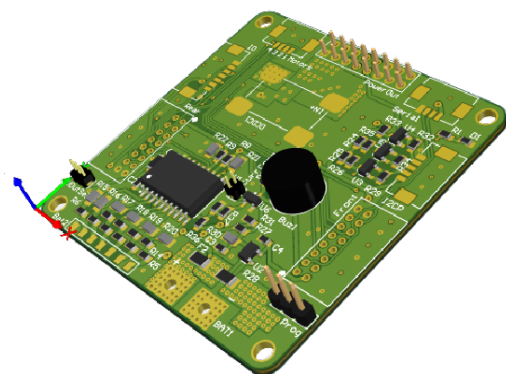
Figure E.5: SmartBat and Router PCB.
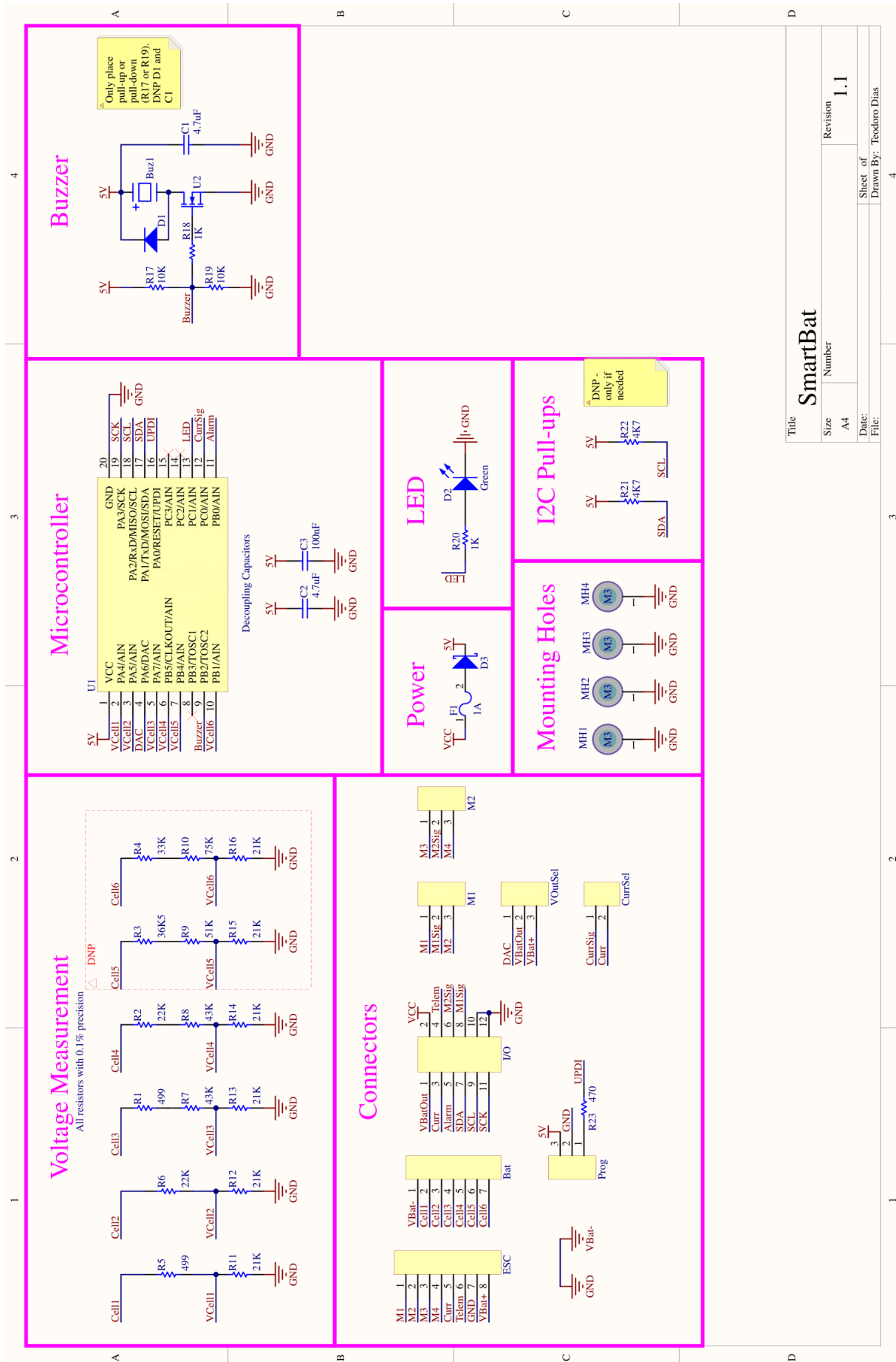
Figure E.6: SmartBat schematic.
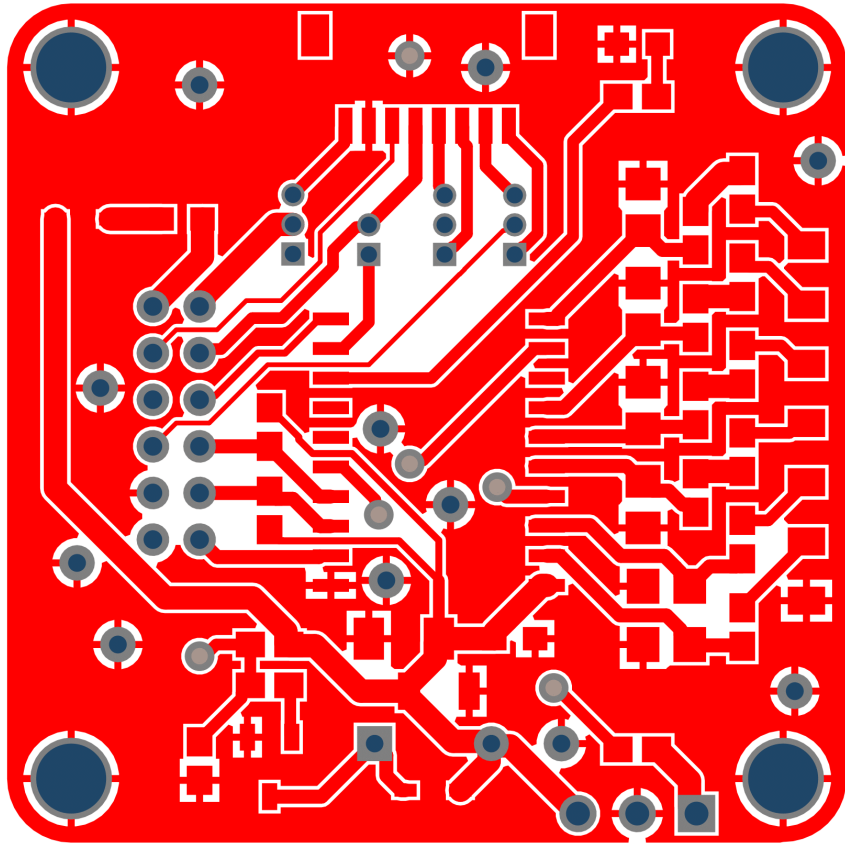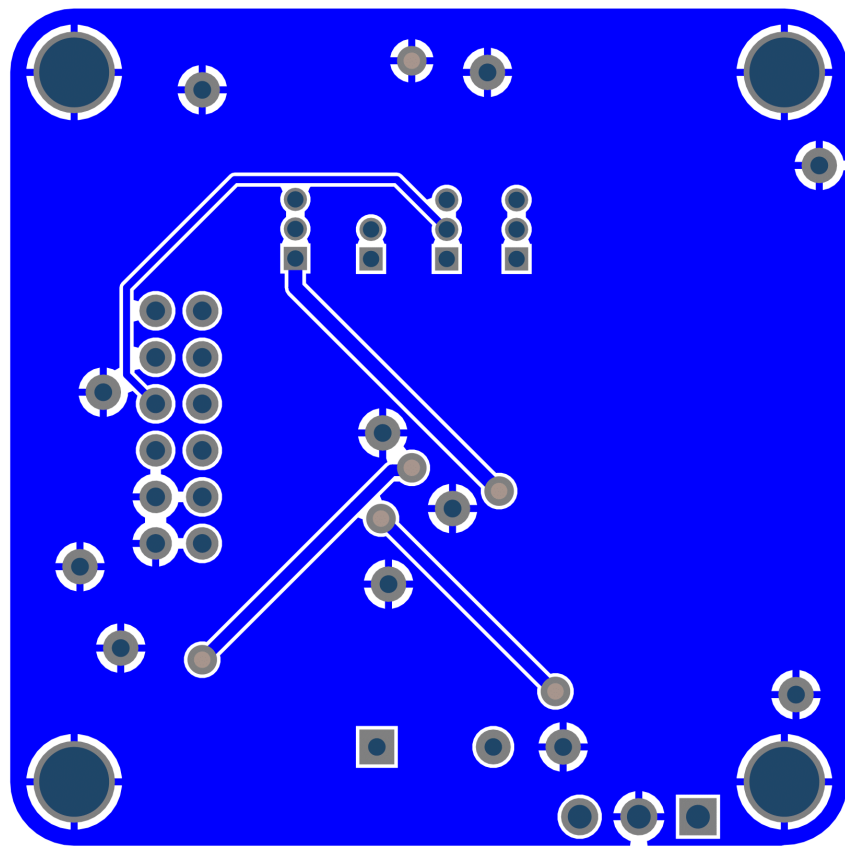
Figure E.7: SmartBat layout and layers: (a) Top (b) Bottom.
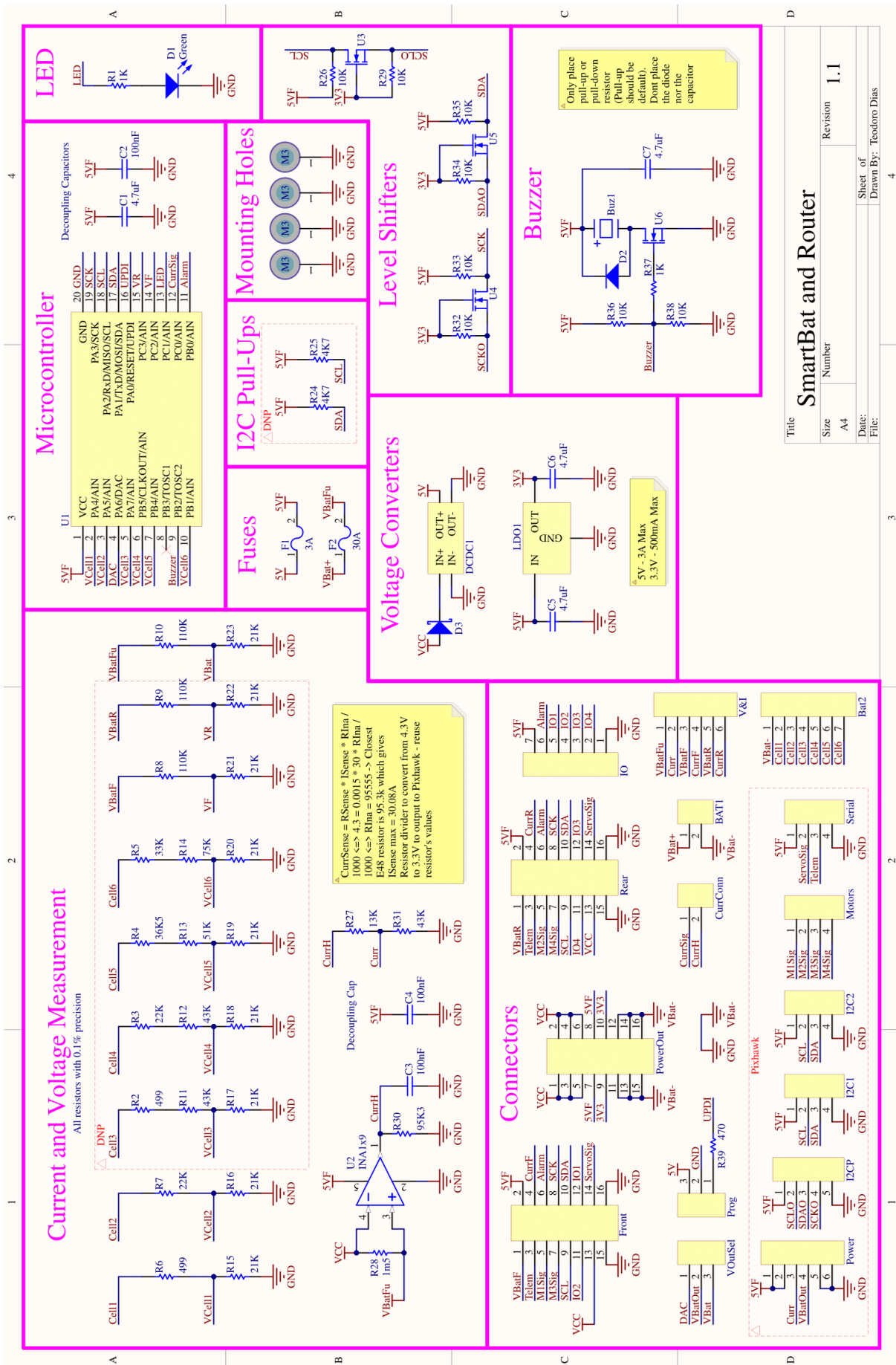
Figure E.8: SmartBat and Router schematic.
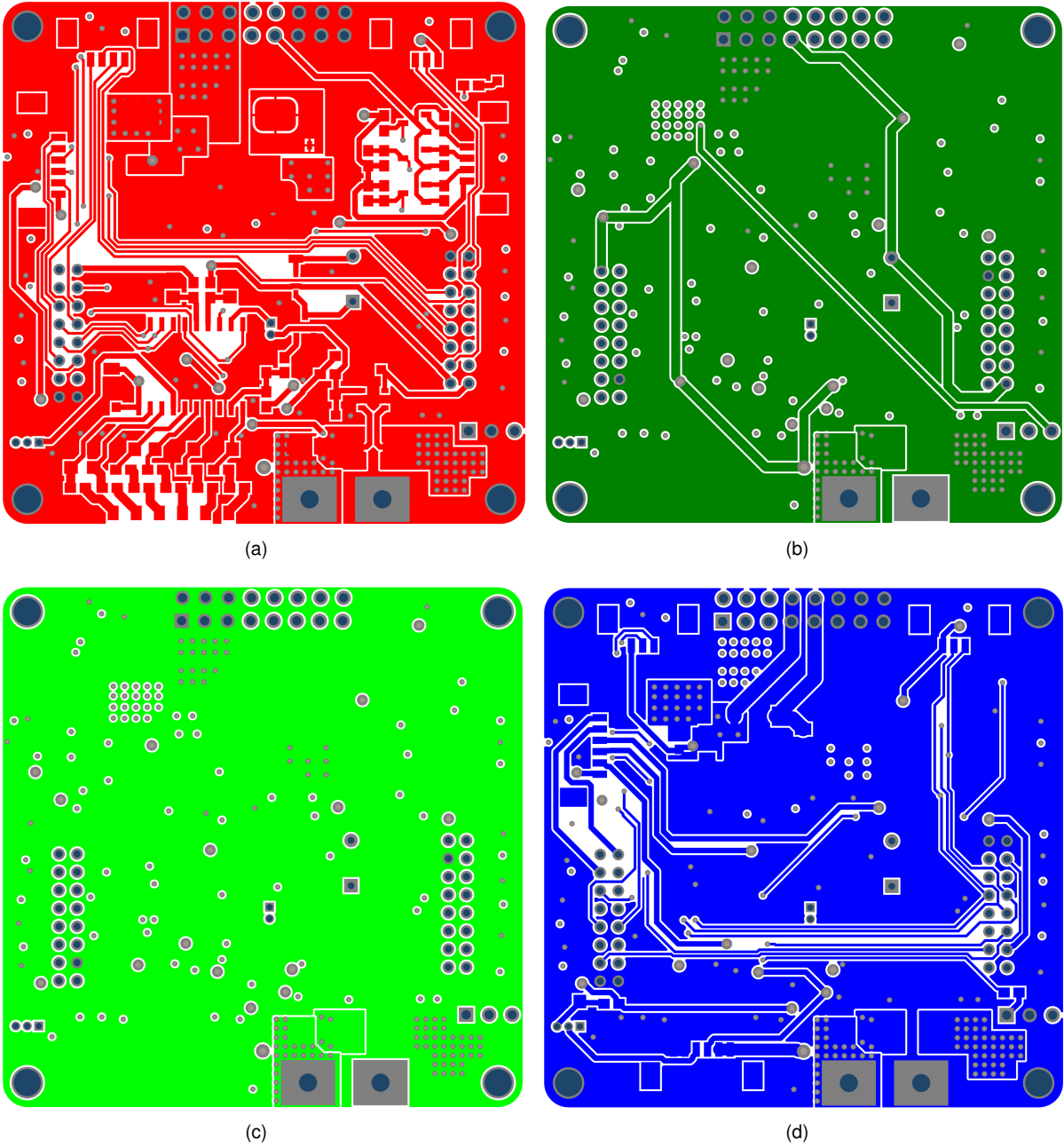
Figure E.9: SmartBat and Router layout and layers: (a) Top (b) Middle 1 (c) Middle 2 (d) Bottom.

Appendix F

Design Naming

F.1 Introduction

In this appendix, the naming of the different components of BogieCopter is presented. It starts by presenting a general overview of the names of the different components of BogieCopter, in F.2, and then presents both the extruded view and the naming of the components in two assemblies: the motors' arms, in F.3, and the wheel assembly, in F.4, giving a better knowledge of BogieCopter structure.

F.2 BogieCopter Naming Overview
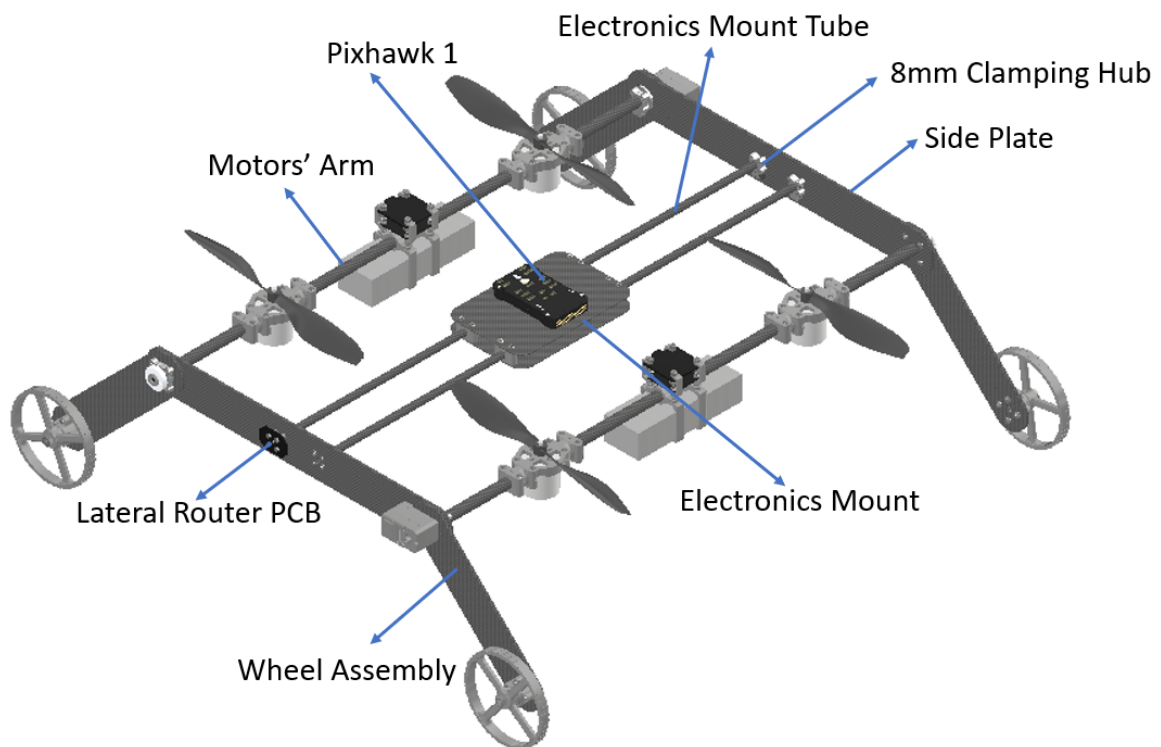
Figure F.1: Name of the general components of BogieCopter.

F.3 Motors' Arms Naming
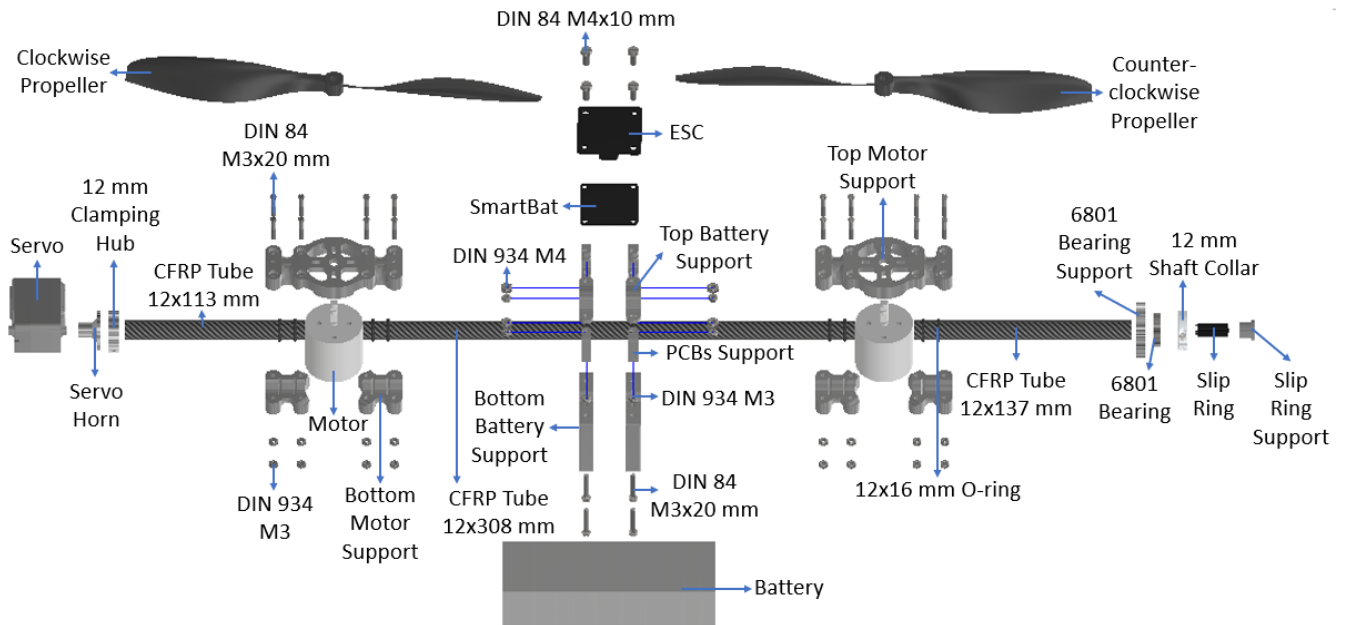
Figure F.2: Extruded view and name of the components of the motors' arm of BogieCopter.

F.4 Wheel Assembly Naming
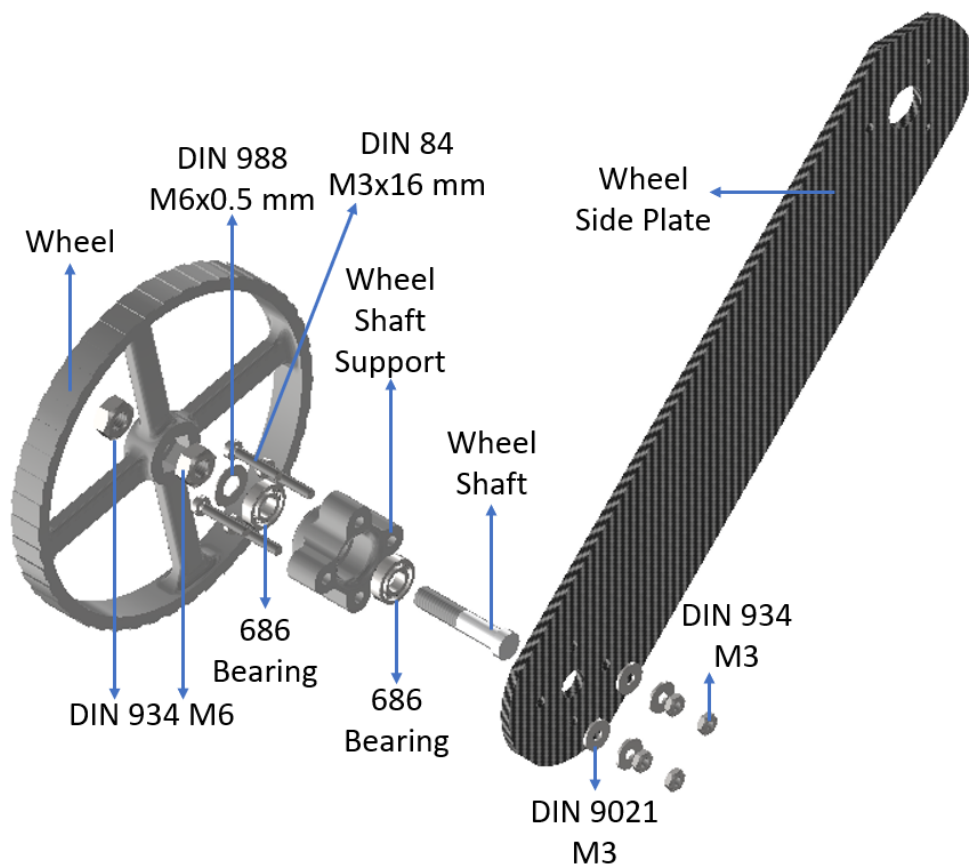
Figure F.3: Extruded view and name of the components of the wheel assembly of BogieCopter.

Appendix G

Thrust Stand

G.1 Introduction

In a rotor static thrust test, the objective is to determine the performance of the rotor, i.e., to determine its rotational velocity, thrust, power, and efficiency for each throttle command level. Static thrust tests are performed in thrust stands. Unfortunately, during this work, there was no access to a readily available thrust stand that could determine all these parameters automatically (such as RCbenchmark test stands [177]) and so, a readily available thrust stand was adapted to be able to measure all the necessary parameters and to realise the tests automatically.

G.2 Adaptation of Thrust Stand

The adaptation of a thrust stand started with the Turnigy Thrust Stand v1, which uses a 5 kg load cell to measure the thrust produced by a rotor. The rotor is mounted on a sliding platform, enabling it to move with the force it creates. The force created can then be determined by the load cell, just like on a common scale. Unfortunately, this thrust stand isn't able to measure rotational velocity or power, only being able to measure thrust. To add the ability to measure rotational velocity, a commonly available RPM sensor was used, the Hobbywing Brushless RPM sensor and to measure the power (current and voltage) a commonly available power module was used, the APM Power module. Both of these components are usually used on custom-made MAVs.

Having the necessary components to measure the desired parameters, a way to measure data automatically and log it was still required. To solve this challenge, an Arduino UNO was used [173], being the code developed available in [178]. To control the throttle level commanded to the ESC, Pixhawk 1 (the autopilot used in the MAV) was used and custom code was developed for the automatic test. The final result was a thrust stand that could measure data automatically and log it on a computer, by using the USB interface, independently of the rotor and the ESC used.

G.3 Final Considerations

To maintain the results constant throughout the multiple tests performed on the different rotors, a power supply with adjustable voltage was used. Using a power supply instead of a battery has the advantage that the voltage output is constant throughout the tests (while with the battery, the voltage

keeps dropping during the test, due to the discharge of the battery). The tests were conducted at the nominal voltage of the propulsive system batteries, 14.8 V and the power supply was required to handle the maximum permissible motor current of 40 A. Due to the availability of power supplies, a 1000 W, 24 V adjustable power supply was used.

Due to the thrust that the rotors produced, the thrust stand had to be attached to a wood panel and weights had to be mounted on top of it. Figure G.1 illustrates the setup used to test the rotors, with the custom adapted thrust stand depicted, and figure G.2 presents a schematic of all the components used. The total cost of this custom adapted thrust stand is presented in table G.1, which ended up being 6x cheaper (power supply included here) than the solution from RCbenchmark.
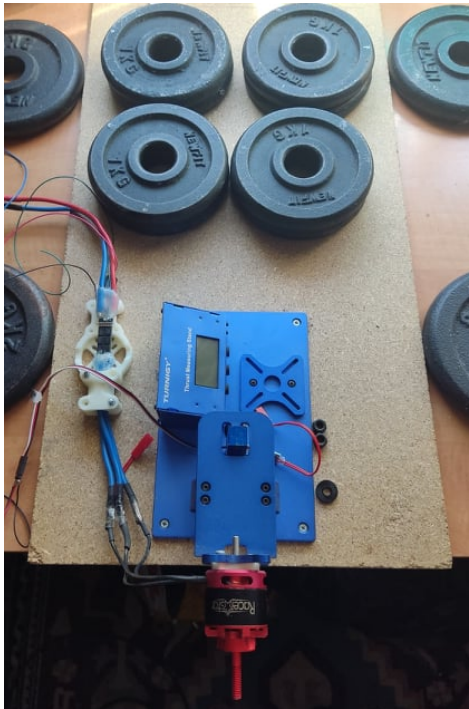
Figure G.1: Thrust stand used in the static tests, with the Racerstar BR2814 assembled. The weights were added due to the thrust created by the rotors, which was able to move the wood panel and the thrust stand.
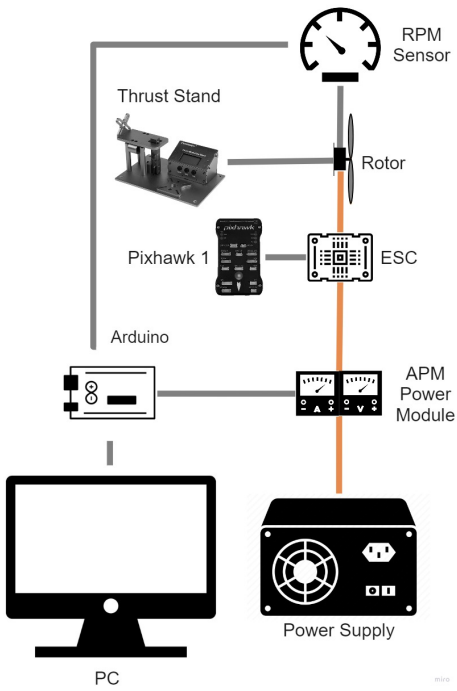
Figure G.2: Schematic of the components used in the thrust stand and their connection. Orange connection represents high current path while grey connection represents low current signals or mechanical connection (in the case of the thrust stand to rotor).

Component	Cost (€)
APM Power Module	5
Hobbywing RPM Sensor	4.5
Power Supply (S-1000-24)	60
Turnigy Thrust Stand V1	40
Total	109.5

Table G.1: Cost of the adapted thrust stand for automatic static thrust tests.

Bibliography

[1] S. Herwitz, L. Johnson, S. Dunagan, R. Higgins, D. Sullivan, J. Zheng, B. Lobitz, J. Leung, B. Gallmeyer, M. Aoyagi, R. Slye, and J. Brass. Imaging from an unmanned aerial vehicle: agricultural surveillance and decision support. *Computers and Electronics in Agriculture*, 44(1):49–61, 2004. ISSN 0168-1699. doi: https://doi.org/10.1016/j.compag.2004.02.006.

[2] A. Pretto, S. Aravecchia, W. Burgard, N. Chebrolu, C. Dornhege, T. Falck, F. Fleckenstein, A. Fontenla, M. Imperoli, R. Khanna, F. Liebisch, P. Lottes, A. Milioto, D. Nardi, S. Nardi, J. Pfeifer, M. Popovic, C. Potena, C. Pradalier, E. Rothacker-Feder, I. Sa, A. Schaefer, R. Siegwart, C. Stachniss, A. Walter, W. Winterhalter, X. Wu, and J. I. Nieto. Building an aerial-ground robotics system for precision farming. *CoRR*, abs/1911.03098, 2019.

[3] A. Ollero, G. Heredia, A. Franchi, G. Antonelli, K. Kondak, A. Sanfeliu, A. Viguria, J. R. Martinez-de Dios, F. Pierri, J. Cortes, A. Santamaria-Navarro, M. A. Trujillo Soto, R. Balachandran, J. Andrade-Cetto, and A. Rodriguez. The aeroarms project: Aerial robots with advanced manipulation capabilities for inspection and maintenance. *IEEE Robotics & Automation Magazine*, 25(4):12–23, 2018. doi: 10.1109/MRA.2018.2852789.

[4] Y. Zefri, A. ElKettani, I. Sebari, and S. Ait Lamallam. Thermal infrared and visual inspection of photovoltaic installations by uav photogrammetry—application case: Morocco. *Drones*, 2(4), 2018. ISSN 2504-446X. doi: 10.3390/drones2040041.

[5] A. Kalantari, T. Touma, L. Kim, R. Jitosho, K. Strickland, B. T. Lopez, and A.-A. Agha-Mohammadi. Drivocopter: A concept hybrid aerial/ground vehicle for long-endurance mobility. In *2020 IEEE Aerospace Conference*, pages 1–10, 2020. doi: 10.1109/AERO47225.2020.9172782.

[6] R. A. Mattar and R. Kalai. Development of a wall-sticking drone for non-destructive ultrasonic and corrosion testing. *Drones*, 2(1), 2018. ISSN 2504-446X. doi: 10.3390/drones2010008.

[7] A. Ortiz, F. Bonnín-Pascual, and E. Garcia-Fidalgo. Vessel inspection: A micro-aerial vehicle-based approach. *Journal of Intelligent & Robotic Systems*, 76:151–167, 2014.

[8] M. Nieuwenhuisen, J. Quenzel, M. Beul, D. Droeschel, S. Houben, and S. Behnke. Chimneyspector: Autonomous mav-based indoor chimney inspection employing 3d laser localization and textured surface reconstruction. In *2017 International Conference on Unmanned Aircraft Systems (ICUAS)*, pages 278–285, 2017. doi: 10.1109/ICUAS.2017.7991427.

[9] S. Waharte and N. Trigoni. Supporting search and rescue operations with uavs. In *2010 International Conference on Emerging Security Technologies*, pages 142–147, 2010. doi: 10.1109/EST.2010.31.

[10] A. Ferworn, J. Tran, A. Ufkes, and A. D'Souza. Initial experiments on 3d modeling of complex disaster environments using unmanned aerial vehicles. In *2011 IEEE International Symposium on Safety, Security, and Rescue Robotics*, pages 167–171, 2011. doi: 10.1109/SSRR.2011.6106781.

[11] A. Lacaze. Pegasus transforming uav/ugv hybrid vehicle. In *NDIA Ground Vehicle Systems Engineering And Technology Symposium—Autonomous Ground Systems (AGS) Technical Session, Novi, MI*, 2017.

[12] M. Hassanalian and A. Abdelkefi. Classifications, applications, and design challenges of drones: A review. *Progress in Aerospace Sciences*, 91:99–131, 2017. ISSN 0376-0421. doi: https://doi.org/10.1016/j.paerosci.2017.04.003.

[13] S. Drones. Drone benefits in photovoltaic solar farms. URL: `https://skylinedrones.ro/drone-benefits-in-photovoltaic-solar-farms`. Accessed on: 2021-09-29.

[14] DJI. Lives Saved: A Survey of Drones in Action, . URL: `https://www.dji.com/newsroom/news/dji-releases-first-count-of-lives-saved-by-drones`. Accessed on: 2021-09-29.

[15] Percepto. The Evolution of Drones: From Military to Hobby & Commercial. URL: `https://percepto.co/the-evolution-of-drones-from-military-to-hobby-commercial`. Accessed on: 2021-09-29.

[16] K. P. Valavanis. Advances in unmanned aerial vehicles: state of the art and the road to autonomy. 2008.

[17] M. Burri, J. Nikolic, C. Hürzeler, G. Caprari, and R. Siegwart. Aerial service robots for visual inspection of thermal power plant boiler systems. In *2012 2nd International Conference on Applied Robotics for the Power Industry (CARPI)*, pages 70–75, 2012. doi: 10.1109/CARPI.2012.6473374.

[18] D. Floreano and R. J. Wood. Science, technology and the future of small autonomous drones. *Nature*, 521:460–466, 2015.

[19] A.-a. Agha-mohammadi, N. K. Ure, J. P. How, and J. Vian. Health aware stochastic planning for persistent package delivery missions using quadrotors. In *2014 IEEE/RSJ International Conference on Intelligent Robots and Systems*, pages 3389–3396, 2014. doi: 10.1109/IROS.2014.6943034.

[20] Kettering Bug. URL: `https://en.wikipedia.org/wiki/Kettering_Bug`. Accessed on: 2021-09-29.

[21] S. Gupta, M. Ghonge, and P. Jawandhiya. Review of unmanned aircraft system (uas). *International Journal of Advanced Research in Computer Engineering & Technology*, 9, 04 2013. doi: 10.2139/ssrn.3451039.

[22] M. Hassanalian, H. Khaki, and M. Khosravi. A new method for design of fixed wing micro air vehicle. *Proceedings of the Institution of Mechanical Engineers, Part G: Journal of Aerospace Engineering*, 229(5):837–850, 2015. doi: 10.1177/0954410014540621.

[23] DJI. DJI Phantom 4 Pro, 2016. URL: `https://www.dji.com/pt/phantom-4-pro`. Accessed on: 2021-09-29.

[24] M. Hassanalian and A. Abdelkefi. Methodologies for weight estimation of fixed and flapping wing micro air vehicles. *Meccanica*, 52(9):2047–2068, 2017.

[25] Blimp toy. URL: `https://www.amazon.com/Remote-Control-Swimming-Inflatable-Balloon/dp/B08NT63FG3`. Accessed on: 2021-09-29.

[26] M. Yamada, M. Nakao, Y. Hada, and N. Sawasaki. Development and field test of novel two-wheeled uav for bridge inspections. In *2017 International Conference on Unmanned Aircraft Systems (ICUAS)*, pages 1014–1021, 2017. doi: 10.1109/ICUAS.2017.7991308.

[27] K. Kawasaki, Y. Motegi, M. Zhao, K. Okada, and M. Inaba. Dual connected bi-copter with new wall trace locomotion feasibility that can fly at arbitrary tilt angle. In *2015 IEEE/RSJ International Conference on Intelligent Robots and Systems (IROS)*, pages 524–531, 2015. doi: 10.1109/IROS.2015.7353422.

[28] J. A. Tsanakas, L. D. Ha, and F. Al Shakarchi. Advanced inspection of photovoltaic installations by aerial triangulation and terrestrial georeferencing of thermal/visual imagery. *Renewable Energy*, 102:224–233, 2017. ISSN 0960-1481. doi: https://doi.org/10.1016/j.renene.2016.10.046.

[29] B. Muhammad, R. Prasad, M. Nisi, A. Mennella, G. Gagliarde, E. Cianca, D. Marenchino, A. Angrisano, M. Bernardi, P. Addabbo, and S. Ullo. Automating the maintenance of photovoltaic power plants. In *2017 Global Wireless Summit (GWS)*, pages 6–11, 2017. doi: 10.1109/GWS.2017.8300492.

[30] S. Leva, M. Aghaei, and F. Grimaccia. Pv power plant inspection by uas: Correlation between altitude and detection of defects on pv modules. In *2015 IEEE 15th International Conference on Environment and Electrical Engineering (EEEIC)*, pages 1921–1926, 2015. doi: 10.1109/EEEIC.2015.7165466.

[31] S. Gallardo-Saavedra, L. Hernández-Callejo, and O. Duque-Perez. Technological review of the instrumentation used in aerial thermographic inspection of photovoltaic plants. *Renewable and Sustainable Energy Reviews*, 93:566–579, 2018. ISSN 1364-0321. doi: https://doi.org/10.1016/j.rser.2018.05.027.

[32] S. Hamaza, I. Georgilas, and T. Richardson. An adaptive-compliance manipulator for contact-based aerial applications. In *2018 IEEE/ASME International Conference on Advanced Intelligent Mechatronics (AIM)*, pages 730–735, 2018. doi: 10.1109/AIM.2018.8452382.

[33] M. Fumagalli, R. Naldi, A. Macchelli, F. Forte, A. Q. Keemink, S. Stramigioli, R. Carloni, and L. Marconi. Developing an aerial manipulator prototype: Physical interaction with the environment.

IEEE Robotics & Automation Magazine, 21(3):41–50, 2014. doi: 10.1109/MRA.2013.2287454.

[34] T. Ikeda, S. Yasui, M. Fujihara, K. Ohara, S. Ashizawa, A. Ichikawa, A. Okino, T. Oomichi, and T. Fukuda. Wall contact by octo-rotor uav with one dof manipulator for bridge inspection. In *2017 IEEE/RSJ International Conference on Intelligent Robots and Systems (IROS)*, pages 5122–5127, 2017. doi: 10.1109/IROS.2017.8206398.

[35] W. Myeong and H. Myung. Development of a wall-climbing drone capable of vertical soft landing using a tilt-rotor mechanism. *IEEE Access*, 7:4868–4879, 2019. doi: 10.1109/ACCESS.2018.28 89686.

[36] D. D. Fan, R. Thakker, T. Bartlett, M. B. Miled, L. Kim, E. Theodorou, and A.-a. Agha-mohammadi. Autonomous hybrid ground/aerial mobility in unknown environments. In *2019 IEEE/RSJ International Conference on Intelligent Robots and Systems (IROS)*, pages 3070–3077, 2019. doi: 10.1109/IROS40897.2019.8968276.

[37] A. Kalantari and M. Spenko. Design and experimental validation of hytaq, a hybrid terrestrial and aerial quadrotor. In *2013 IEEE International Conference on Robotics and Automation*, pages 4445–4450, 2013. doi: 10.1109/ICRA.2013.6631208.

[38] K. Kawasaki, M. Zhao, K. Okada, and M. Inaba. Muwa: Multi-field universal wheel for air-land vehicle with quad variable-pitch propellers. In *2013 IEEE/RSJ International Conference on Intelligent Robots and Systems*, pages 1880–1885, 2013. doi: 10.1109/IROS.2013.6696605.

[39] W. Mielniczek. B-unstoppable all terrain tank-quadcopter drone, 2015. URL: `https://www.kick starter.com/projects/2017062404/b-unstoppable`. Accessed on: 2021-09-29.

[40] S. Morton and N. Papanikolopoulos. A small hybrid ground-air vehicle concept. In *2017 IEEE/RSJ International Conference on Intelligent Robots and Systems (IROS)*, pages 5149–5154, 2017. doi: 10.1109/IROS.2017.8206402.

[41] K. Tanaka, D. Zhang, S. Inoue, R. Kasai, H. Yokoyama, K. Shindo, K. Matsuhiro, S. Marumoto, H. Ishii, and A. Takanishi. A design of a small mobile robot with a hybrid locomotion mechanism of wheels and multi-rotors. In *2017 IEEE International Conference on Mechatronics and Automation (ICMA)*, pages 1503–1508, 2017. doi: 10.1109/ICMA.2017.8016039.

[42] W. Wang, C. y. Li, L. h. Chu, and C. y. Qu. Study on air-ground amphibious agricultural information collection robot. In *2016 13th International Conference on Ubiquitous Robots and Ambient Intelligence (URAI)*, pages 938–944, 2016. doi: 10.1109/URAI.2016.7734115.

[43] A. R S and M. M. Dharmana. Multi-terrain multi-utility robot. *Procedia Computer Science*, 133: 651–659, 2018. ISSN 1877-0509. doi: https://doi.org/10.1016/j.procs.2018.07.100. International Conference on Robotics and Smart Manufacturing (RoSMa2018).

[44] Y. Qin, W. Xu, A. Lee, and F. Zhang. Gemini: A compact yet efficient bi-copter uav for indoor applications. *IEEE Robotics and Automation Letters*, 5(2):3213–3220, 2020. doi: 10.1109/LRA. 2020.2974718.

[45] Y. Qin, Y. Li, X. Wei, and F. Zhang. Hybrid aerial ground locomotion with a single passive wheel. *CoRR*, abs/2003.09242, 2020.

[46] JJRC. H3. URL: `https://www.geekbuying.com/item/JJRC-H3-Air-Ground-Airphibian-2-4G-4-Channel-6-Axis-Gyro-RC-Quadcopter-with-2-0MP-Camera-Four-Wheel-UFO---Blue-343423.html`. Accessed on: 2021-09-29.

[47] Syma. X9. URL: `https://www.dhgate.com/product/syma-x9-air-land-dual-mode-rc-flying-car/373183748.html`. Accessed on: 2021-09-29.

[48] A. Kalantari and M. Spenko. Modeling and performance assessment of the hytaq, a hybrid terrestrial/aerial quadrotor. *IEEE Transactions on Robotics*, 30(5):1278–1285, 2014. doi: 10.1109/TRO.2014.2337555.

[49] S. Mizutani, Y. Okada, C. J. Salaan, T. Ishii, K. Ohno, and S. Tadokoro. Proposal and experimental validation of a design strategy for a uav with a passive rotating spherical shell. In *2015 IEEE/RSJ International Conference on Intelligent Robots and Systems (IROS)*, pages 1271–1278, 2015. doi: 10.1109/IROS.2015.7353532.

[50] S. Sabet, A.-A. Agha-Mohammadi, A. Tagliabue, D. S. Elliott, and P. E. Nikravesh. Rollocopter: An energy-aware hybrid aerial-ground mobility for extreme terrains. In *2019 IEEE Aerospace Conference*, pages 1–8, 2019. doi: 10.1109/AERO.2019.8741685.

[51] A. Tagliabue, S. Schneider, M. Pavone, and A. Agha-mohammadi. Shapeshifter: A multi-agent, multi-modal robotic platform for exploration of titan. *CoRR*, abs/2002.00515, 2020.

[52] A. Agha-mohammadi, A. Tagliabue, S. Schneider, B. Morrell, M. Pavone, J. Hofgartner, I. A. D. Nesnas, R. B. Amini, A. Kalantari, A. Babuscia, and J. I. Lunine. The shapeshifter: a morphing, multi-agent, multi-modal robotic platform for the exploration of titan (preprint version). *CoRR*, abs/2003.08293, 2020.

[53] L. J. Gordon. *Principles of Helicopter Aerodynamics*. Cambridge Aerospace Series. Cambridge University Press, New York, 2nd edition, 2006. ISBN 0-521-85860-7.

[54] N. Takahashi, S. Yamashita, Y. Sato, Y. Kutsuna, and M. Yamada. All-round two-wheeled quadrotor helicopters with protect-frames for air–land–sea vehicle (controller design and automatic charging equipment). *Advanced Robotics*, 29(1):69–87, 2015. doi: 10.1080/01691864.2014.991754.

[55] Parrot. Rolling Spider, 2014. URL: `https://www.amazon.com/Parrot-PF723000-ROLLING-SPIDER/dp/B00KZM53NC`. Accessed on: 2021-09-29.

[56] N. Meiri and D. Zarrouk. Flying STAR, a Hybrid Crawling and Flying Sprawl Tuned Robot. In *2019 International Conference on Robotics and Automation (ICRA)*, pages 5302–5308, 2019. doi: 10.1109/ICRA.2019.8794260.

[57] Inkonova. Tilt Scout, 2018. URL: `https://dronemajor.net/brands/inkonova/products/tilt-scout`. Accessed on: 2021-09-29.

[58] J. R. Page and P. E. I. Pounds. The quadroller: Modeling of a uav/ugv hybrid quadrotor. In *2014

IEEE/RSJ International Conference on Intelligent Robots and Systems, pages 4834–4841, 2014. doi: 10.1109/IROS.2014.6943249.

[59] M. Hepperle. How a Propeller Works, 1996. URL: `https://www.mh-aerotools.de/airfoils/propuls4.htm`. Accessed on: 2021-09-29.

[60] B. Theys, G. Dimitriadis, P. Hendrick, and J. De Schutter. Influence of propeller configuration on propulsion system efficiency of multi-rotor unmanned aerial vehicles. In *2016 International Conference on Unmanned Aircraft Systems (ICUAS)*, pages 195–201, 2016. doi: 10.1109/ICUAS.2016.7502520.

[61] S. Bouabdallah. *Design and control of quadrotors with application to autonomous flying*. PhD thesis, École Polytechnique Fédérale de Lausanne, February 2007.

[62] A. Nemati, N. Soni, M. Sarim, and M. Kumar. Design, Fabrication and Control of a Tilt Rotor Quadcopter. Volume 2 of *Dynamic Systems and Control Conference*, 10 2016. doi: 10.1115/DSCC2016-9929.

[63] D. Mellinger, M. Shomin, and V. Kumar. Control of quadrotors for robust perching and landing. In *Proceedings of the International Powered Lift Conference*, pages 205–225, 2010.

[64] G. Hoffmann, H. Huang, S. Waslander, and C. Tomlin. Quadrotor helicopter flight dynamics and control: Theory and experiment. In *AIAA guidance, navigation and control conference and exhibit*, page 6461, 2007.

[65] B. J. Emran and H. Najjaran. A review of quadrotor: An underactuated mechanical system. *Annual Reviews in Control*, 46:165–180, 2018. ISSN 1367-5788. doi: https://doi.org/10.1016/j.arcontrol.2018.10.009.

[66] A. Roza and M. Maggiore. A class of position controllers for underactuated vtol vehicles. *IEEE Transactions on Automatic Control*, 59(9):2580–2585, 2014. doi: 10.1109/TAC.2014.2308609.

[67] R. Naldi, M. Furci, R. G. Sanfelice, and L. Marconi. Global trajectory tracking for underactuated vtol aerial vehicles using a cascade control paradigm. In *52nd IEEE Conference on Decision and Control*, pages 4212–4217, 2013. doi: 10.1109/CDC.2013.6760536.

[68] PX4. Controller Diagrams, 2021. URL: `https://docs.px4.io/master/en/flight_stack/controller_diagrams.html`. Accessed on: 2021-09-29.

[69] Y. Yamamoto and X. Yun. Coordinating locomotion and manipulation of a mobile manipulator. *IEEE Transactions on Automatic Control*, 39(6):1326–1332, 1994. doi: 10.1109/9.293207.

[70] R. M. DeSantis. Modeling and path-tracking control of a mobile wheeled robot with a differential drive. *Robotica*, 13(4):401–410, 1995. doi: 10.1017/S026357470001883X.

[71] T. J. de Vries, C. van Heteren, and L. Huttenhuis. Modeling and control of a fast moving, highly maneuverable wheelchair. In *Proceedings of the International Biomechatronics workshop*, number April, pages 110–115, 1999.

[72] R. Dhaouadi and A. A. Hatab. Dynamic modelling of differential-drive mobile robots using lagrange and newton-euler methodologies: A unified framework. *Advances in Robotics & Automation*, 2(2): 1–7, 2013.

[73] K. Kotay. Robo-Rats Locomotion: Skid-steer Drive, 2001. URL: `https://groups.csail.mit.edu/drl/courses/cs54-2001s/skidsteer.html`. Accessed on: 2021-09-29.

[74] R. Carona, A. P. Aguiar, and J. Gaspar. Control of unicycle type robots Tracking, Path Following and Point Stabilization. In *IV Jornadas de Engenharia Electrónica e Telecomunicações e de Computadores, Lisbon, Portugal*, pages 180–185, 2008.

[75] C. Ordonez, N. Gupta, B. Reese, N. Seegmiller, A. Kelly, and E. G. Collins. Learning of skid-steered kinematic and dynamic models for motion planning. *Robotics and Autonomous Systems*, 95:207–221, 2017. ISSN 0921-8890. doi: https://doi.org/10.1016/j.robot.2017.05.014.

[76] M. Bronz, J.-M. Moschetta, P. Brisset, and M. Gorraz. Towards a long endurance MAV. In *EMAV 2009, European Micro Aerial Vehicle Conference and Flight Competition*, Volume 1, pages pp 241–254, Delft, Netherlands, Sept. 2009. SAGE.

[77] M. Hassanalian, M. Radmanesh, and A. Sedaghat. Increasing flight endurance of mavs using multiple quantum well solar cells. *International Journal of Aeronautical and Space Sciences*, 15 (2):212–217, 2014.

[78] G. Hawkins. F450 dimensions, 2019. URL: `https://george-hawkins.github.io/arf-drone/docs/f450-dimensions`. Accessed on: 2021-09-29.

[79] Y. Mulgaonkar, M. Whitzer, B. Morgan, C. M. Kroninger, A. M. Harrington, and V. Kumar. Power and weight considerations in small, agile quadrotors. In T. George, M. S. Islam, and A. K. Dutta, editors, *Micro- and Nanotechnology Sensors, Systems, and Applications VI*, Volume 9083, pages 376 – 391. International Society for Optics and Photonics, SPIE, 2014. doi: 10.1117/12.2051112.

[80] C. Ampatis and E. Papadopoulos. Parametric design and optimization of multi-rotor aerial vehicles. In *2014 IEEE International Conference on Robotics and Automation (ICRA)*, pages 6266–6271, 2014. doi: 10.1109/ICRA.2014.6907783.

[81] M. Biczyski, R. Sehab, J. F. Whidborne, G. Krebs, and P. Luk. Multirotor sizing methodology with flight time estimation. *Journal of Advanced Transportation*, 2020, 2020.

[82] K. Karydis and V. Kumar. Energetics in robotic flight at small scales. *Interface focus*, 7(1): 20160088, 2017.

[83] A. Tagliabue, X. Wu, and M. W. Mueller. Model-free online motion adaptation for optimal range and endurance of multicopters. In *2019 International Conference on Robotics and Automation (ICRA)*, pages 5650–5656, 2019. doi: 10.1109/ICRA.2019.8793708.

[84] A. U. Tech). How to choose the right motor for your multicopter drone. URL: `https://www.dronetrest.com/t/how-to-choose-the-right-motor-for-your-multicopter-drone/568`. Accessed on: 2021-09-29.

[85] A. Propellers. . URL: `https://www.apcprop.com/`. Accessed on: 2021-09-29.

[86] APC propellers performance data. URL: `https://www.apcprop.com/technical-information/performance-data/`. Accessed on: 2021-01-08.

[87] T. Dias. Propeller's Constraint Script Repository, . URL: `https://github.com/teoPiD/Propeller-Selection-Custom-Script`. Accessed on: 2021-10-30.

[88] APC. 10x5E, . URL: `https://www.apcprop.com/product/10x5e/`. Accessed on: 2021-09-29.

[89] Y. Al-Rihani. Development of a dual axis tilt rotorcraft uav: design, prototyping and control. Master's thesis, Cranfield University, 2012.

[90] APC. 10x7E, . URL: `https://www.apcprop.com/product/10x7e/`. Accessed on: 2021-09-29.

[91] I. Penkov and D. Aleksandrov. Analysis and study of the influence of the geometrical parameters of mini unmanned quad-rotor helicopters to optimise energy saving. *International Journal of Automotive and Mechanical Engineering*, 14:4730–4746, 2017.

[92] C. Persson. Drive Calculator. URL: `http://www.drivecalc.de`. Accessed on: 2021-09-29.

[93] M. Müller. eCalc. URL: `https://www.ecalc.ch/`. Accessed on: 2021-09-29.

[94] AXi Model Motors. URL: `https://www.modelmotors.cz/`. Accessed on: 2021-09-29.

[95] BrotherHobby. URL: `https://www.brotherhobbystore.com/`. Accessed on: 2021-09-29.

[96] Cobra Motors. URL: `https://www.cobramotorsusa.com/`. Accessed on: 2021-09-29.

[97] D-Power Modellbau. URL: `https://www.d-power-modellbau.com/`. Accessed on: 2021-09-29.

[98] Dualsky. URL: `http://dualsky.com/`. Accessed on: 2021-09-29.

[99] Dymond Modelsport USA. URL: `https://www.dymondusa.com/`. Accessed on: 2021-09-29.

[100] EMAX. URL: `https://emaxmodel.com/`. Accessed on: 2021-09-29.

[101] Hacker Motor. URL: `https://www.hacker-motor.com/`. Accessed on: 2021-09-29.

[102] Plettenberg Elektromotoren. URL: `https://plettenberg-motoren.net/en/products/modeler/brushless-motors`. Accessed on: 2021-09-29.

[103] Scorpion Power Systems. URL: `https://www.scorpionsystem.com/`. Accessed on: 2021-09-29.

[104] Sunnysky. URL: `http://en.rcsunnysky.com`. Accessed on: 2021-09-29.

[105] Racerstar. URL: `https://www.racerstar.com/`. Accessed on: 2021-09-29.

[106] T-Motor. URL: `https://uav-en.tmotor.com/`. Accessed on: 2021-09-29.

[107] Dualsky. ECO-C V2 series brushless outrunners. URL: `http://dualsky.com/ECO_Series/ECOv2.shtml`. Accessed on: 2021-09-29.

[108] Racerstar. BR2814 1000KV, . URL: `https://m.racerstar.com/racerstar-br2814-1000kv-3-4s-brushless-motor-for-rc-airplane-model-p-294.html`. Accessed on: 2021-09-29.

[109] Sunnysky. X2814-III. URL: `http://en.rcsunnysky.com/x-fixedwingseries/54.html`. Ac-

cessed on: 2021-09-29.

[110] T-Motor. AS2814 Long Shaft, . URL: `https://store.tmotor.com/goods.php?id=939`. Accessed on: 2021-09-29.

[111] T-Motor. AT2814 Long Shaft, . URL: `https://store.tmotor.com/goods.php?id=791`. Accessed on: 2021-09-29.

[112] Felix. Dshot, testing a new digital parallel ESC throttle signal. URL: `https://www.rcgroups.com/forums/showthread.php?2756129-Dshot-testing-a-new-digital-parallel-ESC-throttle-signal`. Accessed on: 2021-09-29.

[113] blckmn. DSHOT – The new kid on the block. URL: `https://blck.mn/2016/11/dshot-the-new-kid-on-the-block/`. Accessed on: 2021-09-29.

[114] G. Cook. Catalogue of parametrised CRC algorithms. URL: `https://reveng.sourceforge.io/crc-catalogue/all.htm`. Accessed on: 2021-09-29.

[115] O. Liang. ESC for Racing Drones & Mini Quad. URL: `https://docs.google.com/spreadsheets/d/1SYzJWKTu2vFVL99mt5tQxc2sTiHCXNAEZyGodfy3uE0/edit#gid=0`. Accessed on: 2021-09-29.

[116] Racerstar. Air50 3-6S 50A 4In1 ESC, . URL: `https://www.racerstar.com/30_5+30_5mm-racerstar-air50-3-6s-50a-4in1-esc-blheli_s-dshot600-compatibled-with-airf7-lite-p-430.html`. Accessed on: 2021-09-29.

[117] G. Ace. Gens Ace Bashing 4S 5000 mAh 50C. URL: `https://www.gensace.de/gens-ace-5000mah-14-8v-4s1p-50c-lipo-battery-pack-with-xt90-plug-bashing-series.html`. Accessed on: 2021-09-29.

[118] Z. Power. ZOP Power 4S 3200 mAh 75C. URL: `https://www.banggood.com/2Pcs-ZOP-Power-14_8V-3200mAh-75C-4S-Lipo-Battery-XT60-Plug-for-RC-Airplane-p-1762866.html`. Accessed on: 2021-09-29.

[119] G. Gress. Using dual propellers as gyroscopes for tilt-prop hover control. In *2002 Biennial International Powered Lift Conference and Exhibit*, page 5968, 2002.

[120] F. Kendoul, I. Fantoni, and R. Lozano. Modeling and control of a small autonomous aircraft having two tilting rotors. *IEEE Transactions on Robotics*, 22(6):1297–1302, 2006. doi: 10.1109/TRO.2006.882956.

[121] N. dos Santos Fernandes. Design and construction of a multi-rotor with various degrees of freedom. Master's thesis, Instituto Superior Técnico, 2011.

[122] F. RC. STS3215. URL: `https://www.feetechrc.com/74v-19-kgcm-plastic-case-metal-tooth-magnetic-code-double-axis-ttl-series-steering-gear.html`. Accessed on: 2021-09-29.

[123] AXADD. RW16W. URL: `http://www.axadd.com/products/robot-servo/360robot-servo/2948.html`. Accessed on: 2021-09-29.

[124] Robotis. DYNAMIXEL XC430-W240-T, . URL: `https://www.robotis.us/dynamixel-xc430-w240-t/`. Accessed on: 2021-09-29.

[125] Panasonic NCR18650B. URL: `https://www.nkon.nl/pt/panasonic-ncr18650b-made-in-japan.html`. Accessed on: 2021-09-29.

[126] S. S. B. System. Smart Battery Data Specification, Revision 1.1, . URL: `http://sbs-forum.org/specs/sbdat110.pdf`. Accessed on: 2021-09-29.

[127] S. S. B. System. System Management Bus Specification, Revision 1.1, . URL: `http://smbus.org/specs/smbus110.pdf`. Accessed on: 2021-09-29.

[128] M. V. Pimentel. Design and control of a bimodal aerial robot for locomotion in flat and inclined surfaces. Master's thesis, Instituto Superior Técnico, April 2021.

[129] D. Aleksandrov and I. Penkov. Optimal gap distance between rotors of mini quadrotor helicopter. In *Proceedings of the 8th DAAAM Baltic Conference, Tallinn, Estonia*, pages 19–21, 2012.

[130] X. Zhang. Uav design and manufacture. *Singapore, National University of Singapore*, 2010.

[131] Autodesk Inventor Product Page. URL: `https://www.autodesk.eu/products/inventor/overview`. Accessed on: 2021-09-29.

[132] Blocks 3D Printer Manufacturer Website. URL: `https://www.blockstec.com/`. Accessed on: 2021-09-29.

[133] DragonPlate. What is carbon fiber? URL: `https://dragonplate.com/what-is-carbon-fiber`. Accessed on: 2021-09-29.

[134] Design215. Tubing Calculator. URL: `https://design215.com/dcal/toolbox/tubing-calculator`. Accessed on: 2021-09-29.

[135] Protech. Standard Thicknesses. URL: `https://protechcomposites.com/resources/standard-thicknesses`. Accessed on: 2021-09-29.

[136] RobotDigg. SHF8 Linear Shaft Rail Support Unit, . URL: `https://www.robotdigg.com/product/119/SHF8-Linear-Shaft-Rail-Support-Unit`. Accessed on: 2021-09-29.

[137] RobotDigg. 8 mm Clamping Hub, . URL: `https://www.servocity.com/8mm-0-770-clamping-hub/`. Accessed on: 2021-09-29.

[138] F. Furrer, M. Burri, M. Achtelik, and R. Siegwart. *RotorS—A Modular Gazebo MAV Simulator Framework*, pages 595–625. Springer International Publishing, Cham, 2016. ISBN 978-3-319-26054-9. doi: 10.1007/978-3-319-26054-9_23.

[139] Gazebo. URL: `http://gazebosim.org/`. Accessed on: 2021-09-29.

[140] ArduPilot, . URL: `https://ardupilot.org/`. Accessed on: 2021-09-29.

[141] PX4. URL: `https://px4.io/`. Accessed on: 2021-09-29.

[142] ArduPilot. Vehicle Types Supported by ArduPilot, . URL: `https://ardupilot.org/plane/docs`

/common-all-vehicle-types.html. Accessed on: 2021-09-29.

[143] ArduPilot. AntennaTracker Home, . URL: https://ardupilot.org/antennatracker/index.html. Accessed on: 2021-09-29.

[144] ArduPilot. Copter Home, . URL: https://ardupilot.org/copter/index.html. Accessed on: 2021-09-29.

[145] ArduPilot. Plane Home, . URL: https://ardupilot.org/plane/index.html. Accessed on: 2021-09-29.

[146] ArduPilot. Rover Home, . URL: https://ardupilot.org/rover/index.html. Accessed on: 2021-09-29.

[147] ArduSub. Overview. URL: https://www.ardusub.com/. Accessed on: 2021-09-29.

[148] ArduPilot. ArduCopter-4.0.7 stable branch, . URL: https://github.com/ArduPilot/ardupilot/tree/Copter-4.0.7. Accessed on: 2021-09-29.

[149] ArduPilot. ArduCopter Beta branch, . URL: https://github.com/ArduPilot/ardupilot/tree/ArduCopter-beta. Accessed on: 2021-09-29.

[150] Robotis. DYNAMIXEL Protocol 1.0, . URL: https://emanual.robotis.com/docs/en/dxl/protocol1/. Accessed on: 2021-09-29.

[151] T. Dias. TTL Servo Protocol Code Branch, . URL: https://github.com/teoPiD/ardupilot/tree/TTLServo-Copter-4.0.7. Accessed on: 2021-10-30.

[152] T. Dias. Multiple External SMBus Battery Monitors Code Branch, . URL: https://github.com/teoPiD/ardupilot/tree/customSMBusBattery-Copter-4.0.7. Accessed on: 2021-10-30.

[153] ArduPilot. Connect ESCs and Motors, . URL: https://ardupilot.org/copter/docs/connect-escs-and-motors.html. Accessed on: 2021-09-29.

[154] A. van Beek. Coefficient of friction, Rolling resistance and Aerodynamics. URL: https://www.tribology-abc.com/abc/cof.htm. Accessed on: 2021-09-29.

[155] E.-M. Design. Manufacturing laboratory. *Drive Wheel Motor Torque Calculations. Faculty of Engineering. University of Florida, University of Florida*, 2011.

[156] Spektrum. DX8. URL: https://www.spektrumrc.com/Products/Default.aspx?ProdId=SPM8800. Accessed on: 2021-09-29.

[157] ArduPilot. Rover Control Modes: Manual Mode, . URL: https://ardupilot.org/rover/docs/manual-mode.html. Accessed on: 2021-09-29.

[158] T. Dias. Flat and Inclined Surface Locomotion Code Branch, . URL: https://github.com/teoPiD/ardupilot/tree/groundMode-Copter-4.0.7. Accessed on: 2021-10-30.

[159] T. Dias. Wall Climb Test Code Branch, . URL: https://github.com/teoPiD/ardupilot/tree/Copter-4.0.7-wallClimb. Accessed on: 2021-10-30.

[160] N. Iboshi, N. Itoga, J. Prasad, and L. N. Sankar. Ground effect of a rotor hovering above a confined area. *Frontiers in Aerospace Engineering*, 3(1):7–16, 2014.

[161] P. Sanchez-Cuevas, G. Heredia, and A. Ollero. Characterization of the aerodynamic ground effect and its influence in multirotor control. *International Journal of Aerospace Engineering*, 2017, 2017.

[162] S. Prothin, C. F. Escudero, N. Doué, and T. Jardin. Aerodynamics of mav rotors in ground and corner effect. *International Journal of Micro Air Vehicles*, 11:1756829319861596, 2019. doi: 10.1177/1756829319861596.

[163] DJI. Zenmuse H20 Series, . URL: `https://www.dji.com/pt/zenmuse-h20-series`. Accessed on: 2021-09-29.

[164] FLIR. VUE® TZ20-R. URL: `https://www.flir.com/products/vue-tz20-r/`. Accessed on: 2021-09-29.

[165] WORKSWELL. WIRIS Security. URL: `https://workswell-thermal-camera.com/drone-secur ity-thermal-imaging-camera-night-vision-uav/`. Accessed on: 2021-09-29.

[166] Yuneec. CGOET, . URL: `https://us.yuneec.com/cgoet/`. Accessed on: 2021-09-29.

[167] Yuneec. E10Tv, . URL: `https://us.yuneec.com/e10tv/`. Accessed on: 2021-09-29.

[168] Livox. MID-70. URL: `https://www.livoxtech.com/mid-70`. Accessed on: 2021-09-29.

[169] Velodyne. Puck, . URL: `https://velodynelidar.com/products/puck/`. Accessed on: 2021-09-29.

[170] Velodyne. Puck Lite, . URL: `https://velodynelidar.com/products/puck-lite/`. Accessed on: 2021-09-29.

[171] Parallel Axis Theorem. URL: `https://en.wikipedia.org/wiki/Parallel_axis_theorem`. Accessed on: 2021-09-29.

[172] O. J. Borgersen. Multicell battery monitoring and balancing with avr. Master's thesis, Norwegian University of Science and Technology, June 2009.

[173] Arduino Website, . URL: `https://www.arduino.cc/`. Accessed on: 2021-09-29.

[174] Microchip. ATtiny1616. URL: `https://www.microchip.com/en-us/product/ATTINY1616`. Accessed on: 2021-09-29.

[175] T. Dias. Custom Made PCBs Firmware, . URL: `https://github.com/teoPiD/SmartBat-SW`. Accessed on: 2021-10-30.

[176] T. Instruments. INA139. URL: `https://www.ti.com/product/INA139`. Accessed on: 2021-09-29.

[177] T. Robotics. RCbenchmark Series 1580/1585 Test Stand. URL: `https://www.tytorobotics.c om/pages/series-1580-1585`. Accessed on: 2021-09-29.

[178] T. Dias. Custom Adapted Thrust Stand Code Repository, . URL: `https://github.com/teoPiD/ Thrust-Stand-Code`. Accessed on: 2021-10-30.